Energetics and Structural Aspects of Cation-Coupled Drug Transport by NorM Multidrug Transporters

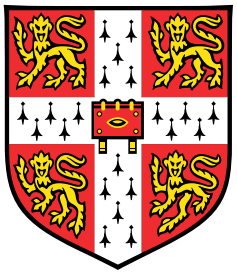

Sagar Raturi

Department of Pharmacology
University of Cambridge

This dissertation is submitted for the degree of
Doctor of Philosophy

Clare Hall

October 2018

Dedicated to my family.

Declaration

I hereby declare that the contents of this dissertation are original and have not been submitted in whole or in part for consideration for any other degree or qualification in this, or any other, university. The data shown in shown in figures 3.7, 3.13, 4.5, 5.7 and 6.2 were generated and analysed by Dr Asha Nair. The rest of the work presented in this dissertation is my own work and contains nothing which is the outcome of work done in collaboration with others. This dissertation contains fewer than 60,000 words including appendices, bibliography, footnotes, tables and equations and has fewer than 150 figures.

Sagar Raturi
October 2018

Acknowledgements

Any piece of work, directly or indirectly, is a resultant of innumerable personal efforts and events. Even though I might fall prey to my lack of good memory, I shall try my best to acknowledge every person who has helped me conduct the research work presented here. The prime mover for this research has been my PhD supervisor, Dr Hendrik van Veen. I am extremely grateful to him for taking me under his supervision and providing guidance and care throughout the last four years. I have learnt a lot from him and that is something that will stay with me beyond this PhD. I am also very grateful to Dr Andreas Bender, who encouraged and guided my application for this PhD.

Dr Asha Nair, who I collaborated with, let me use her substrate binding data and I thank her for that. I thank my lab members Dr Lisa Fagg, Dr Kelvin Agboh, Dr Zhen Tong, Dr Himansha Singh, Arthur Neuberger, Robbin De Kruijf, Megan Ansbro, Brendan Swain, Alex Kong, Soeren Pfitzer, and David Guo for being extremely supportive co-workers and great friends. The Department of Pharmacology has been a very positive place to work at and I shall always cherish the friends I have made here.

I am grateful to the Cambridge Commonwealth Trust and Nehru Trust for Cambridge University for funding my doctoral studies and stay at the University. I must acknowledge the personal support provided by the directors of these two funding bodies, Ms Helen Pennant and Dr Anil Seal, respectively.

Thanks to the Institute of Bioinformatics and Applied Biotechnology (IBAB) and the affiliated faculty members for providing me what I consider the best education of my life and for providing me with financial loan to help me arrive at Cambridge. I have had unconditional support (moral and financial) from Clare Hall. I thank them, in particular the senior tutor Dr Iain Black, who has always been very understanding and supportive. Every college needs an Iain!

We are what our parents make us and I am certainly who my parents made me. I take the opportunity to thank them and my siblings. Finally, I consider my friends to be the highlight of my life. Thanks to Darshana Joshi for providing me endless support 24/7 (for the last four years!). Thanks to Martina Kuvalja, Bhaskaran Nair, Vijay Venugopalan, Michael Rice, and Mark Williams. You guys are literally the best!

Abstract

NorM multidrug transport proteins belong to the multiple antibiotics and toxins extrusion (MATE) family of secondary active transporters. Members of this family are present across all species including bacteria, plants and humans. In bacteria, their over-expression can lead to antibiotic resistance, whereas in the human body, the transporters can alter the plasma levels of drugs. NorM proteins are therefore relevant for the pharmacokinetic properties of drugs. Previously, NorM from *Vibrio cholerae* (NorM-VC) was shown to export drug (ethidium) in an antiport reaction that is coupled to the simultaneous uptake of protons and sodium ions down their electrochemical gradients across the plasma membrane. But NorM from *Pseudomonas stutzeri* (NorM-PS) was shown to transport DAPI by utilising proton cycling exclusively. NorM-VC and NorM-PS share 42% identical amino-acid residues and yet their functions differ in terms of their ion coupling properties. These differences in functionality of two highly homologous proteins provide an excellent opportunity to carry out a comparative study. The work presented in this thesis investigates the energetics of drug transport processes by NorM-VC and NorM-PS and the structural basis for ion-coupled drug transport by NorM-VC. Ethidium efflux assays in intact *Lactococcus lactis* cells were used to study the effect of the magnitude and composition of the proton- and sodium-motive force on transport activity. Furthermore, ethidium binding assays were used to study partial reactions in drug efflux processes. These biochemical data were supplemented by computational studies and analyses of current protein structures. Based on the observations detailed here, a novel transport model for NorM-VC is proposed, which explains published findings for NorM-VC and other MATE transporters. The model represents a potentially universal mechanism for MATE transporters that can be used to predict further structure-function relationships in this important family of member transporters.

Table of contents

List of figures

List of tables

Chapter 1

Introduction

"Good fences make good neighbours."

Robert Frost, *Mending Wall*

1.1 Drug-resistance: a global health problem

Drug-resistance poses one of the biggest threats to human health. In 2017, the World Health Organisation published a list of 12 pathogenic bacteria that cannot be treated with currently available antibiotics [1]. The list includes certain strains of stomach ulcer and cancer causing *Helicobacter pylori*, pneumonia and meningitis causing *Haemophilus influenza* and several other deadly pathogens. The threats posed by drug resistance on current drug therapies is evident if one looks at the vanishing number of antimicrobial agents that have been developed over the past few decades. As shown in Figure 1.1, no novel antibiotic class has emerged from drug development projects since the 1980's.

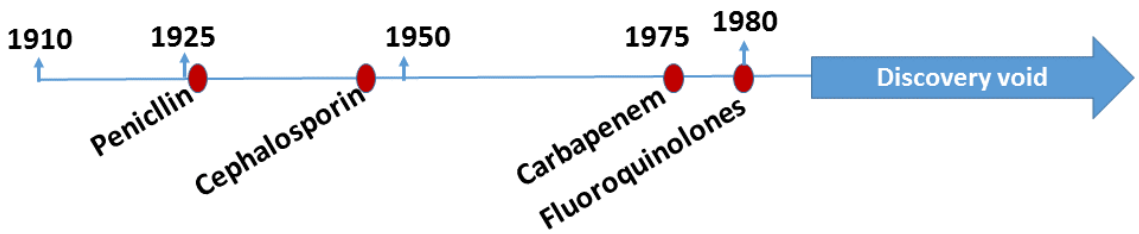

Fig. 1.1 A brief timeline of some of the major antibiotic discoveries followed by a discovery void.

Several factors are involved in the underlying mechanisms of drug resistance: the composition of cell walls [2], enzymatic modification or degradation of drug molecules [3], altered sensitivity of the targets via mutations [4] or conformational alterations [5], and extrusion of drug molecules [6]. The drug extrusion process is facilitated by the notoriously promiscuous multidrug transporters (MDTs). MDTs are integral membrane proteins and act as gateways for their substrates. These proteins, which perhaps evolved as housekeeping agents for the disposal of cellular metabolic waste, later also served to protect cells from external harmful chemicals. Such primordial function of transporter proteins is supported by their ubiquity. As of 2016, the Transporter Classification DataBase (TCBD) contains more than 10,000 non-redundant transport systems [7].

The overexpression of MDTs has led to ever increasing cases of drug-resistant pathogens [8] and chemotherapy-resistant tumour cells (overexpression of P-Glycoprotein [9] and/or ABCG2 [10]). The importance of MDTs is further accentuated by the fact that they are heavily expressed in human liver [11] and kidney [12] tissues where they affect drug pharmacokinetics and the redistribution of endogenous metabolites and xenobiotics. For example, cimetidine, a H2-blocker used to prevent and treat gastric ulcers, interacts with other co-administered drugs by competitively inhibiting a human multidrug transporter, hMATE1, during the final secretion step of drugs in the kidney [13]. The implications of MDTs in pharmacokinetics makes it crucial to consider drug-transporter interactions for developing better novel drug candidates and for such information to be a part of drug toxicity guidelines.

1.2 Multidrug transporters: they come in all shapes and sizes

On the basis of the energy dependence and phylogeny, MDTs, and solute transporters in general, have been classified into six different superfamilies [14]. These are: the ATP-binding cassette (**ABC**) superfamily, the major facilitator superfamily (**MFS**), the resistance/nodulation/division (**RND**) superfamily, the small multidrug resistance (**SMR**) family, the multidrug and toxic compound extrusion (**MATE**) family, and the recently added proteobacterial antimicrobial compound efflux (**PACE**) family [15]. The following table lists a few examples of each class of multidrug transporters together with their physiological and clinical relevance.

Table 1.1 Transporter proteins and their relevance

Family	Member proteins	Physiological/Clinical relevance
ABC	MDR1 (ABCB1)	Resistance to anticancer agents [16], [17]
	BCRP (ABCG2)	Gene mutation causes cystic fibrosis [18]
MFS	RFC (SLC19A1)	Folate transport, methotrexate resistance [19]
	Glucose transporters	Type-2 diabetes [20], implicated in cancer [21]
RND	BepDE and BepFG	Antibiotic resistance in *Brucella suis* [22]
SMR	EmrE	Antibiotic resistance [23]
MATE	NorM, YdhE, DinF	Antibiotic resistance [24]
	Human MATE1	Drug-drug interactions & pharmacokinetics [12]
PACE	AceI	Resistance to biocides [15]

1.3 The energetics of transport

The transport process can either be passive or active. Passive transport occurs in the direction of a concentration gradient of the substrate and requires no other energy source. In contrast, the active transport of a substrate requires energy derived from biochemical reactions such as ATP-hydrolysis, ion gradients or, in the case of a charged substrate, electrical potential difference. With access to an energy source, cellular transport systems can transport a substrate against its concentration gradient. The ion gradient dependent secondary active transport is called symport or co-transport when both the driving ion and driven ion or molecule move in the same direction, and antiport or exchange when the driving ion and driven ion or molecule move in the opposite directions.

The different modes of transport are summarised in Figure 1.2.

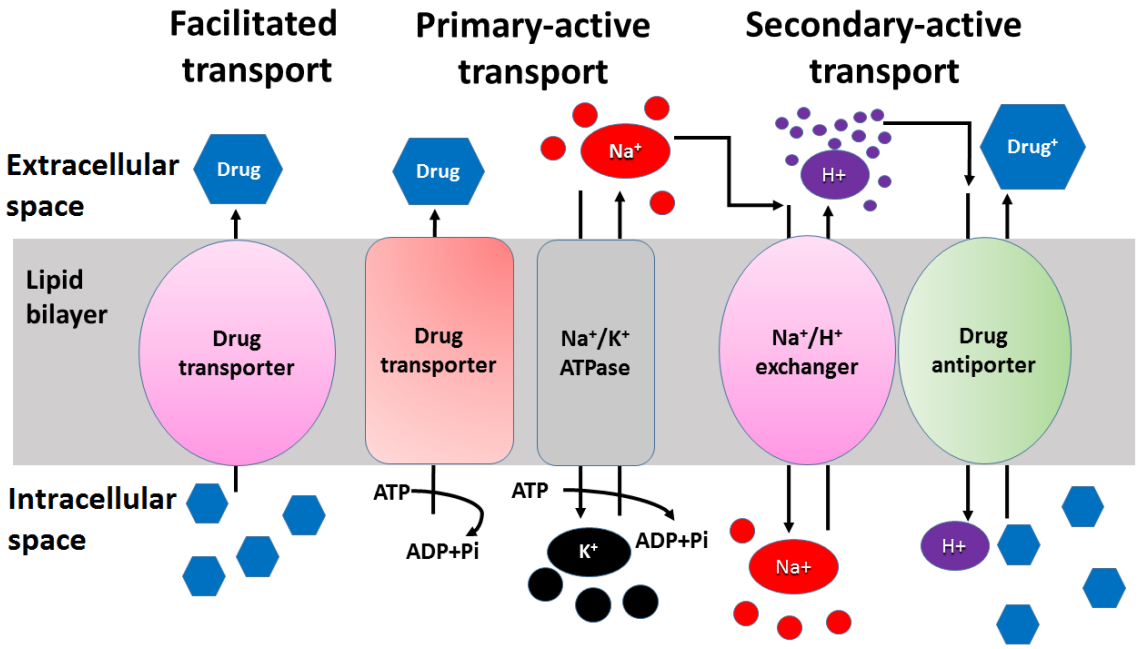

Fig. 1.2 Schematic of different membrane transport systems. Facilitated transporters allow passage of drugs down their concentration gradient. Primary-active transporters, also known as ABC transporters, utilise ATP-hydrolysis to transport drugs against their concentration gradient. Another type of ATP-hydrolysing transporters can establish ion-gradients which in turn can be utilised by ion-exchangers to establish ion-gradients of a different type, or by secondary-active drug transporters to transport drugs against their concentration gradients.

The separation of ions by transporters has two consequences: a) formation of a chemical ion gradient and, b) an electrical potential difference. Collectively, these are known as the electrochemical ion gradient. The interiors of metabolically active cells are alkaline and negatively charged relative to the exterior, therefore the total energy conserved by a membrane is the sum of the proton gradient (ΔpH) and the electrical potential difference ($\Delta\psi$).

For protons, the proton motive force = Electrical potential difference + proton gradient

The corresponding formula is: Δp (in mV) = $\Delta\psi$ - 59.1$\times\Delta$pH

The Gibbs energy change when 1 mole of a monocation X^+ is transported down an electric potential of $\Delta\psi$ mV from a concentration of $[X^+]_A$ to $[X^+]_B$ is given by:

Δ G(kJmol$^-$) = -F$\Delta\psi$+2.3RT$\log_{10}([X^+]_A/[X^+]_B)$

where R is the gas constant and T is the absolute temperature.

For protons: $\Delta\mu_{H+}$ = -F$\Delta\psi$ - 2.3RT$\times\Delta$pH

The term proton motive force (pmf or Δp) is defined in units of voltage where:

Δp (mV) = -($\Delta\mu_{H+}$)/F

Hence: $\Delta p = \Delta\psi$ - 2.3RT$\times$ ΔpH

Substituting values for R and T at room temperature: $\Delta p = \Delta\psi$ - 59$\times$ ΔpH

The active export of Na^+ across the membrane to the exterior of the cell generates the equivalent sodium motive force (ΔpNa). Hence, in principle, a secondary-active transport system has two sources of energy: the first of which is the concentration gradient of ions, and the second is the potential difference.

1.3.1 Bio-energetic consequences of different stoichiometries: is more always better?

With the emergence of cells that maintain ion gradients and voltage difference across the membrane, cellular transport systems might have adapted to utilise the components of such energy reservoirs differently. An antiporter with 1:1 stoichiometry does not perturb the membrane potential and hence there will be no build-up of a by-product. In contrast, an antiporter with a different stoichiometry will lead to a build-up of a net charge that, depending on the nature of charged species, would enhance or inhibit the transport. For positively charged species X and Y, the schematic of electroneutral and electrogenic transports can be summarised as following:

Electroneutral: $X^+_{in}/Y^+_{out} \leftrightarrow X^+_{out}/Y^+_{in}$

Electrogenic: X^+_{in}/Y^+_{out} & $Z^+_{out} \leftrightarrow X^+_{out}/Y^+_{in}$ & $Z^+_{in} + \Delta\psi$

For secondary active transporters, a net incoming positive charge should be favoured due to the negative nature of the cytosol. Hence a transporter that imports more than one cation while exporting one cationic drug should be more efficient than a transporter with a simple 1:1 stoichiometry (discounting the osmotic effects). Furthermore, a transport system with more than one incoming ion, will have more choice in terms of what type of ions can be used. For instance, a system capable of importing one H^+ and one Na^+ at once should be more successful as it would function in the absence of either ion gradient. These are purely hypothetical speculations and the biochemical feasibility is a concern of a different kind. It is, however, also important to consider that there is a distinction between binding stoichiometry and transport stoichiometry. Amongst sodium-phosphate cotransporters, the subtype NaPi-IIa/b can translocate three Na^+ at once while NaPi-IIc only transports two Na^+ despite binding three Na^+ [25]. The possibility of Na^+-binding site(s) in pfMATE , an H^+-coupled MATE transporter from *Pyrococcus furiosus*, has been speculated [26], but no experimental evidence exists.

1.4 Functionally diverse yet structurally similar MATE transporters

The work presented in this thesis investigates members of the secondary-active MATE transporters. Hence the rest of this chapter explores MATE transporters in detail. The structural aspect, ion-coupling mechanisms, and modes of ion binding are discussed further. MATE transporters share 40% similar residues and hence have a similar architecture. MATE transporters are divided into two classes: the Na^+-coupled MATEs and the H^+-coupled MATEs. The first bacterial MATE transporter to be characterized was the Na^+-coupled NorM of *Vibrio parahaemolyticus* [27]. Subsequently, NorM orthologs from *Neisseria gonorrhoeae* [28], and *Vibrio cholerae* [29] were also characterised. The human genome harbours H^+-coupled MATE transporters that are primarily expressed in the kidney and liver where they facilitate the final step in the excretion of organic compounds [30] including compounds of high clinical importance such as metformin, a fist line medication used for the treatment of type 2 diabetes [31]. Besides affecting drug pharmacokinetics, MATE transporters are also involved in pathophysiology. For instance, the *Escherichia coli* MATE transporter CIbM transports colibactin, a neoplastic genotoxin, and is also involved in the activation of colibactin [32].

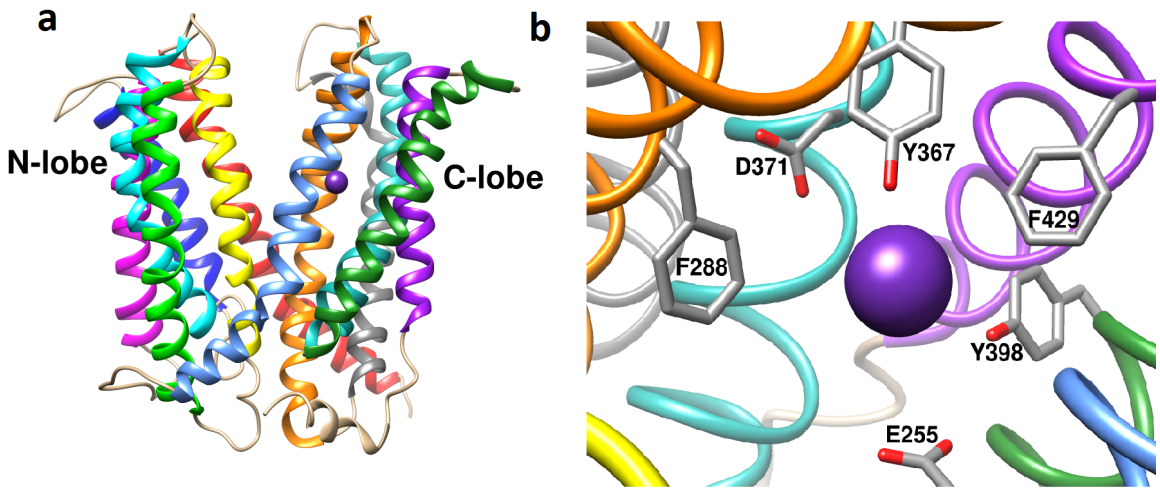

Fig. 1.3 **a,** The crystal structure of NorM-VC in the outward-open state (PDB IDs 3MKT and 3MKU). The protein has twelve transmembrane helices which cluster into two distinct lobes. **b**, the Rb^+-binding site in the C-lobe is composed of amino acid side-chains of differing chemical natures. Rb^+ shown as purple ball.

Owing to their relatively late discovery, less is known about MATE transporters. The first structural insight into them came when the NorM protein from *V. cholerae* (NorM-VC) was crystallised in an outward-open conformation with rubidium ion, and caesium ion, both of which are more electron-dense analogs of sodium ion [29]. As shown in Fig. 1.3, the transporter showed a structural organisation different from MFS family proteins; 12 transmembrane helices (TMHs) organise in two distinct bundles (referred to as the N- and C-lobe) and show a pseudo-two-fold symmetry. The cation-binding cavity is composed of residues from TMH7, TMH8, and TMH10–TMH12.

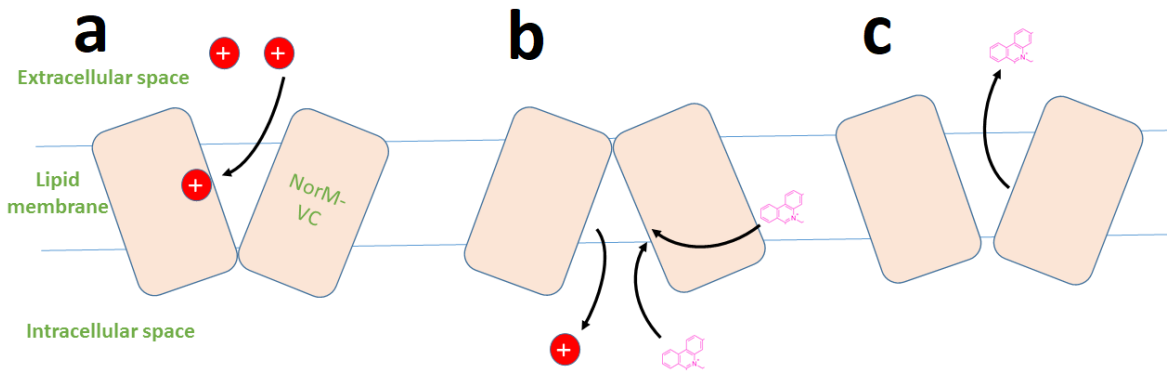

Fig. 1.4 A two-state transport model proposed to explain the drug/cation antiport in NorM-VC. Na^+ shown as red-crossed circle, with the drug shown as pink molecule. **a**, binding of sodium to NorM-VC in the outward-open state causes the switch to the inward-open state as shown in **b**, the sodium is released as the drug binding takes place. **c**, the transporter switches back to the outward-open state and the drug is relased.

Based on the crystal structural, a simple two-state transport model was proposed in which the cation binds to the outward-open state (Figure 1.4a), which leads to switching to the inward-open state. The cation is released, followed by the binding of a drug molecule (Figure 1.4b). This, in turn, leads to return to outward-open state (Figure 1.4c). Drug release resets the transporter for another cycle. The existence of an inward-open conformation, which brings the residues located near the extracellular termini of the helices closer together, has been experimentally demonstrated [33] and could corroborate a two-state model for MATE transporters. However, the existence of relatively short-lived intermediate states can not be excluded.

This minimal model suffers from a few drawbacks. For a monovalent cationic drug, this model should lead to an electroneutral transport reaction. But it has been shown that NorM-VC can transport ethidium in a $\Delta\psi$-dependent manner [34]. Furthermore, this model does not allocate any role to the residue D36 (Figure 1.5), which is ubiquitously conserved in the NorM family of transporters and is likely to have a role in transport. However, in the crystal structure, D36 is located distal to the metal ion biding site and perhaps that is why no functional relevance was allocated to it in this transport model.

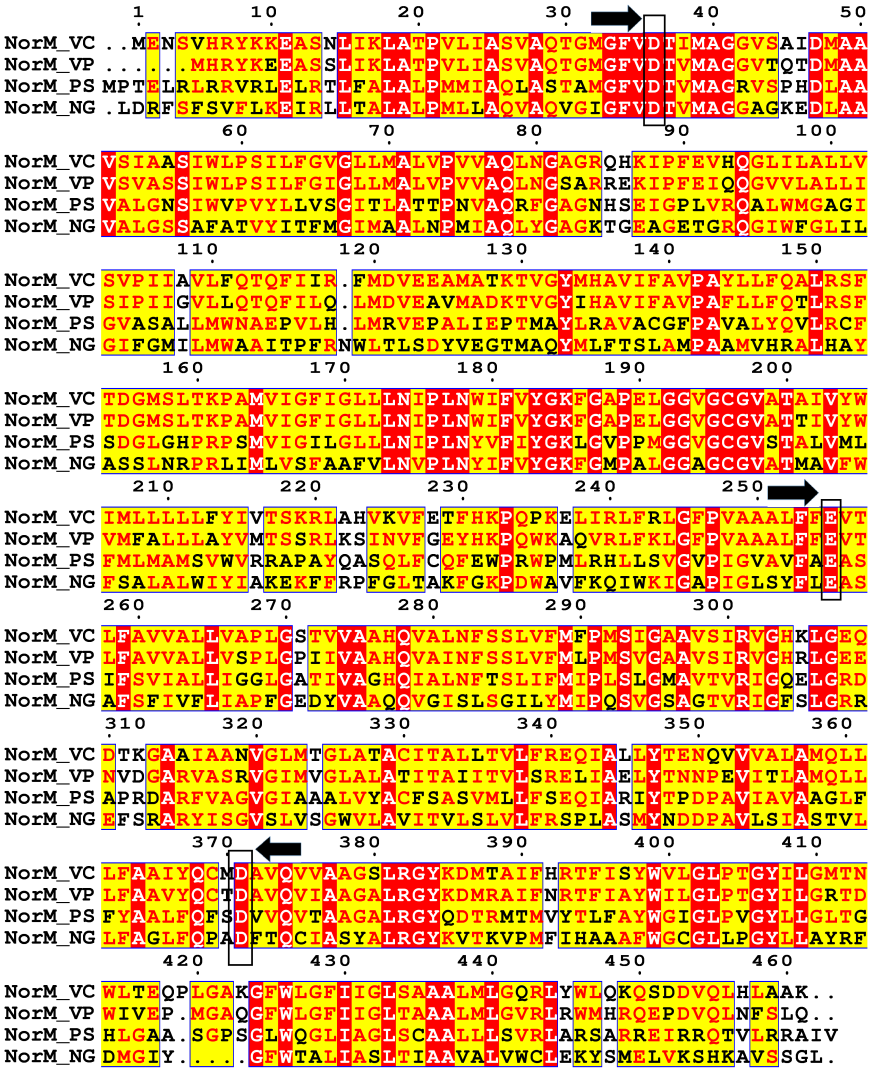

Fig. 1.5 Multiple sequence alignment of different NorM proteins. With the exception of NorM-PS, all NorM proteins shown here have been reported to couple to Na^+. Identities are indicated in red boxes, conserved residues shown in red and the rest shown in black. The thick black arrows show the conserved carboxylates. the alignment was performed with ClustalW and the figure was generated with ESPript 3.0.

Crystal structures for six different MATE transporters have been published to date : NorM-VC [29], NorM-NG [35], pfMATE [36], DinF-BH [37], CIbM [32] and eukaryotic AtDTX14 [38] . With the exception of DinF, which was crystallised in an occluded state, all MATE transporters have been crystallised only in outward-open states. This leaves a big gap in the current knowledge on the role of the inward-open conformation and any other possible intermediate states.

1.4.1 Drug-cation antiport and Na^+ binding in NorM proteins

H^+- and Na^+ binding in NorM-VC

A paradigm shift in MATE transport biology was brought about when NorM-VC was shown to be coupled to H^+ and Na^+ simultaneously [34]. NorM-VC showed improved ethidium transport in the presence of sodium and proton motive forces (termed ΔpNa and Δp hereafter) and the contributions from ΔpNa and Δp were found to be additive. Ethidium transport by NorM-VC was found to be dependent on $\Delta\psi$. Since ethidium bears a single positive charge over a large range of pH values, the dependence on $\Delta\psi$ suggests transport of two cations in exchange for one ethidium molecule.

The D36-region was suspected to be involved in Na^+-binding as the N174A mutation (located in close proximity to D36) leads to a 1200-fold drop in the apparent affinity for Na^+ [34]. A 5-fold decrease in apparent affinity for Na^+ was observed for the F288A mutation (located in the vicinity of E255 and D371), indicating Na^+ binding to this location as suggested by the crystal structure. Furthermore, D371 was shown to be involved in proton binding in biochemical studies [34]. In molecular simulation studies, the protonation of D371 was shown to be an important step for the binding of Na^+ to NorM-VC [39]. Although mutations at D371 were shown to cause loss of Cs^+-binding in NorM-VC crystals [29], the D371N mutant still exhibited Na^+-dependent ethidium transport with unaltered apparent affinity for $Na^+$and ethidium in this reaction. Therefore, D371 appears to directly interact with H^+ but not with Na^+ in biochemical experiments. Or, it could be possible that in order to bind Na^+, only one carbonyl oxygen is required which is still available in the D371N mutant.

Unlike H^+-binding to acidic residues, which is a simpler chemical event, Na^+-binding to protein requires coordination by several side chains or main chain atoms. For example, in the crystal structure of NorM-VC, the binding of Rb^+ or Cs^+ appears to be stabilised by ionic interactions provided by E255 and D371, and also by polar and pi-cationic interactions provided by Y367 and Y398. The residues D36, in the N-lobe, and E255 and D371, in the C-lobe, have been shown to be important for the transport reaction as mutating these leads to either partial or complete loss of transport activity [34]. Substitution of the D371 side chain

by alanine or asparagine disrupts metal ion binding [29], highlighting the importance of an ionisable carboxylate group at this position. However, in the crystal structures, no Na^+ was bound near D36.

In molecular simulation studies, protonation of $D371^{NorM\text{-}VC}$ was found to lead to binding of Na^+ [39]. Another study found that the V-shaped outward-facing conformation of NorM-VC (as seen in the crystal structure) is unstable under physiological conditions [40]. Instead, the protein assumes a conformation with semi-parallel lobes that form an internal cavity open to the external medium via D36. In this conformation, Na^+ interacts with D36 in the N-lobe first, before finally arriving at the E255/D373 dyad in the C-lobe. Na^+ could bind at the E255/D373 dyad in two distinct ways – either by interacting with both residues simultaneously or with one of the two carboxylates. This study corroborated the existence of a conformation different from the outward facing V-shaped state [41] and also confirmed the biochemical data pointing to importance of D36-region in Na^+-binding.

Despite all of the above-mentioned studies, it remains unclear how NorM-VC utilises Na^+ in the transport reaction and what stoichiometry is followed. Also, it remains yet to be investigated how H^+ fits in this reaction. To complicate the situation further, NorM from *Pseudomonas stutzeri* (NorM-PS) has been shown to be exclusively H^+-coupled [42]. Despite having 42% identical residues with additional 24% semi-conserved residues, NorM-VC and NorM-PS appear to have different ion binding preferences. This is surprising given that the three residues predicted to play key roles in ion-coupling in NorM-VC, namely D36, E255 and D371, are conserved in NorM-PS (Figure 1.5). These differences in function raise interesting questions about the cation-binding behaviour in MATE transporters.

Distinct modes of Na^+-binding in different MATE transporters

Similar to observations for NorM-VC, the Cs^+ in NorM-NG (PDB ID 4HUL) makes direct contact with E261 (symmetrical bidentate hence coordination number=2) and Y294 (Pi-cation interactions). Although D377 is too distant (>7 Å) to interact, a potential donor group might be S290 that is 5 Å away.

In contrast to NorM-NG, the Rb^+ in the ClbM crystal structure makes no close contact with any of the nearby amino acid side-chains. Whilst the aromatic ring of Y277 is a potential candidate for pi-cation interactions, the orientation of the F292 ring is unfavourable for the interaction with the bound Rb^+. Overall, the number of interactions evident in NorM-NG and ClbM structure is less than the usually required coordination number of 5-6 for Na^+. It is possible that a structural water molecule mediates interaction between the metal cations and amino acid side chains in these transporters. Another possibility is that the substrate also provides a coordinating group for sodium-binding. Such a case is discussed in the next section.

1.4.2 Substrate binding and its correlation with metal-ion binding in MATE transporters

According to the antiport model suggested for NorM-VC [29], drug binding occurs after the metal cation has been released. This suggests that the binding of Na^+ and the substrate would be mutually exclusive in a biochemical ping-pong mechanism. For NorM-VC, this model is discordant with the observation that the binding of ethidium monoazide, a fluorescent analogue of ethidium that binds covalently, was shown to be enhanced in the presence of Na^+ [34]. Similarly, another study showed that other substrates, but not Na^+, compete with Ruboxyl binding to purified NorM-VC [43].

The existence of a state where Na^+ and the substrate could bind simultaneously is also suggested for NorM-NG [35] where the Cs^+-binding cavity is distal to the tetraphenylphosphonium (TPP) binding site. The drug-bound conformation is not very different from the Cs^+-bound conformation and upon superimposing the two conformations, the Cs^+ ion and TPP do not sterically hinder; instead, under physiological conditions they can be at an optimal distance to interact with each other. Alternatively, they could interact with each other via a water molecular. It is reasonable to suspect that the aromatic phenyl rings of TPP might be one of the coordinating partners. The possibility of direct interactions between the drug (ethidium) molecule and Na^+ in NorM-VC transport cycle cannot be ruled out, either.

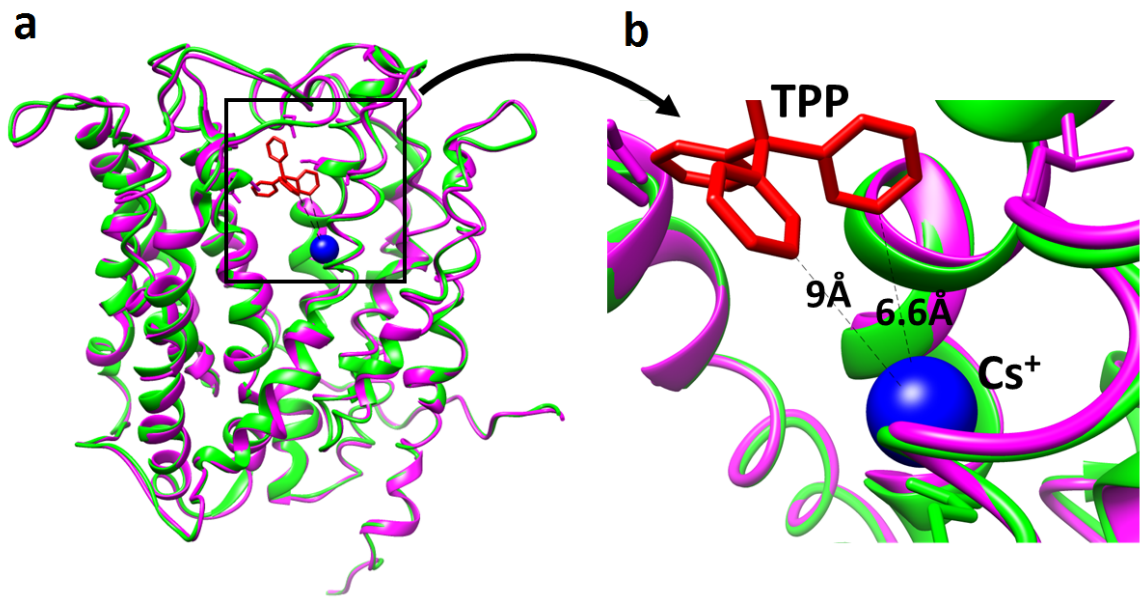

Fig. 1.6 **a**, The substrate and Cs^+ occupy two distant sites in NorM-NG. TPP^+ (shown in red) -bound conformation shown as purple ribbons, Cs^+ (shown in blue)-bound conformation shown as green ribbons. **b**,The distances between the approaching rings of TPP and Cs^+ are shown. The two structures (PDB ID: 4HUL and 4HUK) were superimposed using UCSF Chimera.

In summary, despite having conserved carboxylates, bacterial MATEs probably coordinate metal-ions by different mechanisms. It is also noteworthy that crystal structures are generated under non-native conditions where crystal contacts might influence the protein conformation and subsequently the intra-molecular interactions in the protein.

1.5 H$^+$-coupled MATE transporters

H$^+$-coupled MATE transporters pfMATE and DinF-BH provide a useful contrast to Na$^+$-coupled MATE transporters - both in terms of primary structure and proposed mechanisms of ion-coupling. These proteins do not contain equivalent carboxylates of E255$^{\text{NorM-VC}}$ and D371$^{\text{NorM-VC}}$ in the C-lobe. Instead, in pfMATE, D41 (the counterpart of D36$^{\text{NorM-VC}}$) is complemented by another carboxylate, D184, situated in the N-lobe. The same is true for DinF-BH which contains D40 and D184 in the N-lobe.

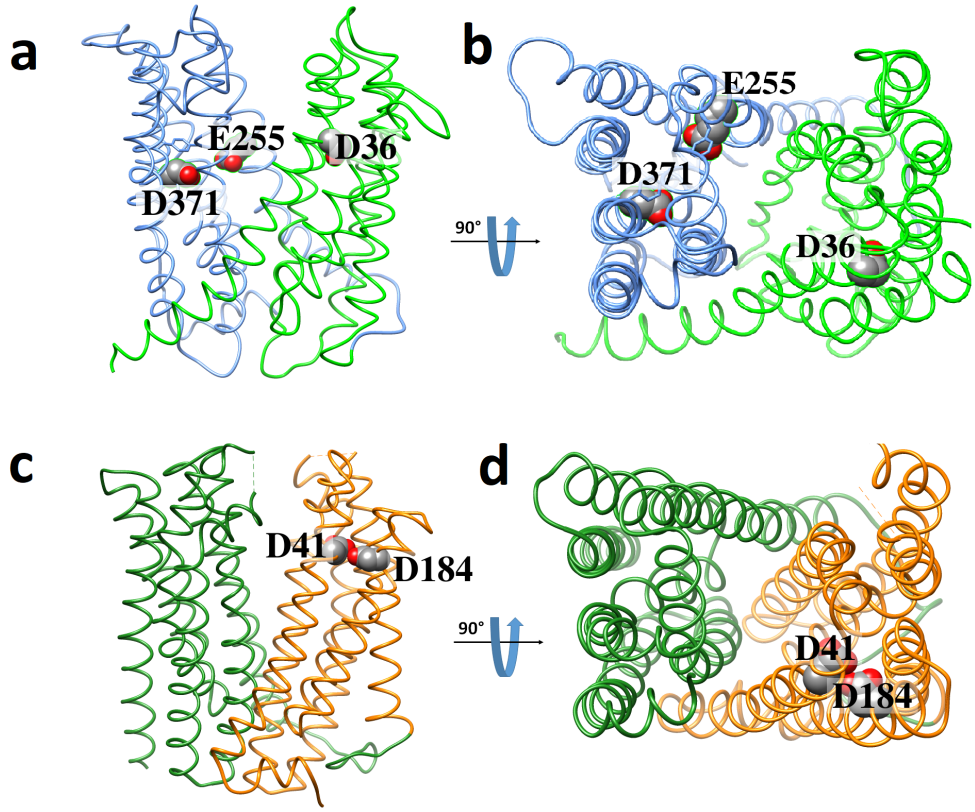

Fig. 1.7 A cartoon representation of NorM-VC (**a** and **b**) and pfMATE (**c** and **d**) crystal structures depicting the positioning of the catalytic carboxylates. H$^+$-coupled pfMATE has two spatially-adjacent carboxylates in the N-lobe that take part in H$^+$-binding, whereas NorM-VC has only one carboxylate in this position but has two vicinal carboxylates in the C-lobe. PDB IDs: 3MKU (NorM-VC) and 3VVN (pfMATE).

In the crystal structure, pfMATE, like most other MATE transporters, is seen in an outward-open conformation but the pH-dependent conformational changes in TMH1 are strikingly different from those seen for any of the previously reported MATE structures [36]. At neutral pH, TMH1 has a straight conformation in which either $D41^{pfMATE}$ or $D184^{pfMATE}$ is protonated. But at pH 6.0, the rearrangement of the H-bond network causes TMH1 to assume a bent conformation in which both $D41^{pfMATE}$ and $D184^{pfMATE}$ are occluded in a water-inaccessible cavity and may both be protonated via sharing the same proton. The TMH1 seems to bend at P26 and G30 (significant torsional changes take place at G30). Following these findings in pfMATE, similar observations were made in eukaryotic H^+-coupled MATE transporters as discussed in the next section.

1.6 MATE transporters in eukaryotes

The crystal structure of a eukaryotic MATE transporter from *Arabidopsis thaliana* (AtDTX14) provided new insights into the mechanism of eukaryotic MATE transporters [38]. With 32% sequence identity with the human MATE transporter hMATE1, the mechanism is quite relevant and can be extrapolated to explore hMATE1.

1.6.1 Common structural elements in bacterial and eukaryotic MATE transporters

An interesting pattern emerges upon comparing the positioning of catalytic carboxylates in bacterial and eukaryotic MATE transporters. AtDTX14 does not have an equivalent carboxylate in the N-lobe of NorM proteins. Instead it has $E273^{hMATE1}$ and $E389^{hMATE1}$in the C-lobe. The positioning of carboxylates here is opposite to pfMATE and DinF-BH which lack active site carboxylates in the C-lobe but have two vicinal carboxylates in the N-lobe. The C-lobe carboxylates in AtDTX14 are very close to each other, forming a H-bond, brought about by the low pH of the crystallisation medium. Furthermore, the structural changes in the TMH7 are brought about by a kink introduced at P257 which is part of a GXP motif. This GXP motif is conserved in NorM and DinF family proteins and is replaced by AXP in hMATE1 and hMATE2.

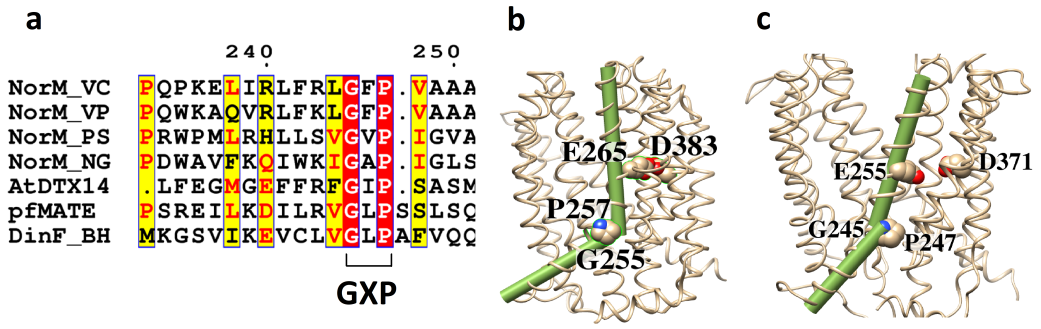

Fig. 1.8 **a**, Multiple sequence alignment of MATE family members showing the conserved GXP motif in the TMH7 that connects N-lobe with the C-lobe. Identities shown in red boxes, semi conserved resideus shown in red, and the rest shown in black. **b**, The TMH7 in eukaryotic MATE AtDTX14 (PDB ID: 5Y5O) bends at G255 (part of the GXP motif). This bending is brought about by protonation of E265/D383 dyad. **c**, The bending of TMH7 in NorM-VC (PDB ID: 3MKU) brings E255 and D371 closer and orients E255 to face D371.

However, the indispensability of these two amino acids in the GXP motif is debatable. In this regard, the observations made for pfMATE are interesting. pfMATE uses a PXXXG motif to induce the kink in TMH1. Upon comparing the straight and bent conformations of pfMATE, the kink is seen at the residues succeeding G30, and the conformation around P26 remains the same. Yet, mutating the P26 (and not G30) causes disruption of drug/H^+ antiport [36]. Perhaps in the absence of a 'flexible' residue, the torsion transmits over a larger distance along the helix which still allows the transport related dynamics to take place. Anyhow, the possibility that these bi-symmetrical transporters probably resulted via a gene duplication event cannot escape one's notice. The mirroring of $TMH1^{pfMATE}$ by $TMH7^{AtDTx14}$ further supports this hypothesis.

This thesis is presented in 7 chapters. A brief description of the contents of these chapters follows here.

Chapter 1 introduces MATE transporters and provides a summary of the current views on their mechanisms of transport. The chapter also summarizes the structural information available for MATE transport proteins.

Chapter 2 provides an overview of the methods and materials used to conduct this research. Relevant molecular biology and biochemical techniques are described in detail.

Chapter 3, the first of four results chapters, details fundamental differences between the ion requirements of NorM-VC and NorM-PS. The chapter gives an account of the properties of chimeric proteins that I prepared using NorM-VC and NorM-PS. It also provides evidence for cooperativity between the two transmembrane helical bundles (lobes), which allows Na^+ transport by NorM-VC.

Chapter 4 demonstrates a relationship between proton and sodium ion availability, and the observed ion-dependence of NorM-VC. Evidence for a correlation between pH and Na^+ coupling, and correlation between pH and substrate binding is also provided.

Chapter 5 describes the rational design of NorM-PS and NorM-VC mutants with the objective of achieving altered ion specificity in the drug transport process. The structure-function relationships of the two transporters are discussed.

Chapter 6 describes a novel pathway for Na^+ movement through NorM-VC. Biochemical experimental evidence is presented which confirm the pathway. The prediction of this pathway explains the observations made in chapter 3.

In the final **Chapter 7**, a transport model is proposed to explain my observations and those in published studies. The model is discussed with respect to the findings presented by other studies. The thesis finishes with a discussion of further lines of research.

1.7 Scope of this thesis

The work presented here focuses on the ion-coupled drug transport by NorM-VC and NorM-PS. The basic premise of the study is the difference in the ion-coupling in transport reactions by otherwise highly homologous proteins. A bioenergetics aspect, supplemented with structural relevance, is provided. The work begins by laying down some fundamental differences in the energetics of the two transporters and concludes with an experimentally confirmed novel transport mechanism for NorM-VC. The work here deals with some fundamental questions relating to transport across energy-conserving membranes and, at the same time, bears high clinical significance. Such knowledge will add to the current understanding of transport biology and has the potential to help address the issue of drug resistance.

Chapter 2

Methods and Materials

2.1 Risk assessment and safety procedures

The laboratory protocols were risk assessed as per Department of Pharmacology safety guidelines and local rules. A chemical safety course was taken prior to the lab work. Non-virulent *E. coli* strain DH5α was used for molecular biology purposes. For expression of proteins, *L. lactis* (subsp. *cremoris*) was used. *L. Lactis* is a food grade bacterium and is safe to use at the lowest biosafety class 1 containment level. Ethidium bromide was used with caution while avoiding contact with body parts. Ethidium bromide containing waste was decanted into a container with charcoal bags, which were disposed of by incineration. 2-4, dinitrophenol (DNP) was weighed wearing personal protection equipment, and waste was collected for disposal by the Safety Office, University of Cambridge. Protocols involving use of high-speed centrifuges, UV-based gel visualisation units and liquid nitrogen tanks were carried out after risk assessment and safety inductions.

2.2 Bacterial strains, media and growth conditions

The drug-hypersensitive *L. lactis* Δ*lmrA* Δ*lmrCD* [44], [45] was used as the host for protein expression and transport studies. It contains expression vector pNZ8048 derived plasmids [45] with a chloramphenicol resistance marker gene, nisin A-inducible Pnis promoter and N-terminally 6× His-tagged proteins of interest. The same strain with empty control vector (pNZ8048) was used as a negative control. The cells were grown in M17 broth supplemented with 25 mM glucose containing 5 μg/mL chloramphenicol at 30°C in all experiments unless stated otherwise. Glycerol stocks were streaked on M17-agar plates supplemented with 25 mM glucose containing 5 μg/mL chloramphenicol, and incubated for 24-36 hours at 30°C.

Single colonies were grown overnight and stored in 25% glycerol at -80°C. For molecular biology purposes, *E. coli* DH5α cells were used. The cells were grown in LB medium supplemented with 100 μg/ml carbenicillin when required.

For preparing competent *E. coli* cells, cells were grown to an O.D.$_{600nm}$ (optical density at 600 nm) of 0.35-0.4 and washed twice with chilled 100 mM $CaCl_2$. The cells were kept on ice prior to use. The plasmid DNA (2-5 μL of ligation product containing 5 ng total DNA) was added to 50 μL aliquots of competent cells and the cells were further kept on ice for 30 minutes. The cells were heat shocked by incubating cells at 42°C for 45 seconds. The cells were incubated on ice for 2-5 minutes and 1 mL of LB media was given to induce recovery. The cells were then incubated at 37°C with constant shaking at 200 rpm for an hour after which the cells were collected by centrifugation. Finally, the pellet was resuspended in LB medium and plated on carbenicillin containing LB-agar. The plates were incubated at 37°C overnight.

Electrocompetent *L. lactis* cells were prepared as described previously [46]. The cells were grown in an osmotically-stabilised M17 medium containing 0.5 M sucrose, 1% glycine and 25 mM glucose. The presence of glycine ensures growth of single-celled *L. lactis* population. An overgrown culture was diluted 100-fold in fresh medium and incubated at 30°C to an O.D.$_{660nm}$ of 0.4. The cells were then washed twice using wash solution containing 0.5 M sucrose and 10% glycerol. The cells were snap-frozen and stored at -80°C.

2.3 Cloning, subcloning and mutagenesis

2.3.1 Cloning the *norM-PS* gene into pET19b vector

All the molecular biology experiments were performed on *E. coli* vector pET19b prior to subcloning into *L. lactis* pNZ vector. The reason behind not using pNZ vectors directly was that in the experiments, parental pNZ vectors did not get digested by DpNI. DpNI digestion is a critical step for separating parental plasmid DNA from mutated plasmid DNA after PCR reaction.

The molecular biology enzymes used, were ordered from ThermoScientific (unless stated otherwise) and the reactions were carried out as per the product manual. All restriction enzymes were of the FastDigest category and required the same universal buffer. The DNA was eluted in nuclease-free water and stored at -20°C until use.

The *norM-PS* sequence (GenBank ID EHY79494.1) was codon-optimised for *L. lactis* subspecies *cremoris* using the online codon optimisation tool from Integrated DNA Technology (IDT). The NdeI and XhoI restriction sites were added on the ends and the resulting

sequence was synthesised by IDT. 250 ng of the synthesised gene was digested using NdeI and XhoI restriction enzymes, and spin column purified using the Thermo Scientific GeneJET Gel Extraction Kit. The DNA concentration was determined using UV absorbance at 260 nm.

The pET19b vector harbouring the *norM-VC* gene [29] was digested with NdeI and XhoI restriction enzymes and was agarose-gel purified. The *norM-PS* gene insert was ligated as an NdeI and XhoI fragment into the digested vector. The ligated vector was used to transform chemically competent *E. coli* DH5α cells and transformed cells were selected by growing overnight on 100 μg/ml carbenicillin containing LB-agar plates at 37°C. Single colonies were picked, grown overnight in LB medium supplemented with carbenicillin and subsequently the plasmid DNA was purified. Prior to subcloning into pNZ vector, all genes were sequenced by using the tube sequencing service provided by Eurofins Genomics.

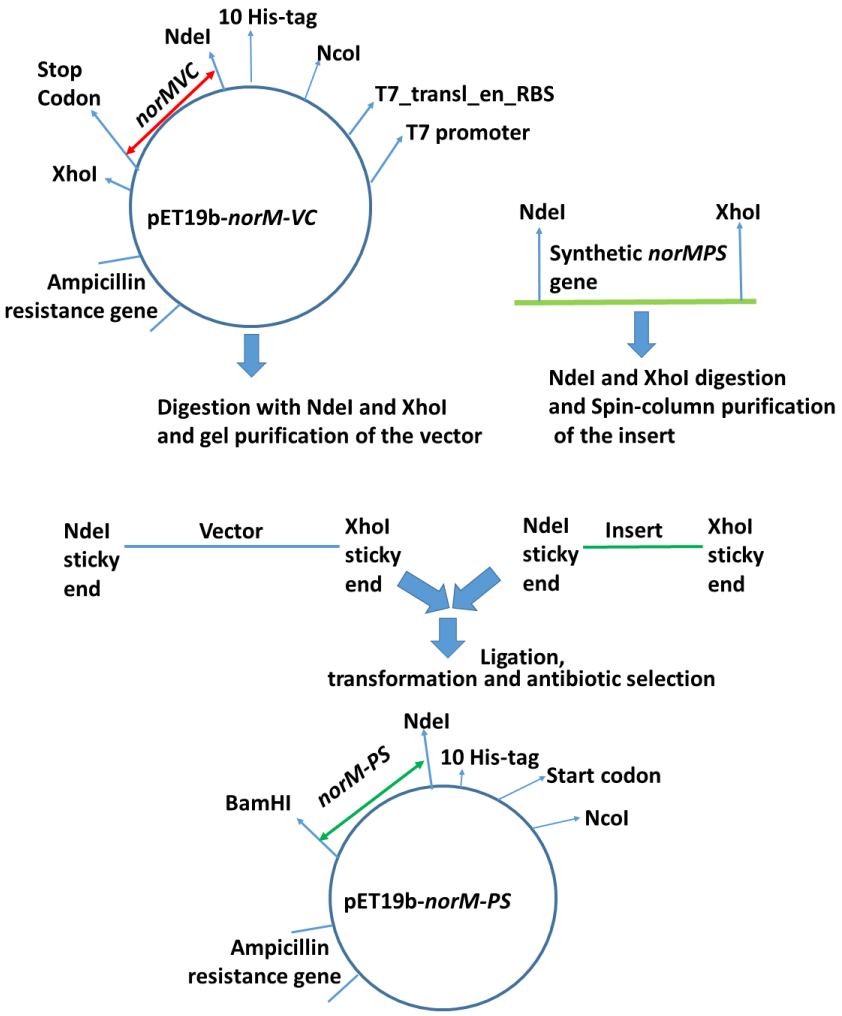

Fig. 2.1 The molecular biology workflow for cloning the synthetic *norM-PS* gene into pET19b vector.

2.3.2 Subcloning the *norM-PS* gene into pNZ vector

The pET19b-*norMPS* vector was digested with NcoI and BamHI and the released insert was agarose gel purified. The insert was ligated into pNZ-NorM-VC which had been digested with the same enzymes.

The ligation product was used to transform electrocompetent *L. lactis* cells. The electrocompetent cells were mixed with plasmid DNA and electroporated using a MicroPulser™ electroporater from BioRad. The pulse was given using the preset conditions EC3 3.00 kV, single pulse, 0.2 cm cuvette. After the pulse, an ms value of 5.4-6.0 was achieved. The cells were quickly mixed with recovery buffer (M17 supplemented with 0.5 M sucrose, 25 mM glucose, 20 mM $MgCl_2$ and 2 mM $CaCl_2$) and kept on ice for 10 minutes followed

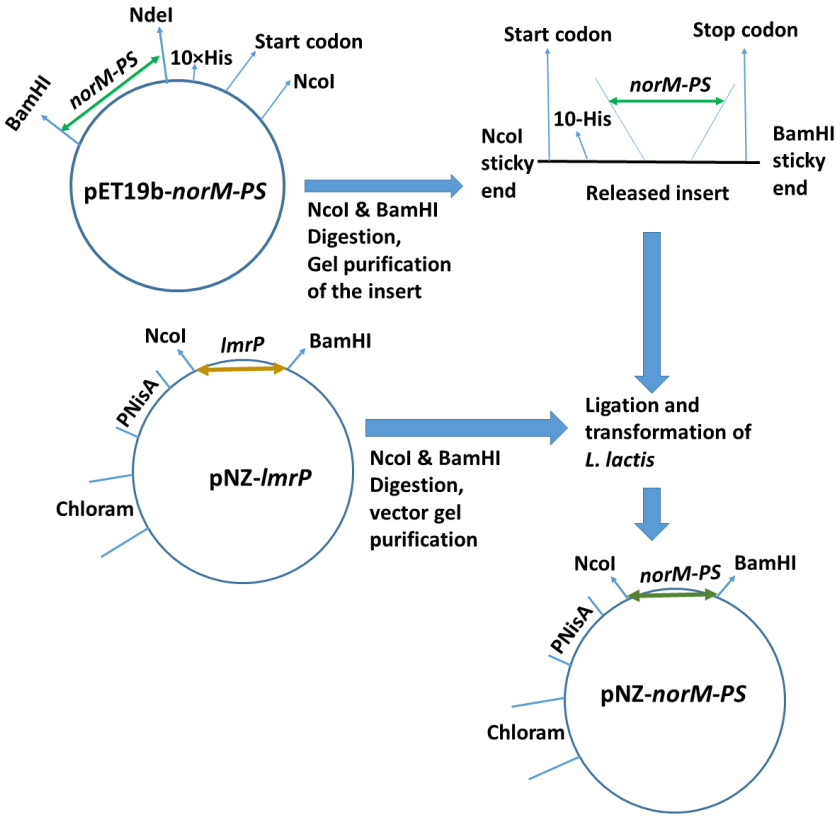

Fig. 2.2 The molecular biology workflow for cloning the synthetic *norM-PS* gene into pET19b vector and the subcloning into pNZ vector.

by incubation at 30°C for 2 hours. The cells were centrifuged and the resulting pellet was resuspended in 100 μL of recovery buffer and plated on M17-agar plates containing 0.5 M sucrose, 25 mM glucose and 5 μg/ml chloramphenicol. After incubation at 30°C for 36-48 hours, single colonies were picked and grown overnight for plasmid isolation.

2.4 Site directed mutagenesis

For the introduction of point mutations in *norM* genes, the QuikChange site-directed mutagenesis method was used as per manufacturer's instructions. Alternatively, the method described here [47] was also used in cases where the QuikChange method was not efficient due to primer-dimer formation. This method, colloquially referred to as the Round-the-Horn method, utilises two non-overlapping primers, one of which contains the desired mutation at the 5' end (Figure 2.3).

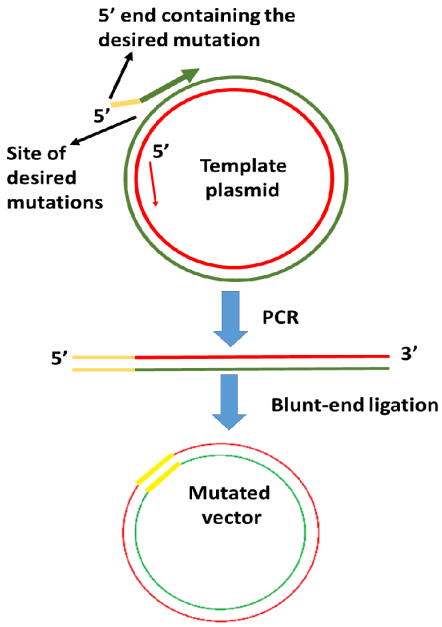

Fig. 2.3 The *Round-the-horn* (RTH) method of site-directed mutagenesis. In contrast to the QuikChange method, this method requires phosphorylation of the primers and an additional ligation step but due to short length (∼20 bases) of primers, the annealing temperature of the primers can be regulated more easily. Also, as the mutagentic primers contain the mutations at the 5' end, the annealing is better controlled. RTH also allows introduction of multiple subsequent mutations in one PCR reaction.

The primers were designed to have a melting temperature of 60°C and were phosphorylated using polynucleotide kinase (PNK) as per product manual. The phosphorylated primers were directly used in the mutagenic PCR reactions. A typical 50 μl PCR reaction consisted of 1X HF buffer (provided with the DNA polymerase kit), 0.2 mM dNTPs, 10 μM forward and reverse primer, 10 ng plasmid DNA template and 1 unit of Phusion DNA polymerase. The PCR cycling parameters were 98°C for 1 min, (98°C for 15 sec, 55°C for 30 sec, 72°C for 30 sec/kb) × 20-25 cycles, 72°C for 5 minutes. The amplified product was detected using agarose gel electrophoresis. After PCR amplification, parental DNA was digested by adding 1 μL of FastDigest DpnI to 20 μL of DNA mixture containing 1x FastDigest buffer and the reaction mixture was incubated at 37°C for 30-60 minutes (1 μL of FastDigest enzyme cleaves 1 μg of substrate DNA in 5 to 15 minutes in 20 μL of FastDigest buffer). Undigested DNA was gel purified and ligated (optional in case of QuikChange). The DNA was finally used to transform chemically ($CaCl_2$) competent *E. coli* (DH5α) cells.

Table 2.1 Primers used for site-directed mutagenesis

Mutation	**Method**	**Primer sequence**
NorM-VC F429L	Round the horn	ttaatcatcggactctcggcgg
		tccgagccagaaacctttggc
NorM-VC L430F	Round the horn	tttatcgcgggtttaagttgtgc
		cccttgccataacccagatgg
NorM-VC L426F	Round the horn	ttttggcaagggttaatcgcggg
		cccagatggaccgctagctg
NorM-PS F369Y	Round the horn	taccagttcagcgatgtagtacagg
		aagagcggcgtaaaaaaaaagccc
NorM-PS S201A	Round the horn	gcaactgcccttgtgatgttatttatgc
		gacaccacaacccactcccc
NorM-VC Q278A	QuikChange	aaattgagcgccactgcgtgtgccgccacgac
		gtcgtggcggcacacgcagtggcgctcaattt
NorM-VC N282A	QuikChange	aaacaccaaagaagagaaagcgagcgccacttggtgtgcc
		ggcacaccaagtggcgctcgctttctcttctttggtgttt

2.5 Chimeric genes generation

The first chimera is named NorM-VC(NL)NorM-PS(CL) referring to the protein consisting of N-lobe (NL) of NorM-VC (amino acid residues 1-225) and C-lobe (CL) of NorM-PS (amino acids residues 227-464). Similarly, the second chimera is named NorM-PS(NL)NorM-VC(CL) referring to the protein consisting of N-lobe of NorM-PS (amino acids 1-227) and C-lobe of NorM-VC (amino acid residues 226-461). The NorM-VC and NorM-PS chimeras were generated using FastCloning method as described previously [48]. The flow chart below summarises the overall procedure and primer design.

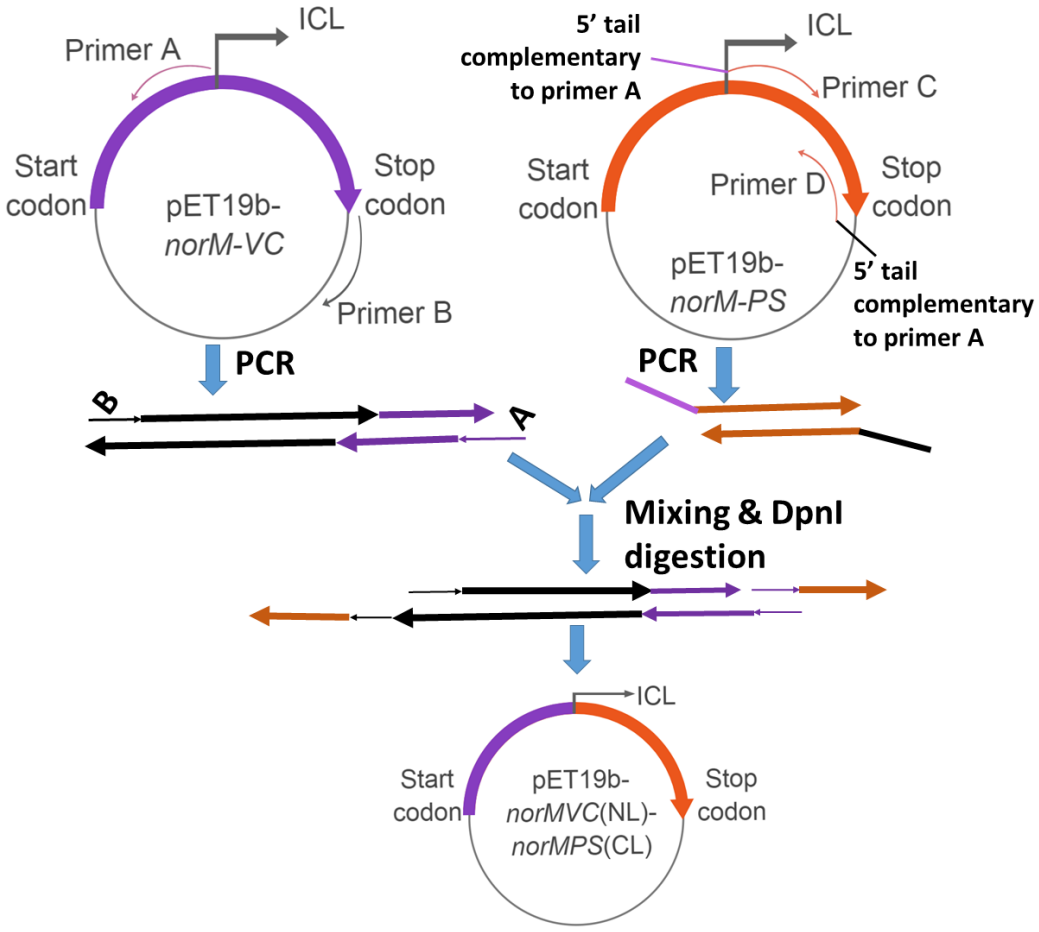

Fig. 2.4 The FastCloning method workflow for chimera generation. This method is digestion and ligation free and allows quick generation of chimeras is a three-step (PCR, DpnI digestion and transformation) protocol.

A 50 µl PCR reaction mixture consisted of 1X HF buffer (provided with polymerase kit), 0.2 mM dNTPs, 5 picomoles of each primer, 10 ng plasmid DNA template and 0.5 μl of Phusion DNA polymerase. The PCR cycling parameters were 98°C for 1 min, (98°C for 15

sec, 55°C for 30 sec, 72°C for 30 sec/kb) × 18 cycles, 72°C for 5 minutes. The product was confirmed using agarose gel electrophoresis.

Table 2.2 Primers used for chimeric gene generation

Primer	**Sequence**
NorM_VC_A_fw	tacatgtgccagacgcttagagg
NorM_VC_A_rev	ctcgaggatccggctgc
NorM_PS_B_fw	cctctaagcgtctggcacatgtacaattattttgccaatttgaatggc
NorM_PSB_rev	gcagccggatcctcgagttaaacgatagctcgtctaagaacag
NorM_PS_A_fw	cgaccactacaagcatatgcctacagagttgcgtttacg
NorM_PS_A_rev	aaagtctcaaacactttgctggcttggtacgctgg
NorM_VC_B_fw	aaagtgtttgagactttccataaaccac
NorM_VC_B_rev	atgcttgtagtggtcgtcgatatg

The primer pair NorM_VC_A_fw and NorM_VC_A_rev were used to amplify the first half of NorM-VC (residues 1-225) along with the pET19b vector. The primer pair NorM_PS_B_fw and NorM_PS_B_rev were used to amplify the second half of NorM-PS (residues 227-464). After PCR amplification, 1 μl of DpnI was added to the PCR products and, the two reaction mixtures were pooled together in the ratios 1:1, 1:2, 1:4 and incubated at 37°C for 1 hour to digest the template DNA. 2 μl of the digested product was used to transform competent *E. coli* DH5α cells.

2.6 Protein expression, purification, quantitation, and purity determination

2.6.1 Preparation of inside-out membrane vesicles (ISOVs) from *L. lactis* cells

For protein expression, M17 growth medium containing 25 mM glucose and 5 μg/ml chloramphenicol was inoculated with 2.5% overnight culture and grown to an $OD_{600\,nm}$ of 0.5-0.6 at 30°C. Protein expression was induced by addition of 0.1% (v/v) of the culture supernatant of the nisin A-producing strain *L. lactis* NZ9700 [49], which gives a final concentration of approximately 10 pg nisinA /ml. Cells were further grown for one hour and were collected by centrifugation at 7,500 rpm for 12 minutes, at 4°C (Sorvall Evolution RC, SLC-6000 rotor). The pellet was resuspended in ice-cold 100 mM potassium phosphate (KP_i) buffer (pH 7.0) and centrifuged at 4,400 rpm for 30 minutes at 4°C. The cell pellet

(collected from 1 L culture) was resuspended in 20 ml KP_i (pH 7.0) containing 5 mg/mL lysozyme (from chicken egg white) and a tablet of Complete-Protease inhibitor cocktail and incubated for 30 minutes at 30°C. Cell lysis was performed by passing the cell suspension 2-3 times through a Basic Z 0.75 kW Benchtop Cell Disruptor (Constant Systems, Northlands, UK) at 20 kpsi. The suspension containing lysed cells was supplemented with 10 μg/mL DNAse and 10 mM $MgSO_4$ and incubated for 30 minutes at 30°C to digest cellular DNA. 15 mM K-EDTA (pH 7.0) was added to prevent the aggregation of the membrane vesicles. In order to remove cell debris and unbroken cells, centrifugation was carried out at 4°C for 40 minutes at 8000 rpm (Sorvall Evolution RC-6 PLUS, F21S rotor). Supernatant containing the membrane vesicles was retained and ultra-centrifuged at 37,000 rpm for 50 minutes at 4°C (Beckman Type-50.2-Ti rotor). The pellet was resuspended in 50 mM KP_i (pH 7.0) containing 10% glycerol, and stored in liquid-nitrogen.

2.6.2 Purification of His-tagged proteins

The protein of interest was purified from inside-out membrane vesicles (ISOVs) using metal ion-affinity chromatography. ISOVs (5 mg membrane protein/ml) were added to 50 mM KP_i (pH 8.0), 10% (v/v) glycerol, 0.1 M KCl and 1% (w/v) n-dodecy-β-D-maltopyranoside (DDM) for 4 hours with mild shaking at 4°C. Non-solubilized membrane vesicles and cell debris were removed by centrifuging the mixture at 55,000 rpm , 4°C for 30 minutes (Beckman Type-70.1-Ti rotor). Nickel-nitrilotriacetic acid resin (Ni-NTA) was equilibrated by washing thrice with 5 resin volumes of MilliQ water, and twice with 5 resin volumes of wash buffer A (50 mM KP_i (pH 8.0), 0.1 M KCl, 10% (v/v) glycerol, 0.05% (w/v) DDM and 20 mM imidazole), at a ratio of 10 mg His-tagged protein/mL of resin. The suspension was left on a rotating wheel for overnight binding at 4°C, after which the unbound proteins were removed by centrifugation, and the resin was transferred to a 2 mL volume Biospin disposable chromatography column (Bio-Rad). After subsequent washing with 20 volumes of wash buffer A and 30 volumes of wash buffer B (50 mM KP_i (pH 7.0), 0.1 M KCl, 10% (v/v) glycerol, 0.05% (w/v) DDM and 20 mM imidazole (pH 8.0). The His-tagged protein was eluted with 3-4 volumes of elution buffer (50 mM KP_i (pH 7.0), 0.1 M KCl, 5% (v/v) glycerol, 0.05% (w/v) DDM and 150 mM imidazole (pH 8.0). The eluted purified protein was kept on ice and was immediately used in experiments. The purity of the protein was checked by on a 10% Sodium dodecyl sulphate-poly acrylamide gel (SDS-PAGE) stained with Coomassie Brilliant Blue.

2.6.3 Protein concentration determination

Protein concentration in the membrane vesicles was determined by Bio-Rad DC protein assay kit. A standard curve was prepared by plotting the absorbance at 750 nm versus varying concentrations of bovine serum albumin (BSA). 20 μl of samples containing 0, 0.25, 0.5, 0.75, 1, 1.25, 1.5 mg/ml BSA was mixed with 100 μl of Solution A and 800 μl of Solution B. After 15 minutes of incubation, absorbance at 562 nm was measured. 10, 20, and 50-fold dilutions of the ISOVs were prepared and the absorbance at 750 nm was used to determine the protein concentration by using the standard curve equation. Purified protein was quantified by Micro BCA (ThermoScientific) protein assay kit (catalog number 23235) which is more sensitive and does not cross-react with detergents. A standard curve was prepared by plotting the absorbance versus varying concentrations of bovine serum albumin (BSA). Samples containing 0, 0.5, 1, 2, 5, 10, 15, 20 μg/ml BSA was mixed with equal volume of colouring solution (25 parts solution MA + 24 parts Solution MB + 1 part solution MC). After 15 minutes of incubation, absorbance was measured and the protein concentration was determined by using the standard curve equation.

2.6.4 Protein detection and purity determination

Sodium dodecyl sulphate-polyacrylamide gel electrophoresis (SDS-PAGE) was used to detect the proteins in ISOVs and in purified samples. ISOV samples containing equal amounts of total protein were denatured in SDS sample-loading dye (6X sample buffer: 10% SDS, 30% glycerol, 1.2% bromophenol blue, 62.5 mM Tris-HCl (pH 6.8), 0.715 mM βC-mercapto-ethanol, 6 mM EDTA free-acid , 50 mM dithiotriol) and were separated on 10% resolving/separating gel (pH 8.8) and 5% stacking gel (pH 6.8). A pre-stained protein marker (6μL) was also loaded to estimate protein size by comparing the migration of standard proteins in the marker. The gel was run in 1x tris-glycine running buffer (25mM Tris-base, 250 mM glycine, 0.1 % SDS, pH 8.3) at 80 volts until the dye front reached the resolving gel and then at 100 volts until the dye front ran over. Separated proteins were visualized by staining the gel with Coomassie blue (0.1 % Coomassie Brilliant Blue (w/v), 45 % methanol, 45 % distilled water, 10 % glacial acetic acid). The gel was destained using the destaining solution (45% methanol, 45% distilled water, 10% glacial acetic acid) overnight and finally washed with MilliQ water for visualising the bands.

For western blotting, proteins separated on SDS-PAGE gels were electro-blotted onto PVDF membrane (0.45μm ImmobilonTM Transfer membranes) in cold transfer buffer (12.5 mM Tris-base, 100 mM glycine and 20% methanol) at 100 volts, 4°C for an hour. To avoid non-specific binding, the membrane was blocked using TBST (Tris-buffered saline, 0.1%

Tween-20) containing 5% (w/v) skimmed milk powder for 30 minutes at room temperature with mild shaking. The membrane was washed with TBST three times and a 1:1000 to 1:3000 dilution of anti-His primary antibody (Sigma Aldrich, catalog number SAB1305538) was added and the membrane was incubated for 1 hour at room temperature. The blot was washed thrice with TBST and incubated with 1:5000 dilution of secondary antibody (horseradish peroxidase HRP-conjugated anti-mouse IgG from Sigma Aldrich, catalog number A9917) for 1 hour at RT. The membrane was again washed thrice with TBST. The membrane was incubated with the Enhanced Chemiluminescence system (ECL) solution for 5 minutes. Finally, the signals were detected by exposing the membrane to X-ray film for varying durations or using Biospectrum Imaging System.

2.7 Measurements in whole cells

2.7.1 Ethidium efflux assay

MATE protein expressing cells were harvested by centrifugation and washed with ice-cold 50 mM KP_i (pH 7.0) supplemented with 5 mM $MgSO_4$ by centrifugation at 3000g for 8 -10 minutes. Cell pellet was re-suspended in 0.6 mM 2,4-dinitrophenol (DNP) containing wash buffer at 30°C for 40 minutes. DNP shuttles protons into the cytosol and in order to maintain the pH gradient, cells pump out protons by hydrolysing ATP until the intracellular ATP levels drop to micromolar levels. The deenergised cells were then washed thrice with ice-cold buffer by centrifugation at 3000 g for 8 -10 minutes. the cells were re-suspended in the same buffer to attain a cell density corresponding to $OD_{660\,nm}$ 5.0. The cells were diluted 10 times in 2 ml of the same buffer in a 3 ml cuvette at 30°C. After 30 seconds, 2 μM ethidium bromide was added and fluorescence was monitored (excitation wavelength=500nm, slit width=5 nm and emission wavelength=580 nm, slit width=10 nm) using LS-55B Luminescence spectrometer (Perkin Elmer, Norwalk, CT). After reaching a saturation in fluorescence, 25 mM glucose was added to energise cells and to trigger efflux. The ethidium fluorescence was monitored for 10-15 minutes.

2.7.2 Membrane potential measurement in *L. lactis* cells

The cells expressing NorM-VC or control cells (empty vector pNZ8048) were de-energised by DNP treatment as described in ethidium efflux assay method. The cells were diluted 10 times in 50 mM KP_i (supplemented with 5 mM $MgSO_4$) buffers with different pH values (6, 7, and 8) to attain a cell density corresponding to $OD_{660\,nm}$ 0.5 in a glass cuvette. The cells were re-energised by addition of 12.5 mM glucose and incubation at 25°C for 3

min. A membrane potential-sensitive fluorescent probe, 3,3'-Diethyloxacarbocyanine Iodide ($DiOC_2(3)$) (Thermo Scientific, catalog number D14730) was employed to monitor the transmembrane potential in *L. lactis* using a LS-55B luminescence spectrometer (Perkin Elmer). The parameters were set as follows: (excitation wavelength = 488 nm, slit width=5 nm; emission wavelength= 620 nm, slit width=10 nm). 10 μM $DiOC_2(3)$ was added and when a steady-state level of fluorescence was reached, 0.5 μM nigericin was added to interconvert ΔpH into $\Delta\psi$. After saturation, 0.5 μM valinomycin was added to completely abolish Δp.

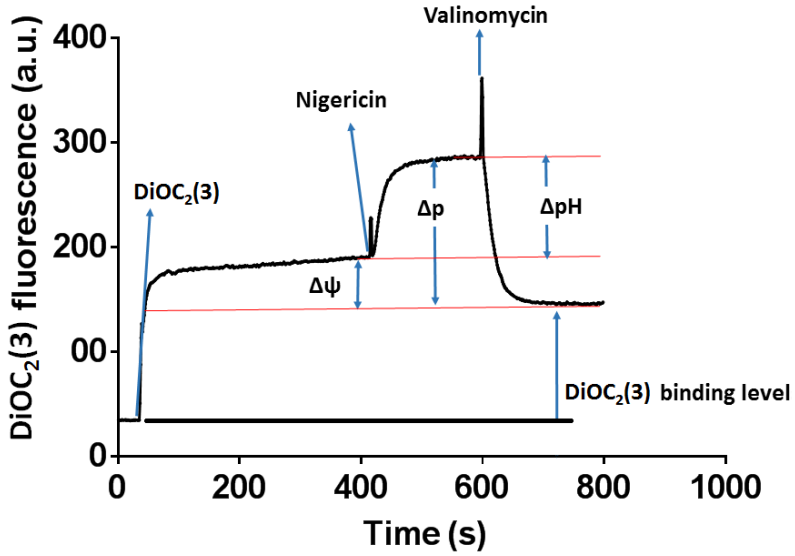

Fig. 2.5 A typical $DiOC_2(3)$ fluorescence trace indicating different components of cellular proton motive force. The probe $DiOC_2(3)$ accumulates in negative cellular compartments and hence indicates the $\Delta\psi$. Upon addition of nigericin, the ΔpH is interconverted into $\Delta\psi$ and a rise in fluorescence is seen with the top value being indicative of the total Δp. Further addition of valinomycin completely abolishes the Δp and the fluorescence drops to the basal level (the value used for baseline correction). The difference between Δp and Δpsi gives ΔpH.

The fluorescence levels corresponding to cells with no Δp were taken as the baseline fluorescence due to $DiOC_2(3)$ binding to cells and was subtracted from the original fluorescence traces. After baseline correction, the fluorescence after $DiOC_2(3)$ addition was taken as $\Delta\psi$, the fluorescence after nigericin addition was taken as Δp. The ΔpH was deduced by subtracting $\Delta\psi$ from Δp. The picture below shows how the various phases of the traces were interpreted and analysed.

2.8 Ethidium binding assays using fluorescence anisotropy

The anisotropy measurements shown in figures 3.7, 3.13, 5.7, 6.2 and 4.5 were made using a Perkin Elmer LS55 spectrophotometer. The instrument uses the following formula to calculate anisotropy:

Anisotropy = $(I_{vv}\text{-}(GF\times I_{vh}))/(I_{vv}+(2\times GF\times I_{vh})$

Where I_{vv} is the intensity with both polarisers (excitation and emission) vertical, I_{vh} is the intensity with polarisers vertical and horizontal (excitation and emission). The GF (grating factor) is instrumental polarisation correction factor and was calculated using the software.

The anisotropy measurements shown in Figure 6.7 here , were made using CLARIOstar microplate reader from BMG LABTECH. The samples were read in a 96-well plate with black bottom. The focus adjustment was done at a well with least amount of protein. The gain was maintained at 10%. Other parameters were kept the same as for the readings with Perkin Elmer LS-55 spectrophotometer.

For measuring the anisotropy, a protein solution at a concentration of 0.4 mg/ml was used. Increasing amounts of the proteins were added to 2 ml of assay buffer containing 50 mM KP_i (pH7.0), 0.2 M KCl, 0.05% DDM and 2 μM EtBr. The excitation and emission wavelengths were the same those in the ethidium efflux assay. The protein concentration ranged from 0.036 μM to 1 μM. 0.5 mM of Na_2SO_4 was added to the buffer to test the effect of Na^+ on ethidium binding to the proteins. To test the effect of protons on ethidium binding, the pH of the buffer was varied from 6 to 9 in 0.2 steps by addition of either HCl or KOH. The protein elution buffer was used as a negative control to generate the base line.

2.9 Computational studies and data processing

2.9.1 The pKa estimations of the ionisable groups in the target proteins

The pKa calculations were done using the online tool H++. The submitted files were either the original PDB files (without the metal-ion) or homology models based on the crystal structures. The parameters were kept to their default values.

2.9.2 Homology modelling

The MurJ based homology model of NorM-VC was made by using SWISS-MODEL. The "User Template" option was selected to provide NorM-VC sequence (PDB IS: 3MKU) and MurJ structure (PDB ID: 5T77).

2.9.3 Data analysis and plotting

The data were analysed and plotted using GraphPad Prism 6.0 packages.

All molecular visualisation images were generated using UCSF chimera. A list of online resources and URLs has been provided in Appendix A.

2.9.4 Statistical analyses

All measurements were done in independent triplicate studies unless indicated otherwise. Two-way ANOVA (multiple comparisons) test provided with GraphPad Prism 6.0 was employed to test for statical significance between pairs of data sets. A description of the symbols used to indicate statistical significance in this thesis is given below.

Table 2.3 P-Value symbols

Symbol	P-Value
ns	$P > 0.05$
*	$P \leq 0.05$
**	$P \leq 0.01$
***	$P \leq 0.001$
****	$P \leq 0.0001$

Chapter 3

Different ion-coupling requirements of NorM-VC and NorM-PS

Transporters in the MATE family were originally thought to be either Na^+- or H^+-coupled. For example, the NorM subfamily is thought to be solely dependent on Na^+ cycling whereas the DinF family is dependent on H^+ cycling. However, the transport assays with NorM-VC in cells and proteoliposomes [34] indicated that NorM-VC couples to H^+ and Na^+ simultaneously. In contrast, NorM-PS was reported to be exclusively H^+-coupled [42]. In this Chapter, I examined these claims by testing the ion coupling and overall energetics of NorM-VC and NorM-PS proteins under identical experimental conditions.

3.1 Cloning of the *norM-PS* gene

The NorM-PS gene was custom synthesised and cloned between the Nde1 and Xho1 sites of the pET19b vector. The product was used to transform *E. coli* DH5α cells. Single transformant colonies were picked and grown overnight to isolate the plasmid DNA. The purified plasmid DNA was double digested and run on a 1% agarose gel to visualise the inserted NorM-PS gene. The insert was verified by DNA sequencing and the translated polypeptide chain had 100% identity with the original sequence (GenBankTM EHY79494.1).

The NorM-PS gene was isolated from pET19b-NorM-PS by digesting with NcoI and BamHI. The digested fragment was then ligated into digested pNZ8048 vector (derived from pNZ-NorM-VC construct). The subcloned gene was sequenced and had 100% amino acid identity with the original sequence.

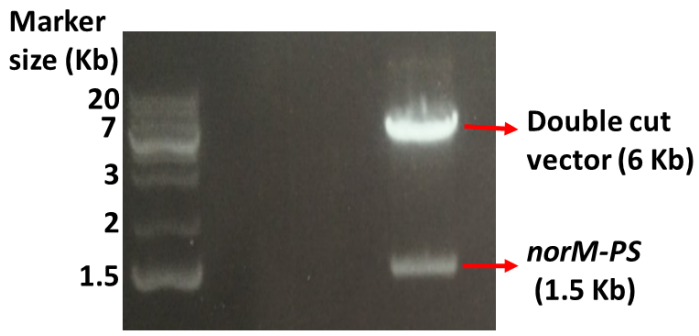

Fig. 3.1 The vector pET19b-NorM-PS was digested with NdeI and XhoI and run on an agarose gel to confirm the presence of the insert. Besides the double-cut vector, a fragment consistent with the size of *norM-PS* gene was seen which was cut out and purified for subcloning into the pNZ8048 vector.

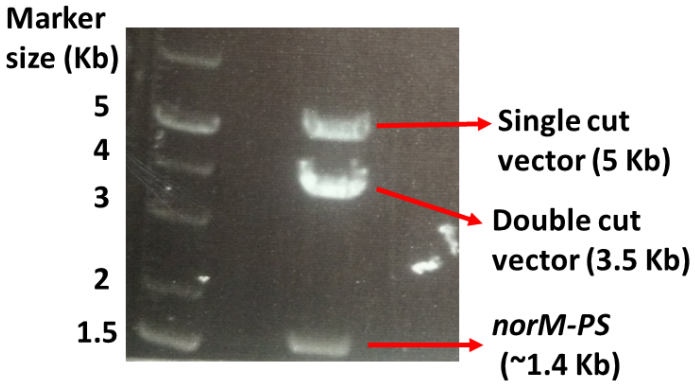

Fig. 3.2 The vector pNZ-NorM-PS was digested with NcoI and BamHI and run on an agarose gel to confirm the presence of the insert. Besides a single-cut and a double-cut band, a band consistent with the size of *norM-PS* gene was seen.

3.2 NorM-VC and NorM-PS couple differently to ion gradients to export ethidium

Ethidium is a substrate for many multidrug transporters and has been used to assay their transport activity [50]. It is a lipophilic cationic compound that upon accumulation into the intracellular compartment, binds to nucleic acids and shows enhanced fluorescence emission. In preparation for the ethidium export assay, the protein-expressing cells were first de-energised in presence of dinitrophenol (protonophore), washed with Kp_i buffer and finally resuspended in the same buffer. The cells were then incubated with ethidium and after the fluorescence eqillibrated, glucose was added to cells, optionally along with different cation salts. As shown in Fig. 3.3, NorM-VC exported ethidium in the presence of Δp which

further improved in the presence of Na^+. Whereas NorM-PS also exported ethidium in a Δp dependent manner, no stimulation of efflux by Na^+ was observed.

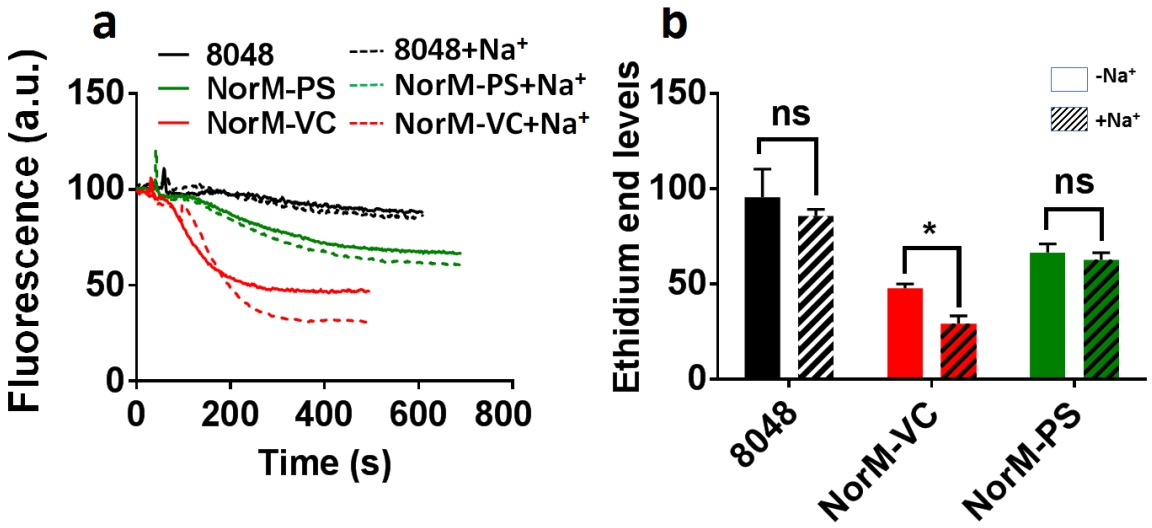

Fig. 3.3 **a**, NorM-VC as well as NorM-PS expressing cells show significant ethidium extrusion compared to control cells containing empty vector pNZ8048. The addition of 1 mM Na^+ caused enhanced extrusion activity for NorM-VC. In contrast, no stimulation was observed for NorM-PS. Solid and dotted lines refer to the absence and presence of Na^+. **b**, The bar chart shows mean ($\pm$SD) end levels of ethidium fluorescence after extrusion. N=3 (independent studies).

To further test the ion selectivity of NorM-VC and NorM-PS, a transport assay similar to Figure 3.3 was employed where KP_i buffer was replaced by 25 mM Tris buffer (pH 7.0) supplemented with 5 mM $MgSO_4$. K^+ has been shown to be involved in generation of a pH gradient via an indirect K^+/H^+ exchange reaction in bacterial cells [51]. Under deenergised conditions, cells are dependent on extracellular K^+ for generating a proton gradient. Under these conditions, cells loaded with ethidium can be selectively given either K^+ (to allow generation of ΔpH) or Na^+ (to generate ΔpNa).

As shown in Fig. 3.4, after loading the cells with ethidium and further energisation with glucose, neither NorM-VC nor NorM-PS exported ethidium due to the lack of ΔpH in the absence of K^+.

However, upon addition of K_2SO_4 along with glucose, both NorM-VC and NorM-PS showed a considerable ethidium export, further corroborating the H^+-coupled ethidium transport by the two. Finally, in presence of glucose and Na_2SO_2, only NorM-VC exported ethidium pointing to direct Na^+ coupling in NorM-VC (Fig. 3.4b). It could be argued that upon addition of Na^+, ΔpNa is converted into ΔpH in *L. lactis* cells which, in turn is coupled to ethidium export but the inability of NorM-PS to export ethidium under these conditions

(Fig. 3.4a) proves that NorM-VC-mediated efflux is directly coupled to Na^+ cycling. These results indicate that NorM-VC is more versatile in terms of its ion requirements in the antiport reaction. But how is this versatility achieved?

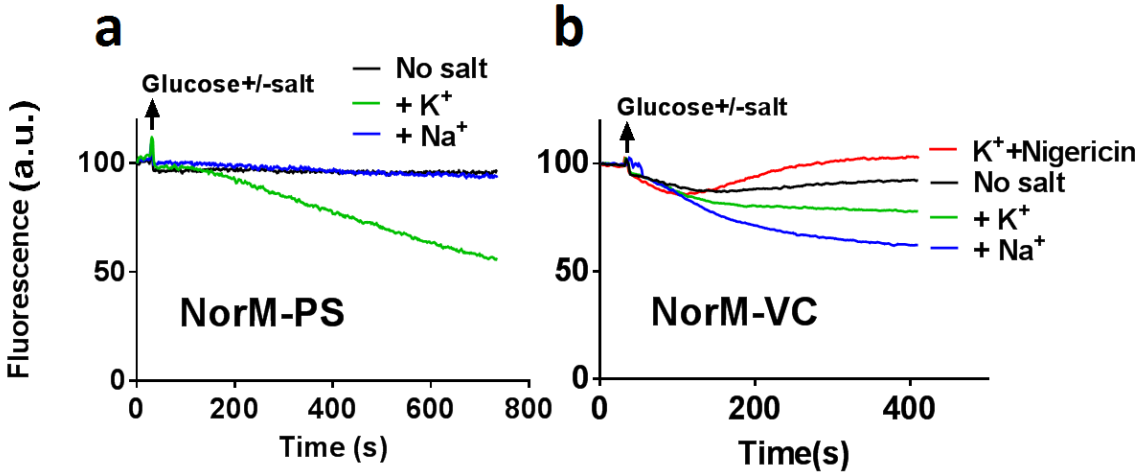

Fig. 3.4 **a**, In absence of extracellular K^+, the *L. lactis* cells expressing NorM–PS showed no ethidium export upon addition of glucose only. However, ethidium export was seen upon addition of 10 mM K^+ (Δp) alongside glucose **b**, NorM-VC can export ethidium in presence of 10 mM K^+ or 10 mM Na^+. The transport was abolished following the addition of nigericin which dissipates the ΔpH.

To test whether the pH of the assay buffer has any effects on the ion preference of NorM-PS, the same assay was performed at acidic and basic pH values. It was hypothesised that an altered protonation state of the donor group (the side chain group that binds the coupling ion) might facilitate interactions between NorM-PS and Na^+, and hence, might convert a H^+-coupled system to a Na^+-coupled one.

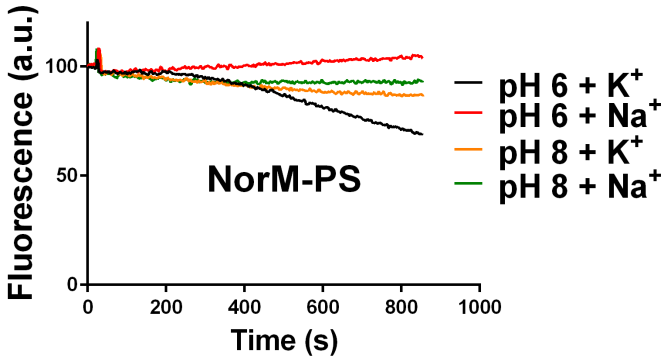

Fig. 3.5 The ethidium export activity of NorM-PS at acidic and basic pH values. In *L. lactis* cells under acidic conditions, Δp largely consists of ΔpH (see Fig. 4.2) and hence a significant export activity is seen. At basic pH (pH_{in}=pH_{out}), Δp is largely composed of $\Delta\psi$, hence no transport is observed in the presence of added K^+.

NorM-PS remained exclusively H^+-coupled at acidic, basic, or neutral pH values and no stimulation by Na^+ was observed. These results establish the specificity of H^+-coupling in NorM-PS and rule out the possibility that NorM-PS might utilise Na^+ under proton-scarce conditions.

3.3 The Na^+-dependent ethidium transport by NorM-VC

To study the dose-response relationship between the extracellular concentration of Na^+ and NorM-VC-mediated ethidium efflux rates, the NorM-VC expressing *L. lactis* cells were de-energised and resuspended in K^+-free Tris-Cl buffer (pH 7) supplemented with 5 mM $MgSO_4$. After loading the cells with ethidium , glucose was added as a source of metabolic energy and increasing amounts of Na^+ (Na_2SO_2) were added along with the glucose. Ethidium efflux by NorM-VC was stimulated in presence of Na^+. The stimulation was observed at Na^+ concentrations as low as 50 μM, until a saturation phase was reached at concentrations around 10 mM.

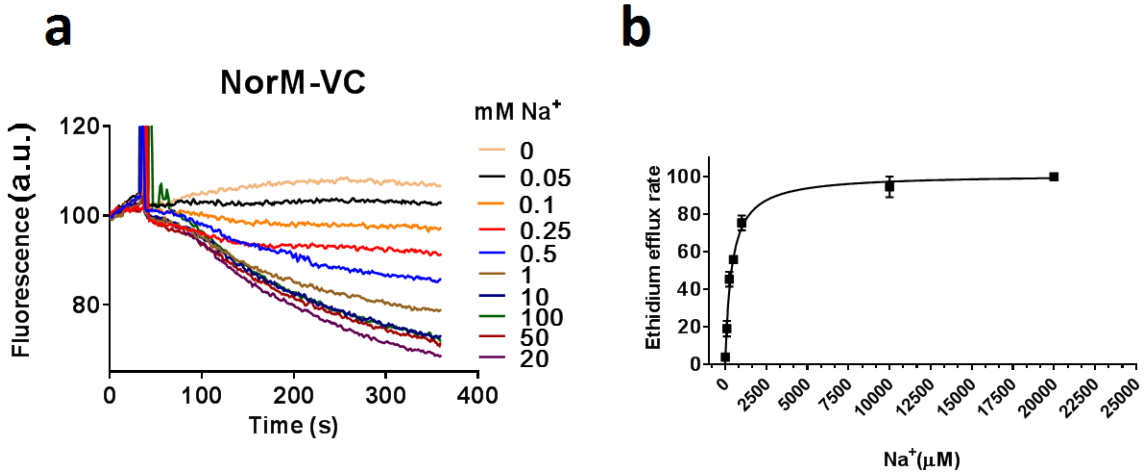

Fig. 3.6 **a**, In the absence of Δp, NorM-VC can export ethidium in a Na^+-dose dependent manner. The NorM-VC expressing cells showed efflux in presence of as low as 50 μM Na^+. The stimulation by Na^+ saturated in the mM range of concentrations. **b** , The ethidium export rate (Δfluorescence/time) is plotted against the Na^+ concentration, and is fitted to a hyperbole. N=3 from independent studies.

To determine the apparent Na^+-binding affinity of NorM-VC in the cells, the rate of ethidium efflux was calculated between the first 100-250 seconds by dividing the change in fluorescence by time. The ethidium export rates were plotted against the Na^+ concentrations and fitted to a hyperbole using GraphPad Prism. The apparent transport constant (K_t) for Na^+ was 393 $\pm$ 61 μM which is comparable to values reported previously [34].

3.4 Na^+-binding improves ethidium-binding to purified NorM-VC but not to NorM-PS

Ethidium export assays in live bacterial cells simulate the most biologically-relevant scenario, however they also suffer with issues such as background signal by non-specific cellular proteins. To address these issues, purified NorM (VC and PS) proteins were used to test: a) their ethidium binding properties, and, b) the effect of metal-ions on the ethdium-binding to proteins. The proteins were purified from inside-out membrane vesicles using Ni^+-affinity chromatography. Equal amounts of proteins were diluted in assay buffer and the ethidium binding was monitored by measuring fluorescence anisotropy. Fluorescence anisotropy occurs when a fluorophore emits light of unequal intensities along different axes of polarisation. Hence when a small fluorophore binds a macromolecule the fluorescence anisotropy increases and the increase in anisotropy can be used to quantify the binding.

To study ethidium binding, the proteins were added in a stepwise manner to a buffer containing a fixed concentration of ethidium bromide. Na_2SO_4 was added where required. The results suggested that purified NorM-VC and NorM-PS bind ethidium in a concentration dependent manner (K_d= 0.56 $\pm$ 0.04 μM and 1.01 $\pm$ 0.09 μM, respectively). NorM-VC binds ethidium with a higher affinity compared to NorM-PS. The addition of 1 mM Na^+ leads to a $\sim$10-fold increase in the binding affinity of NorM-VC (K_d value of 0.06$\pm$0.01 μM) but in unaltered binding for NorM-PS (K_d=0.78 $\pm$ 0.09 μM).

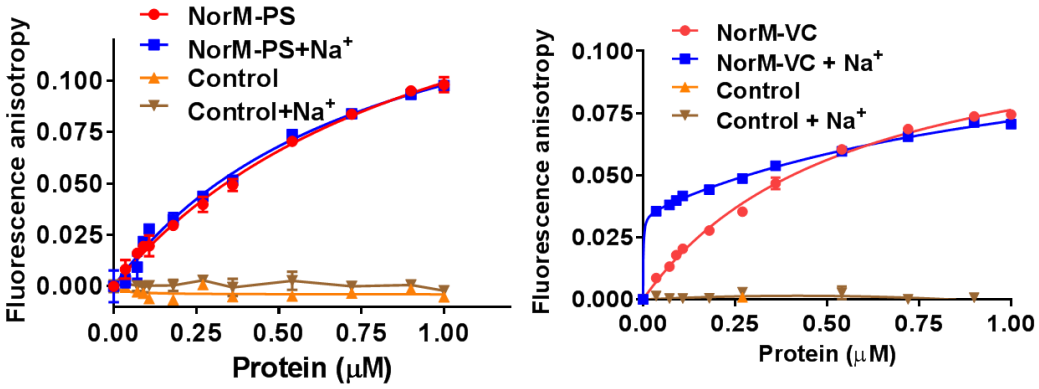

Fig. 3.7 **a**, Purified NorM-PS and **b**, NorM-VC proteins bind ethidium in a dose-dependent manner (fixed ethidium and varying protein concentrations). Upon addition of 1 mM Na^+ to the assay buffer, the affinity of NorM-VC for ethidium increases. NorM-PS shows no such stimulation upon additions of Na^+. The elution buffer was used as control to generate the baseline. N=3 (independent studies).

These data are in agreement with the ethidium efflux studies in intact cells. Evidently, the two highly similar proteins differ in their Na^+ binding behavior. It raises two questions: what are the structural features that entail this difference? And what is the biological (and evolutionary) context of this difference? In the following section, the first question will be explored further.

3.5 NorM-VC and NorM-PS give rise to transport-active chimeric transporters

3.5.1 Construction of chimeric transporters

In order to look for structural differences in NorM-VC and NorM-PS that might be responsible for their ion preferences, further studies on the Na^+-binding site(s) are required. The crystal structure of NorM-VC has Rb^+/Cs^+ bound at the C-lobe (near the E255/D373 centre) [29], but previously the mutagenesis data had suggested that the N174A mutation in NorM-VC leads to a 1200-fold drop in the binding affinity for Na^+ [34]. These two sites are in two different lobes in the published crystal structure of NorM-VC (PDB IDs 3MKT and 3MKU) and seem to be far apart in the outward-facing conformation in which NorM-VC was crystallised.

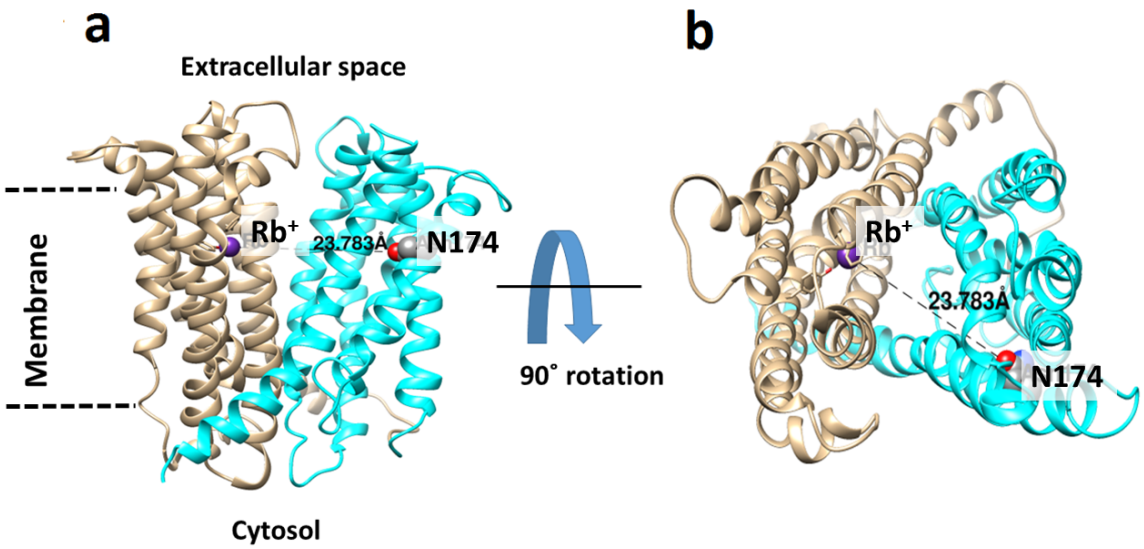

Fig. 3.8 NorM-VC crystallised with Rb^+ (PDB ID 3MKT). **a**, In the crystal structure, the Na^+ analogue binds in the C-lobe (shown as golden), whereas N174A mutation in N-lobe (shown as cyan) causes a drastic drop in affinity for Na^+. The distance between these two locations is very large (about 23 angstroms). **b**, Same structure seen from a 90°angle (top view).

To dissect whether the Na^+-binding site is in the C-lobe or in the N-lobe, a set of chimeric proteins from NorM-VC and NorM-PS was made. The reasoning behind this was to swap the N- and C-lobes of NorM-VC and NorM-PS to create two different chimeric proteins. The ion dependence of the resulting chimeric proteins could indicate the location of the Na^+-binding site in NorM-VC.The overall experiment and the hypothesis are summarised in the flow chart below:

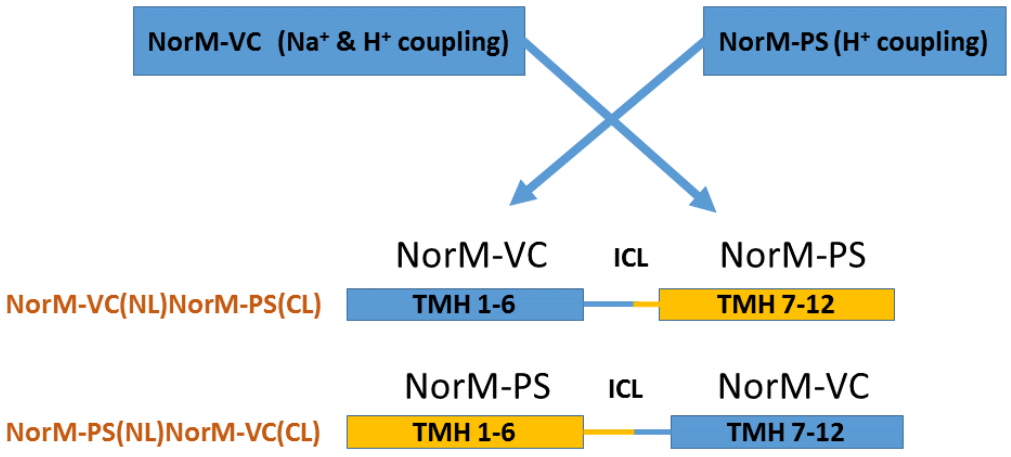

Fig. 3.9 A brief schematic of the overall design of chimeric NorM proteins.

The chimeras were constructed using the FastCloning method as described in Chapter 2 section 2.5. The genes were cloned in the pNZ8048 vector and *L. lactis* cells were transformed with the resulting vectors. The NorM-VC(NL)-NorM-PS(CL) chimera was constructed by fusing the NorM-VC residues 1-225 with NorM-PS residues 227-464 and the NorM-PS(NL)-NorM-VC(CL) chimera was constructed by fusing the NorM-PS residues 1-227 with NorM-VC residues 226-461. Analyses by western blots showed that the chimeric proteins expressed equally well in the plasma membrane of the lactococcal cells.

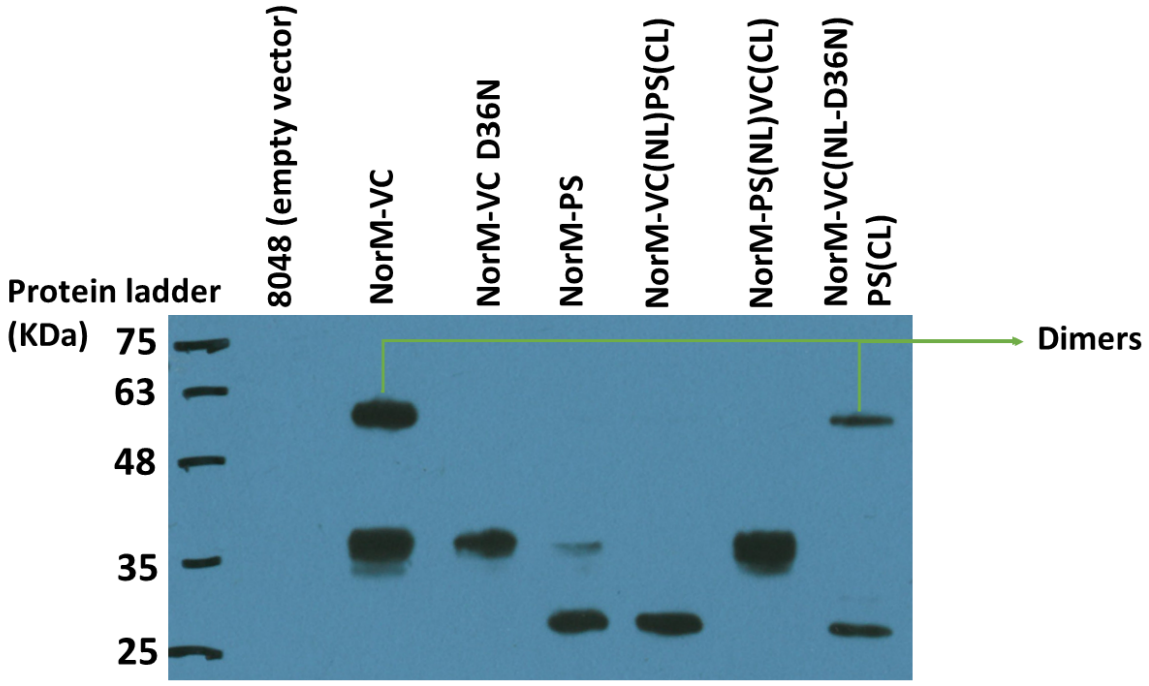

Fig. 3.10 Anti-His immunoblot showing the expression of NorM-VC, NorM-PS and the chimeric proteins. 2 μg of total membrane proteins was loaded onto each lane. Besides the primary bands, the NorM-VC and NorM-VC(NL-D36N)NorM-PS(CL) chimera show a secondary band consistent with the size of a dimer. NorM-PS and chimeras containing the CL part of NorM-PS show a smaller molecular weight band which might be due to intramolecular cross-linking between the two closely located cysteins in the C-lobe or due to enhanced SDS binding.

3.5.2 The NorM chimeric transporters transport ethidium in strictly proton-coupled and electroneutral manner

The cells expressing the chimeric transporters were tested for their transport activities in ethidium export assays. Both the chimeric transporters were found to be transport-active compared to the chimeric transporters containing the inactivating D36N point mutation in the chimera containing N-lobe of NorM-VC.

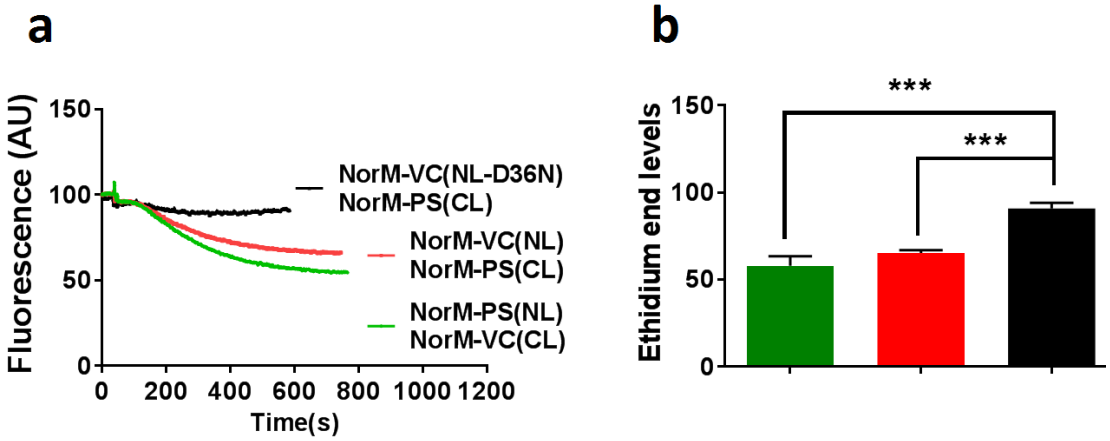

Fig. 3.11 **a**, The chimeric transporters exhibit significant ethidium export compared to the inactive chimeric mutant (containing NorM-VC (NL) D36N). **b**, The bar chart shows mean (±SD) end levels of ethidium fluorescence after export. N=3 (independent studies).

However, when Na^+ was provided alongside glucose, neither of the chimeric transporters showed any response to millimolar concentrations of extracellular Na^+.

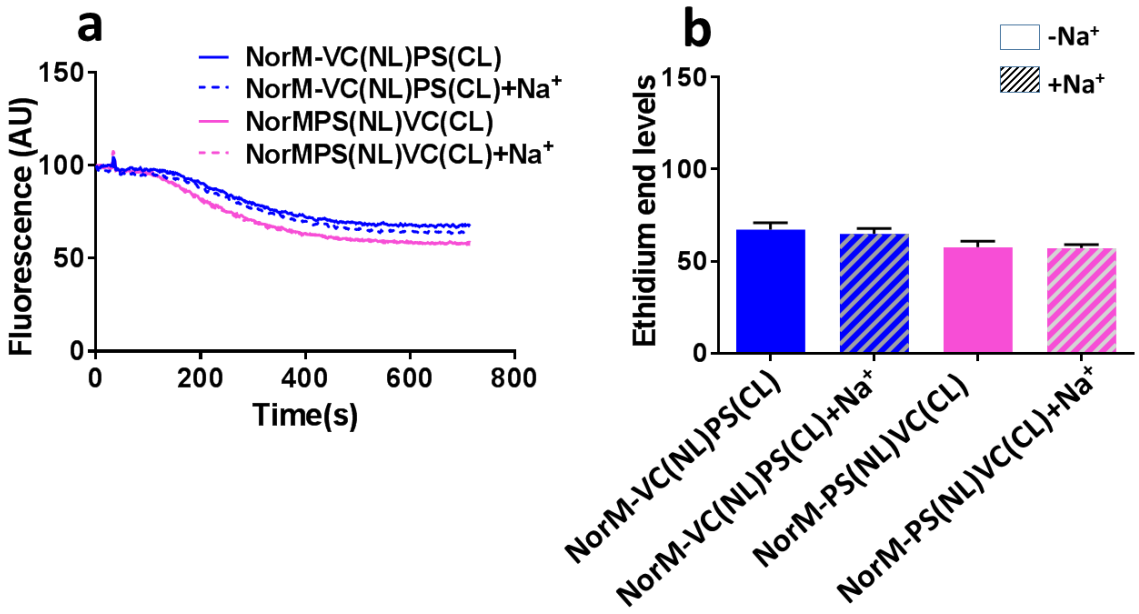

Fig. 3.12 **a**, The chimeric transporters show no Na^+-dependent stimulation of ethidium transport. The traces shown here are those closest to the mean value of replicates. **b**, The bar chart shows mean ($\pm$SD) end levels of ethidium fluorescence after extrusion. N=3 (independent studies).

To corroborate these findings, the effect of Na^+ on ethidium-binding to the purified chimeric proteins was measured using fluorescence anisotropy. The purified chimeric proteins exhibited no stimulation in ethidium binding in presence of Na^+, confirming the loss of Na^+-binding site(s) or allosteric interaction. Interestingly the chimera NorM-VC(NL)NorM-PS(CL) displayed ethidium binding akin to that of NorM-VC (K_d=0.01137 μM) and the chimera NorM-PS(NL)NorM-VC(CL) showed ethidium binding similar to NorM-PS (K_d=0.1221 μM). The difference in the K_d values of ethidium binding to the two chimeras was statistically significant (P value < 0.0001). This might suggest that the ethidium binding site in both NorM-VC and NorM-PS is in the N-lobe.

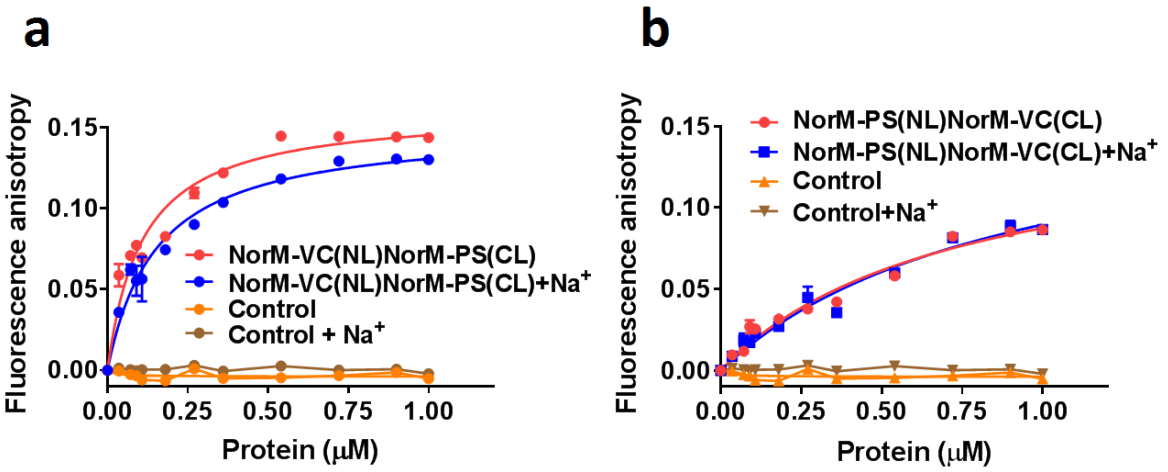

Fig. 3.13 Ethidium binding to purified chimeric transporters, **a**, NorM-VC(NL)NorM-PS(CL), and **b**, NorM-PS(NL)NorM-VC(CL) measured by fluorescence anisotropy. Neither of the chimeric transporters show the Na^+-dependent enhancement of ethidium binding as is observed for NorM-WT. Increasing amounts of the purified chimeric proteins were added to the assay buffer containing 2 μM ethidium in the absence or presence of 1 mM Na^+. The elution buffer was used to generate baseline (control). N=3 (independent studies).

The loss of Na^+-coupling in the chimeric transporters indicates that the Na^+-coupling mechanism in NorM-VC employs both the N-lobe and C-lobe, and, that this mechanism is completely lost upon replacement of either lobe by those of H^+-coupled NorM-PS. To ensure that the loss of Na^+-coupling was due to the complete disruption of the Na^+-binding site and not due to a shift in ion-specificity, the ethidium export assay was carried out at pH $\sim$8. At this pH, the relative concentration of Na^+ ions relative to protons will be higher and a promiscuous ion-binging site might then preferentially bind Na^+.

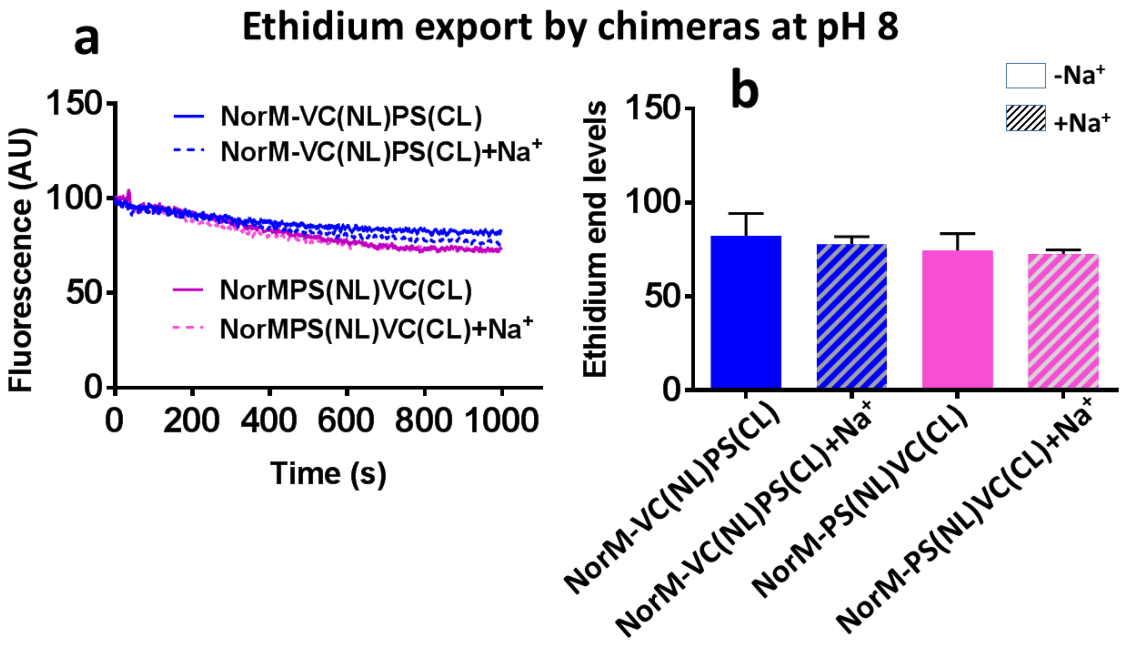

Fig. 3.14 At pH 8, the Δp- dependent transport activity of the chimeric transporters is disrupted. Furthermore, addition of Na^+ does not cause any stimulation of the transport activity. **a**, the traces shown are those nearest to the mean value of the replicates. **b**, The bar chart shows mean (±SD) end levels of ethidium fluorescence after extrusion. N=3 (independent studies).

At a raised pH, the chimeric transporters elicited highly reduced activity relative to activity at neutral pH. When pH_{out}=pH_{in}, the Δp almost entirely consists of $\Delta\psi$. The absence of transport at high $\Delta\psi$ values indicates that there is no correlation between membrane potential and ethidium transport mediated by the chimeric transporters. Furthermore, the chimeras did not show any Na^+-dependent ethidium transport even at an elevated pH.

Previously, NorM-VC was shown to transport ethidium in an electrogenic manner [34], which is a consequence of the exchange of two (or more) coupling-cations per ethidium molecule. To test whether the chimeras transport ethidium in an electrogenic manner too, the ethidium export assay was conducted while selectively abolishing the different components of Δp using ionophores. Nigericin , a H^+/K^+ exchanger, was used to selectively dissipate the ΔpH. Whereas, valinomycin, a K^+ carrier, was used to selectively dissipate the $\Delta\psi$. A combination of these two ionophores dissipates the Δp completely. If the chimeric proteins transport ethidium in an electrogenic manner, there should still be a net movement of ethidium in presence of the $\Delta\psi$ only.

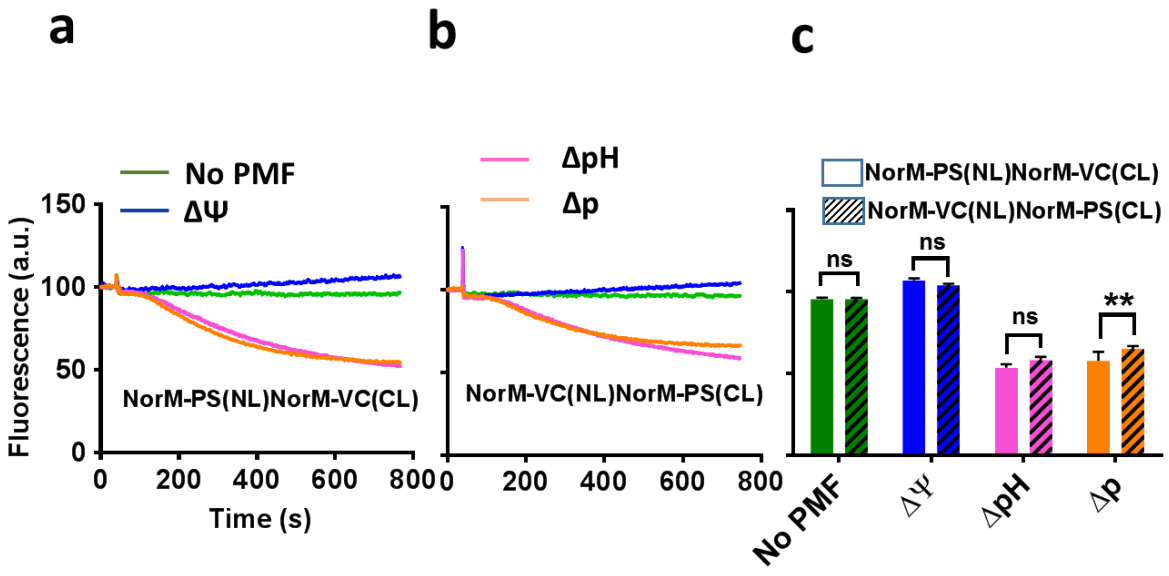

Fig. 3.15 The chimeric transporters **a**, NorM-PS(NL)NorM-VC(CL), and **b**, NorM-VC(NL)NorM-PS(CL) extrude ethidium in a ΔpH-dependent, electroneutral fashion. The control shown here is the ethidium transport without Δp. In the presence of $\Delta\psi$ only, no transport takes place, indicating the electroneutral nature of the transport reaction. **c**, The bar chart shows mean (±SD) ethidium end levels. N=3 (independent studies).

In the whole cell assays, the chimeras appear to transport in an electroneutral manner, i.e., no ethidium transport was seen when only $\Delta\psi$ was provided indicating that only one H^+ was being antiported per molecule of ethdium. This is different from the transport stoichiometry of NorM-VC which has been shown to transport in presence of $\Delta\psi$ only.

3.6 Structural considerations and a potential mechanism for transport-active chimeras

It is remarkable that two different MATE transporters sharing only 42% identity should give rise to functional proteins upon domain swapping. One would expect that these proteins must have highly conserved residues at sites where the two lobes make contact, however this is not apparent at the amino acid sequence level. Also, in absence of a 3D structure for NorM-PS, it becomes difficult to postulate with certainty which structural elements NorM-VC and NorM-PS might have in common. However, a potential explanation can be given by considering the structures of pfMATE$^{Pyrococcus\ furiosus}$ and AtDTX14$^{Arabidopsis\ thaliana}$. In pfMATE, two carboxylates in the N- lobe (D41^{TMH1} and D184^{TMH5}) form the proton-binding

site. Upon protonation of D41, a rearrangement of hydrogen-bond network leads to bending of TM1 at G30. Such an event possibly causes switching from an outward-facing state to an inward-facing state. Interestingly, the AtDTX14 structure suggests a similar mechanism, except that the switch happens in TMH7 - protonation at E265/D383 leads to helix bending at G255. Furthermore, both pfMATE and AtDTX14 do not have any consensus carboxylates in C-lobes and N-lobes, respectively. These two proteins seem to be 'mirror images' of each other, suggesting that MATE transporters evolved via a gene duplication event. A comparison of the two structures reveals a pseudo two-fold symmetry.

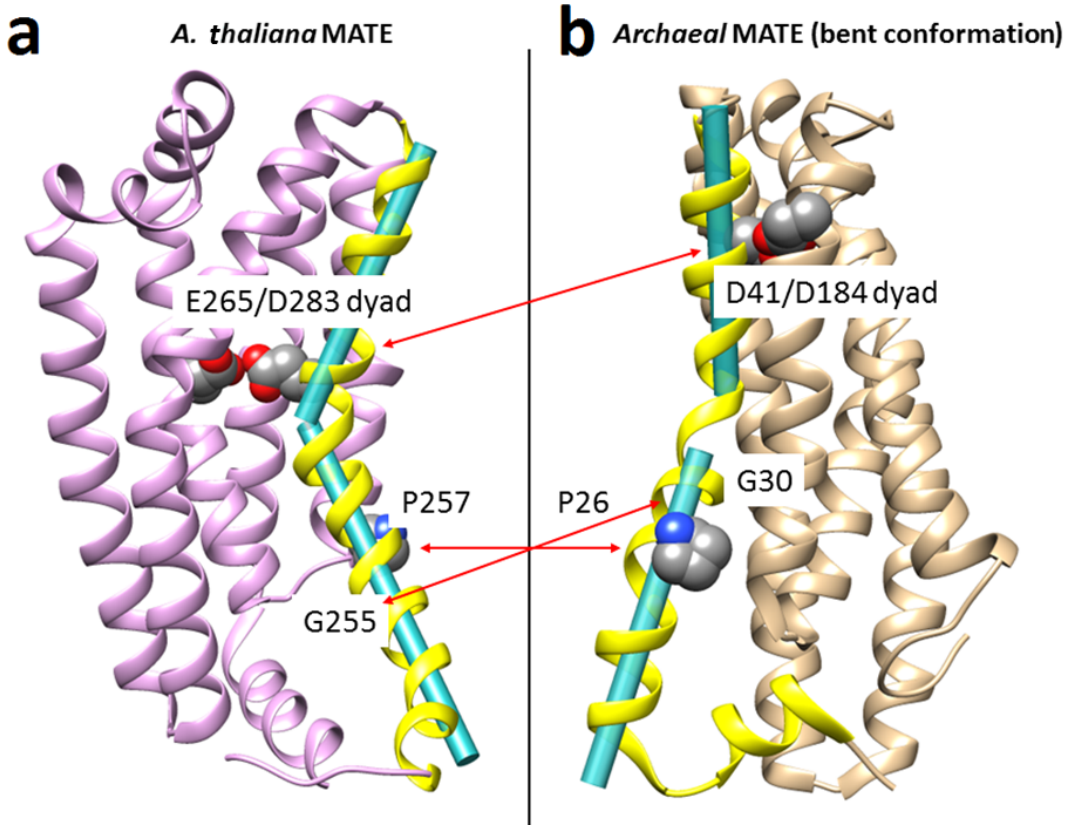

Fig. 3.16 Pseudo two-fold symmetry between **a**, the eukaryotic MATE transporters AtDTX14 and **b** the archael MATE transporter pfMATE. The N-lobe of pfMATE looks like the C-lobe of the *A. thaliana* transporter. The two proteins have a common mechanism of transport which is that protonation at one of the two closely placed carboxylates leads to bending of a helix leading to the inward-open state.

To look for such internal symmetry in NorM-VC, the X-ray structure (PDB ID: 3MKU) was analysed using the online tool TM-align [52]. The N- and C-lobes were compared to each other via structural alignment. On a scale of 0 to 1 (a score of 0.5 - 1.0 indicates the same SCOP (Structural Classification of Proteins) fold. The N- and C-lobe belonging to the same

SCOP fold would indicate existence of a two-fold internal symmetry. Upon such analysis, NorM-VC scores a TM-align value of ∼0.8. Similar values were found when the N-lobe of NorM-VC was structurally aligned to the C-lobe of pfMATE (and vice versa). Table 3.1 lists the structural alignment comparisons scores between N- and C-lobes of different MATE transporters.

Table 3.1 Internal-symmetry scores for MATE transporters

PDB IDs	**Protein and lobe name**		**TM-align score**
3MKU, 3MKU	NorM-VC (N)	NorM-VC (C)	∼0.8
3MKU, 3VVN	NorM-VC (N)	pfMATE (C)	>0.8
3MKU, 3VVN	NorM-VC (C)	pfMATE (N)	∼0.8
5Y50, 3VVN	AtDTX14 (N)	pfMATE (C)	>0.8
5Y50, 3VVN	AtDTX14 (C)	pfMATE (N)	∼0.8

The symmetry between eukaryotic AtDTX14 and archaeal pfMATE indicates the conservation of structural folds across taxonomically distinct species. With such information, it would not be presumptuous to think that NorM-PS will also have these conserved domains and in such case, swapping its domains with those in NorM-VC can result in a protein that has high similarity with the wildtype parent proteins. The concept of such internal symmetry and repeat units has been reported in several transporters and the phenomenon has been utilised to explain the mechanism of transport [53], [54]. Such mechanism could provide a universal mode of transport for MATE proteins and requires extensive computational studies and empirical validation. Despite these speculations, it is still difficult to state why the chimeric transporters discussed here are not Na^+ responsive. The coordination of Na^+ is a multicomponent event and hence the Na^+-binding elements in proteins might be sensitive to small structural changes. In contrast, in order to interact with H^+, only a strategically placed acidic residue (with an optimum pK_a value) is required. Such flexibility in rearrangement of active carboxylate has been demonstrated in the H^+-coupled MFS family transporter, LmrP [55]. In LmrP, the active carboxylate could be placed one helical turn away and the resulting protein retains its H^+-coupled ethidium transport activity. It has been shown that as a compensatory mechanism, sodium translocating systems can translocate H^+ in the absence of sodium gradients[56], but the reverse might not always be true. Perhaps this is why the chimeras retain H^+-coupling but lose Na^+-coupling. The Na^+-binding sites in NorM-VC and the potential to form a Na^+-binding site in NorM-PS are discussed in Chapter 5.

Chapter 4

The pH dependence of Na^+-coupled ethidium transport by NorM-VC

In this chapter, the preferential use of protons and sodium-ions by NorM-PS and NorM-VC was studied with respect to (i) the altered composition and magnitude of the Δp , i.e. ΔpH and $\Delta\psi$, and (ii) the relative availability of H^+ versus Na^+ (ΔpH and ΔpNa).

The energetics of ethidium transport by NorM-PS and NorM-VC was studied by using ionophores that selectively dissipate the components of the Δp . The ionophore nigericin mediates K^+/H^+ antiport and dissipates the ΔpH in an electroneutral manner. Valinomycin acts as a mobile carrier of K^+ and dissipates the $\Delta\psi$. In the presence of nigericin, the Δp is solely composed of $\Delta\psi$, whereas in the presence of valinomycin the Δp is entirely composed of ΔpH. A combination of both the ionophores will completely dissipate the proton motive force and no Δp-dependent substrate transport will take place. In these experiments, ethidium serves as an ideal substrate as the ionisation state of ethidium does not change between pH 6 to 9 (the range of pHs used here). The pK_b values of the two ionisable amines in ethidium have been experimentally determined to be 0.8 and 2 [57], thus eliminating the possibility of proton transport through ethidium binding. For ethidium transport assays, MATE expressing cells (non-expressing cells as negative control) were de-energised using the protonophore DNP and resuspended in KP_i buffer (with different pH values) supplemented with $MgSO_4$. The cells were preloaded with ethidium bromide after which glucose was added (with or without 1 mM Na^+ in case of NorM-VC). To dissipate the components of Δp selectively, the ethidium-loaded cells were incubated with 0.5 μM of nigericin or valinomycin for two minutes before the addition of glucose. The same assay was performed at pH 6, 7, and 8.

4.1 NorM-PS mediated ethidium transport is exclusively ΔpH driven

NorM-PS was previously shown to be H^+-coupled in transport studies in *E. coli* [42] and based on these transport models have been proposed [58]. However, the transport assay employed in these studies suffers from the drawback that it does not directly measure drug transport itself but instead relied on pH-indicating fluorophore acridine orange, which presumably reports drug-proton antiport by NorM-PS in inside-out membrane vesicles. The change in the internal pH in these membrane vesicles does not necessarily originate from drug-proton antiport, but could also be the result of a combination of other factors such as proton pumping by non-specific proteins. The ethidium transport assay employed in my study is more accurate as this assay reports the intracellular concentration of ethidium by measuring the fluorescence of ethidium-nucleic acids complex. Ethidium in this complex shows 10 times more fluorescence emission than free ethidium in aqueous solution. Along with the reversible nature of the ethidium-nucleic acid binding, these properties of ethidium make this assay more accurate.

The ethidium transport in *L. lactis* cells was measured at pH 6, 7 and 8 under conditions where the cells were allowed to generate proton motive force (Δp), proton gradient only (ΔpH), membrane potential only ($\Delta\psi$) and no Δp (control). As shown in Figure 4.1, NorM-PS expressed in *L. lactis* mediates ethidium export by exclusively coupling to proton gradient at pH 6, 7 and 8. Consistent with the observations in Chapter 3, no major correlation between membrane potential and ethidium transport was observed, thus establishing the important role of ΔpH as a driving force for NorM-PS mediated transport and the electroneutral nature of the overall transport reaction. Upon addition of glucose, cells regain their metabolic activity and as a result the cell interior becomes alkaline and negatively charged and a sudden influx of positively charged ethidium is seen in cells that lack NorM-PS-dependent efflux activity. As ethidium bears a single positive charge at these pH values, NorM-PS must mediate the antiport of one H^+ per ethidium molecule to maintain electroneutrality in these experiments.

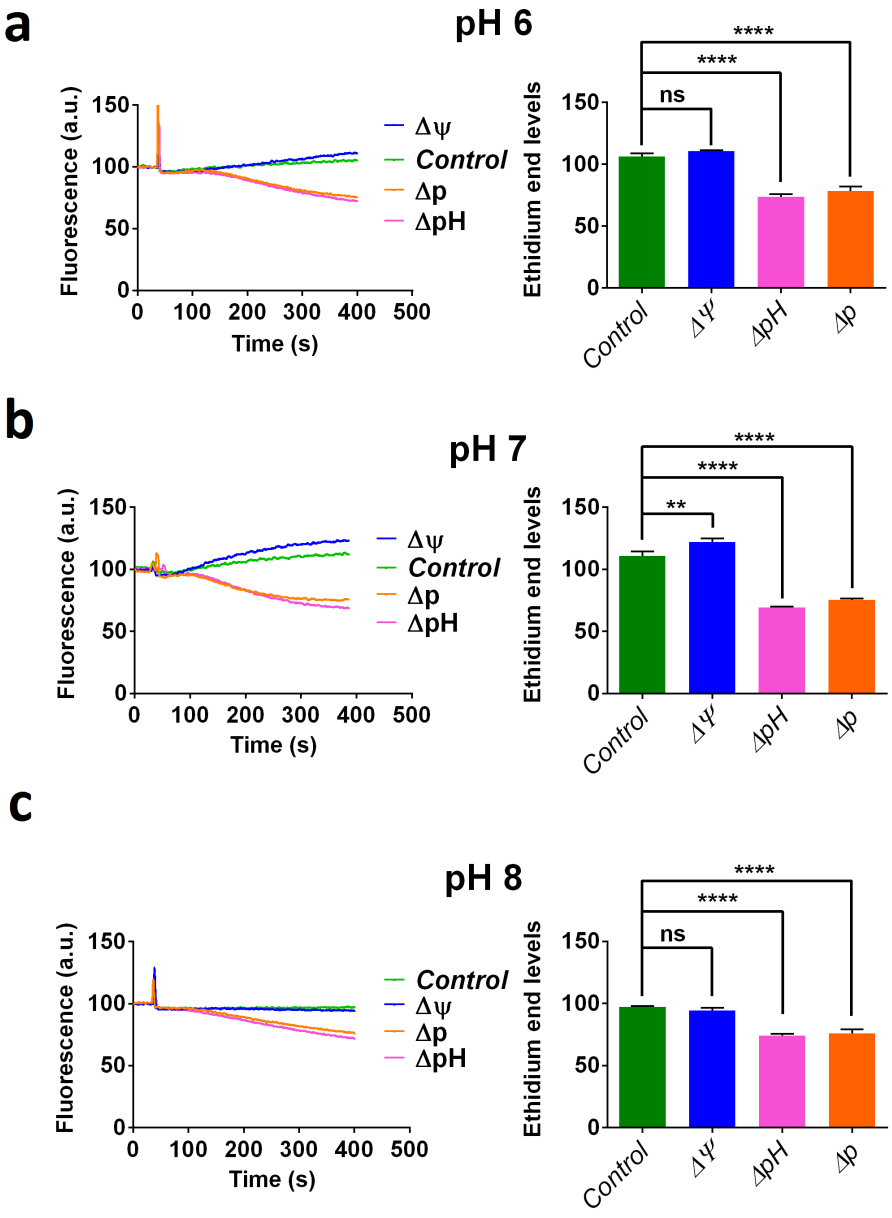

Fig. 4.1 The NorM-PS expressing *L. lactis* cells export ethidium in a ΔpH-dependent and electroneutral manner at **a**, pH 6, **b**, pH 7, and **c**, pH 8. The NorM-PS mediated efflux diminishes with increasing alkalinity. The traces shown on the left are normalised for the initial fluorescence levels and are representative of the mean of the triplicates. The bar chart shows mean (±SD) end levels of ethidium fluorescence after export. N=3 (independent studies).

4.2 Increased alkalinity makes NorM-VC mediated ethidium transport electrogenic

To correlate NorM-VC mediated ethidium export with components of the Δp, the ethidium export assay in non-expressing (8048) cells and NorM-VC expressing cells was performed at different pHs in the absence or presence of ionophores. To better interpret the results, the magnitude of the components of Δp was measured using the lipophilic cationic membrane potential probe $DiOC_2(3)$. The cells used in the transport assays were energised with glucose and loaded with the probe $DiOC_2(3)$. The accumulation of $DiOC_2(3)$ in the cells is indicated by an increase in the red fluorescence (620 nm), with increasing $\Delta\psi$. Upon addition of nigericin, the cellular ΔpH is converted into $\Delta\psi$ and an increase in red fluorescence is seen. Further addition of valinomycin dissipates the $\Delta\psi$ which dissipates the total Δp. In these experiments, NorM-VC-expressing cells exhibited lower levels of $DiOC_2(3)$ accumulation than the non-expressing control. This might be due to the NorM-VC-mediated export of $DiOC_2(3)$ and it might be more useful to consider the $DiOC_2(3)$ responses in the non-expressing cells. The possible export of $DiOC_2(3)$ by NorM-VC can be be investigated n the future studies.

As shown in Figure 4.2, at pH 6, the Δp in *L. lactis* cells is entirely composed of ΔpH with almost no contribution from the $\Delta\psi$. Consequently, the addition of valinomycin has little effect, and the ethidium export activity is fully retained. Upon the addition of nigericin, no ethidium export is seen suggesting that at pH 6, NorM-VC is biased towards the ΔpH. Interestingly, in the presence of 1 mM Na^+, NorM-VC showed enhanced ethidium extrusion (Figure 4.2 b).

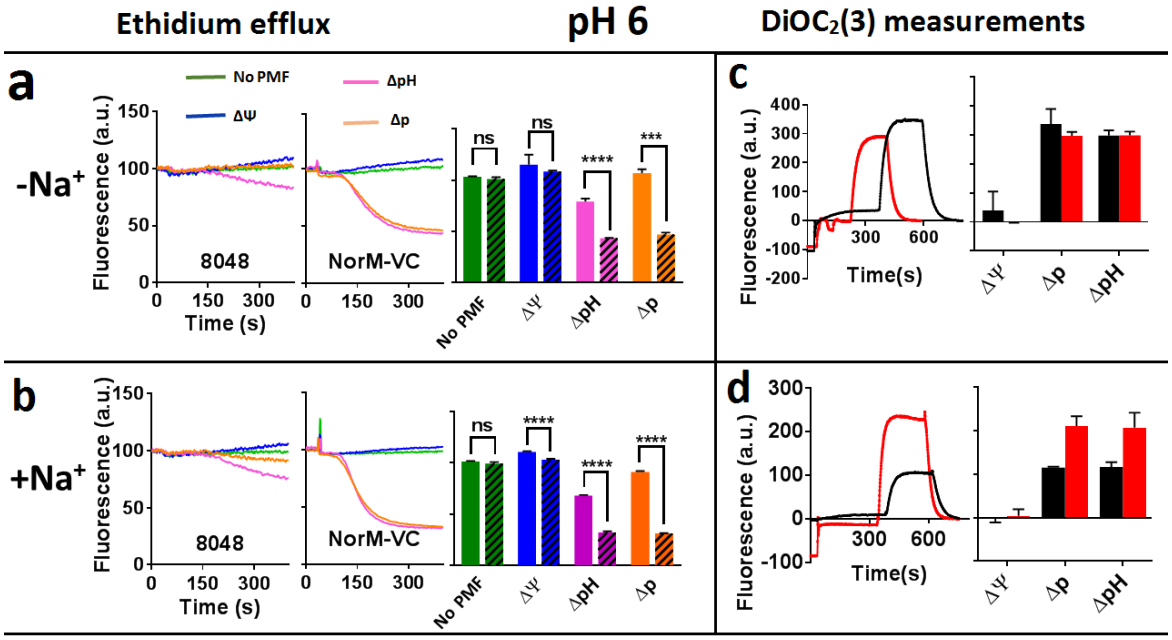

Fig. 4.2 **a**, At pH6, the NorM-VC expressing *L. lactis* cells export ethidium efficiently when compared with non-expressing control (8048) cells. The traces shown here are normalised for the initial fluorescence level and are representative of the mean of the triplicates. The bar chart next to the traces shows end mean (±SD) levels of ethidium fluorescence levels in 8048 cells (no pattern) and NorM-VC cells (ribbed). **b**, Same as **a** except Na^+ was provided alongside glucose. **c**, The $\Delta\psi$ measurements in NorM-VC(red) and control cells (black) show that at pH 6 (± Na^+) the Δp is entirely composed of ΔpH. **d**, same as **c**, except Na^+ was provided. N=3 (independent studies).

At pH 7, the Δp has contributions from the $\Delta\psi$ and the ΔpH, which are utilised by NorM-VC to export ethidium. NorM-VC expressing cells show reduced levels of ethidium accumulation in presence of the $\Delta\psi$ only, as compared with the control (Figure 3a) indicating antiport of two ions ($2H^+$, or $1H^+$ plus $1Na^+$) per ethidium. However, upon addition of 1 mM Na^+ (Figure 4.3b), this $\Delta\psi$-dependent extrusion does not improve in a NorM-VC specific manner indicating that Na^+ might not take part in the antiport reaction under these conditions.

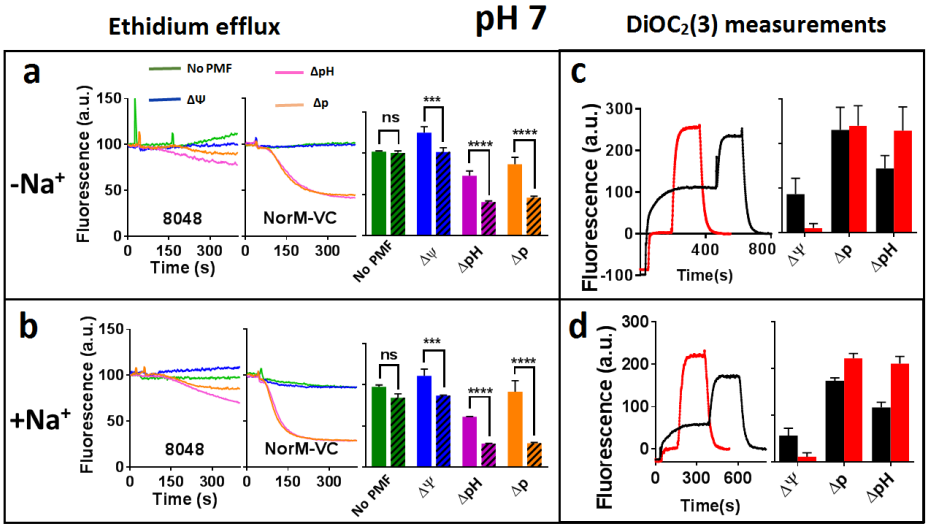

Fig. 4.3 **a**, At pH 7, NorM-VC-mediated ethidium transport becomes electrogenic with contributions from the ΔpH and the $\Delta\psi$. The traces shown here are normalised for the initial fluorescence level and are representative of the mean of the triplicates. The bar chart next to the traces show the end mean (±SD) levels of ethidium fluorescence levels in 8048 cells (no pattern) and NorM-VC cells (ribbed). **b**, Same as **a** except sodium was provided alongside glucose. **c**, The $\Delta\psi$ measurements in NorM-VC (red) and control cells (black) show that at pH 7 (± Na^+) the Δp has contributions from ΔpH and $\Delta\psi$. **d**, same as **c** except Na^+ was provided. N=3 (independent studies).

4.3 Proton scarcity drives NorM-VC to switch to a ΔpH-independent, Na^+-coupled ethidium transport reaction

At pH 8, pH_{out} approaches the pH_{in} in cells, and hence, the ΔpH is close to 0. The Δp is therefore mainly composed of the $\Delta\psi$ (Fig. 3A). In agreement with this, the NorM-VC mediated extrusion of ethidium is driven by the $\Delta\psi$. However, in the presence of valinomycin (Δp = delta pH), NorM-VC also exhibits activity. Thus, similar to the results for pH 7.0, the efflux can be coupled to both components of the Δp (the ΔpH and the $\Delta\psi$). The addition of Na^+ enhances the Δp-dependent export, and interestingly, NorM-VC is able to couple ethidium extrusion to ΔpNa even upon complete dissipation of the Δp (Fig. 4.4). Thus, with the reduced availability of protons, NorM-VC can switch to a ΔpH-independent Na^+-coupled ethidium transport reaction.

This observation becomes relevant upon considering the habitat of *Vibrio cholerae* (VC). One of the biggest reservoirs of *V. cholera* are estuaries where the pH and salinity of the water varies between neutral and fresh to alkaline and saline. Hence, it would be beneficial

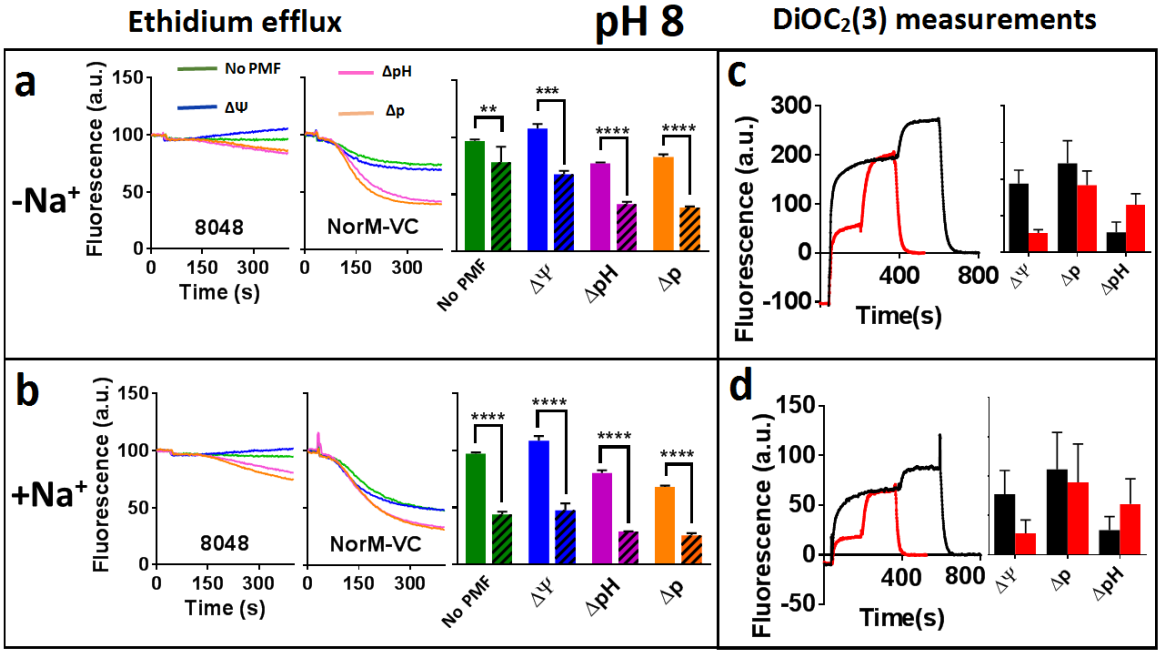

Fig. 4.4 **a**, At pH8, the NorM-VC-mediated ethidium export can be driven by $\Delta\psi$. **b**, In the presence of Na^+, NorM-VC can couple ethidium to ΔpNa exclusively. The traces shown here are normalised for the initial fluorescence level and are representative of the mean of the triplicates. The bar chart next to the traces show end mean ($\pm$SD) levels of ethidium fluorescence levels in 8048 cells (no pattern) and NorM-VC cells (ribbed). **c**, The $\Delta\psi$ measurements in NorM-VC (red) and control cells (black) show that at pH 8 ($\pm Na^+$) the Δp is largely composed of $\Delta\psi$. **d**, same as **c** except Na^+ was provided. N=3 (independent studies).

for the survival of the organism to utilise a transport system that can couple to ΔpH at neutral (or slightly acidic) pH and couple to the ΔpNa at alkaline pH values.

Similar effects of pH on the Na^+-dependent stimulation of enzyme activity have been observed for BCl-MotAB flagellar motor complexes [59]. BCl-MotAB was shown to utilise H^+ at neutral pH but Na^+ at alkaline pH. How these systems fine-tune their ion-binding and transport properties with the environment is fascinating and requires further investigations.

4.4 Increasing alkalinity promotes ethidium binding to NorM-VC

To assess the relationship between the NorM-VC-mediated ethidium transport and the pH, the ethidium binding to NorM-VC and associated mutants was tested by the means fluorescence anisotropy measurements. Previously, sequence analysis and biochemical studies have

identified three critical carboxylate residues (D36, E255 and D371) in NorM-VC. The amide mutants at these positions were used as controls since the amide moiety is basic in nature and mimics their protonated carboxylate counterparts.

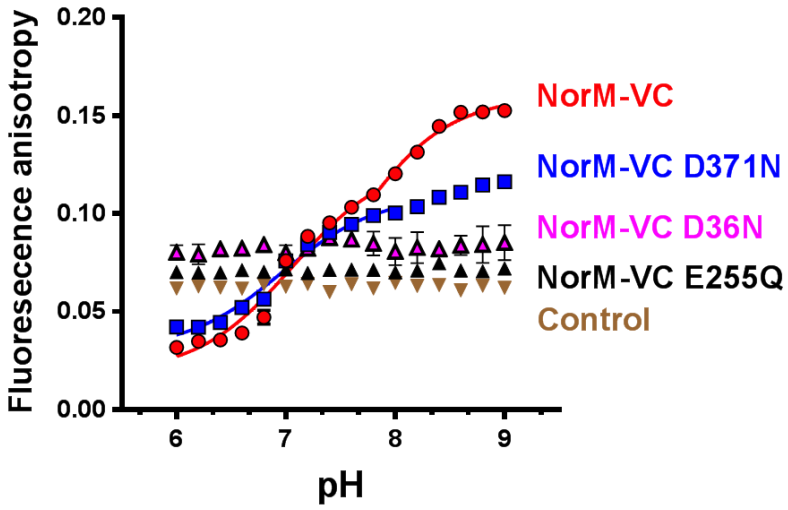

Fig. 4.5 Ethidium binding to purified NorM-VC and mutant proteins at varying buffer pHs. Ethidium binding to NorM-VC WT is promoted as the pH is raised. The D36N and E255Q mutants didn't exhibit any changes in ethidium binding with changes in pH and acted like control (elution buffer). The D371N mutant retains some of the pH dependency of the wild type protein. N=3 (independent studies).

As seen in the Figure 4.5, purified NorM-VC binds increasing amounts of ethidium as the pH of the buffer increases – there is about a 2-fold increase in anisotropy at pH 9 compared with the anisotropy at neutral pH. This indicates competition between ethidium and H^+ binding to NorM-VC and is consistent with the previous reports [34] where NorM-VC was shown to release H^+ upon ethidium-binding. Also, D371N is the only mutation that partially retains the pH-dependent ethidium binding. The two other amide mutants, D36N and E255Q, show no correlation between pH and ethidium binding, pointing towards the importance of ionisable carboxylate groups at these positions for pH-sensitive ethidium binding to NorM-VC.

To explore how the pK_a values of different carboxylates vary upon the outward-open to inward-open conformational switch in NorM-VC, an inward-open homology model of NorM-VC was built by using the structure of the MOP flippase, MurJ (PDB ID: 5T77). A homology model with Qmean of -6.38 was generated using the online server SWISS-MODEL. Figure 4.6 shows a cartoons of the model as seen in different orientations.

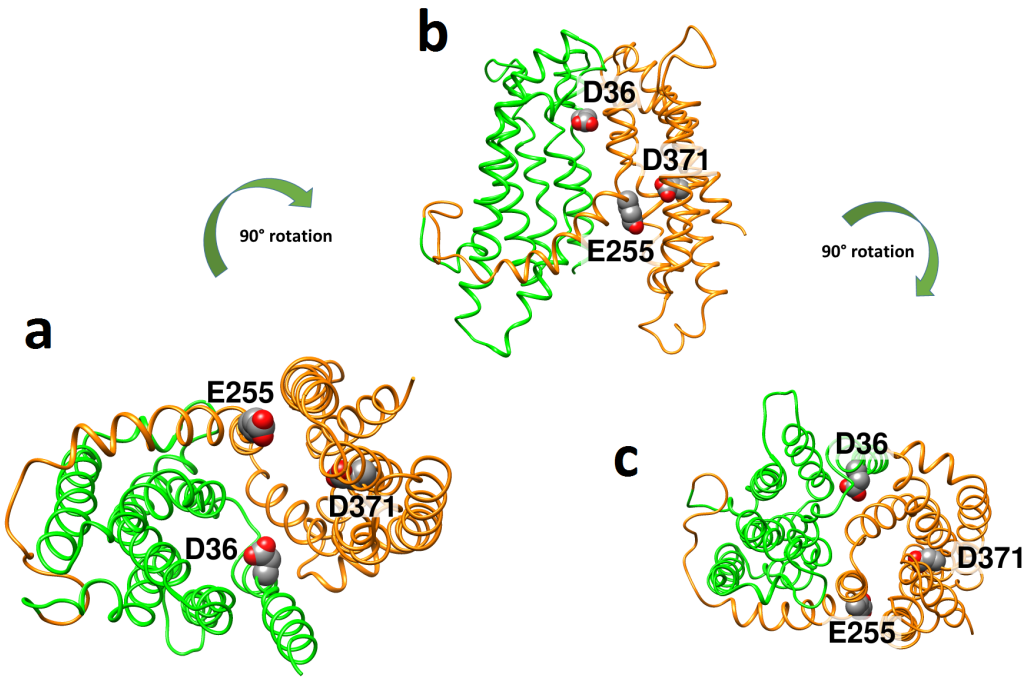

Fig. 4.6 The MurJ-based inward-open homology model of NorM-VC. N-lobe shown as green and C-lobe shown as golden yellow. **a**, The opening of the intracellular interface can be seen. The same structure as seen from the intracellular side **b**, and extracellular side **c**. The extreme bending of the E255 harbouring TMH7 is evident. The distance between E255 and D371 increases by 5 Å compared with that in outward-open crystal structure (PDB ID 3MKT). This might be due to the repulsion caused by deprotonation of these residues upon exposure to the alkaline cell interior.

The outward-open crystal structure of NorM-VC (PDB ID: 3MKU) and the inward-open homology model of NorM-VC were used to calculate the pK_a values of the carboxylates using the online server H++ [60]. All the parameters were kept to their default values. The predicted pK_a values are listed in Table 4.1.

Interestingly, D371 shows a drastic change in the protonation state between the outward-open and inward-open conformations (ΔpK_a= 4.2) which further strengthens the possibility that protonation of D371 can trigger the switch from the outward-open state to the inward-open state and that the release of this proton perhaps leads to the binding of ethidium in the inward-open conformation.

The results presented in this chapter establish fundamental differences between the mechanisms of energy coupling in NorM-PS and NorM-VC. Whereas NorM-PS couples to protons exclusively and antiports one H^+ per ethidium molecule, NorM-VC carries out H^+-coupled electroneutral transport at acidic pH, but H^+- and Na^+-coupled electrogenic

Table 4.1 A comparative list of the pk_a values of NorM-VC carboxylates

Residues	**pKa in outward-facing X-ray structure**	**pKa in inward-facing homology model**
D36	5.2	3.7
E255	6.4	4.4
D371	7.4	3.2

ethidium-transport at basic pH. Furthermore, the observation that the binding of ethidium to purified NorM-VC is promoted at alkaline pH points toward the importance of deprotonation of at least one of the three conserved carboxylates (D36, E255, and/or D371). The binding studies with amide mutants corroborate the latter hypothesis as D36N and E255Q completely lose the pH-dependence of ethidium binding, whereas the effect of D371N is significant but less dramatic.

Chapter 5

Towards altering the coupling-ion requirements of MATE transporters

The Na^+-binding sites in proteins are elusive – partly due to the versatile coordination chemistry of Na^+ and the chemically diverse coordinating side-chains in proteins. Na^+ can interact with proteins in strikingly diverse ways. Besides the main chain carbonyl oxygen, common side-groups that can bind Na^+ are provided by carboxylate, amide and hydroxyl group containing amino acids. However, at times, aromatic residues can also interact with Na^+ via pi-cation interactions. Furthermore, ordered water molecules can be part of a Na^+-binding site. Na^+ usually binds proteins with a coordination number that varies from 5 to 6 (rarely 4 or 7) and the ideal coordination geometry can be octahedral for a coordination number of 6, trigonal bipyramid or tetragonal pyramid for a coordination number of 5, and tetrahedral or square planar for a coordination number of 4 (see Figure 5.1). Such a diversity in terms of the nature of donor groups and coordination numbers (and coordination geometries) can in principle allow many different modes of Na^+-binding to proteins. This is partly why Na^+-binding sites in proteins are difficult to generalise and predict. In this chapter the cation-binding sites in NorM-VC have been dissected using structural and mutational studies, and the information has been used to study the effect of mutations on the ion-requirements of NorM-PS.

5.1 A comparative account of the Cs^+/Rb^+-binding site in NorM-VC and its structural counterpart in NorM-PS

Based on the X-ray crystal structure of NorM-VC and the previous biochemical studies and the studies included in this thesis, NorM-VC seems to have two 'Na^+-binding hotspots' –

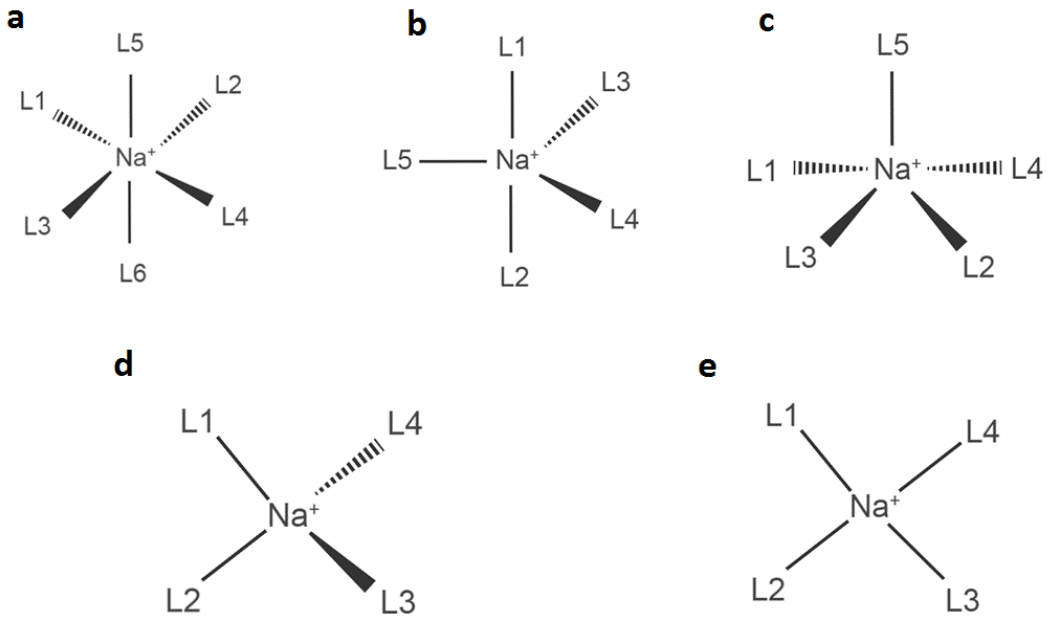

Fig. 5.1 The ideal coordination geometries for Na^+: **a**, octahedral for coordination number 6, **b**, trigonal bipyramidal or **c**, tetragonal pyramidal for coordination number 5, and **d**, tetrahedral or square planar for coordination number 4. L=ligand (donor group).

regions in the tertiary structure that are involved in Na^+ binding and transport. In the 3D structure, these hotspots are centred around three carboxylates, which are D36 in the N-lobe (close to N174) and the E255/D371-dyad in the C-lobe (close to F429 and Y369). The high level of amino acid sequence conservation between NorM-VC and NorM-PS at the 'transport hotspots' provides an excellent opportunity to compare the amino acid sequence variation that might be responsible for the differences in their ion-coupling behaviours. Figure 5.2 depicts a sequence alignment between NorM-VC and NorM-PS highlighting the conservation (underlined by black bars) at sites important for transport activity.

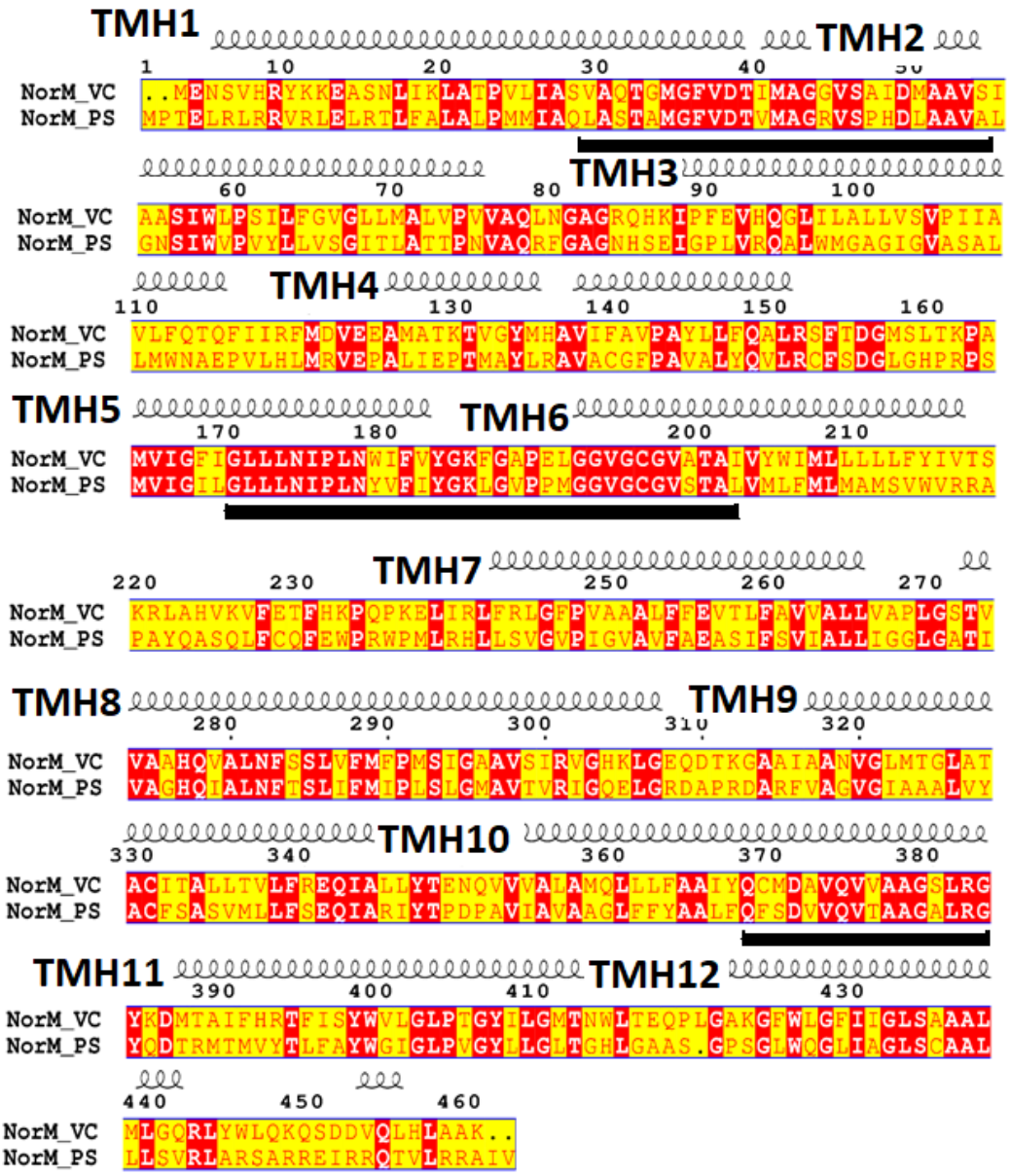

Fig. 5.2 Amino acid sequence alignment of NorM-VC (PDB ID 3MKT) and NorM-PS (GenBank ID EHY79494.1) shows a high level of conservation (conserved residues shown in white against red background) at the regions important for transport (underlined by black bars). Notably, the transmembrane regions (shown as springs) are more conserved than the connecting loops. The indicated helices are based on the NorM-VC structure (PDB ID: 3MKT). Alignment performed using Prabi ClustalW and figure generated using ESPript 3.0.

NorM-VC was co-crystallized with Rb^+ bound in the C-lobe (PDB ID: 3MKU), which was suggested to act as a Na^+ analogue. A quick survey of the Rb^+-binding site in this structure shows that the Rb^+ is in close proximity to three residues, namely F259, Y369 and

F429 (all within 4 Å). The carboxylates E255 and D371 are further away (6 Å or more); it is likely that the situation is different under physiological conditions where water molecules mediate the interactions between the distal metal ion and the carboxylates. Although E255 and D371 are also conserved in NorM-PS (E257$^{\text{NorM-PS}}$ and D373$^{\text{NorM-PS}}$), my experiments demonstrate that NorM-PS does not utilize Na^+-cycling. This raises the question whether there are any residues missing in NorM-PS that would enable Na^+-binding in this location. In the experiments presented here, I therefore focused on the surrounding residues in the Rb^+-binding pocket of NorM-VC that are different in NorM-PS.

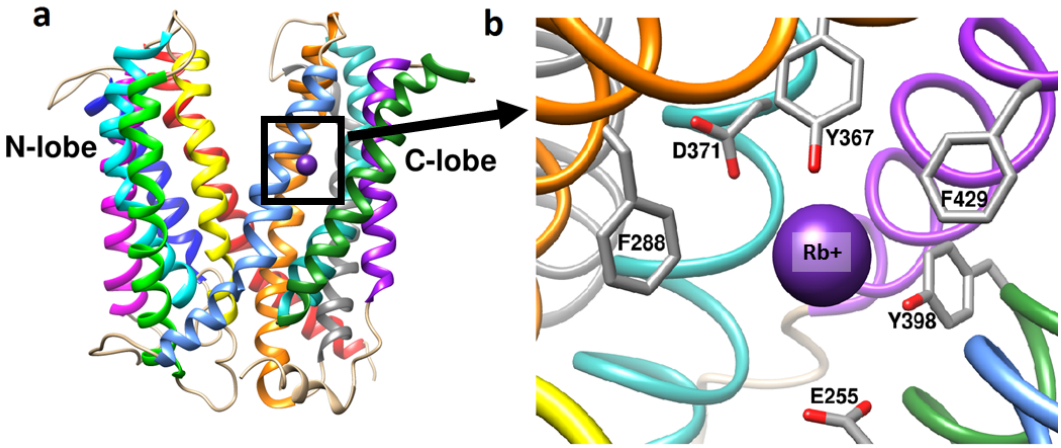

Fig. 5.3 **a**, The crystal structure of NorM-VC. The Rb^+-binding pocket is shown in the rectangle. **b**, The Rb^+ binding site in NorM-VC (3MKT) is shown. The three closest interaction distances are observed for F259, Y367 and F429. The carboxylate E255 and D371 are further away and might be differently positioned under physiological conditions, or might require a structural water molecule to coordinate the metal-ion.

Table 5.1 lists the residues that are believed to be important for drug/ion antiport in NorM-VC and NorM-PS.

Table 5.1 Residues important for drug/cation antiport in NorM-VC and NorM-PS

NorM-VC	**NorM-PS**	**Relevance (putative) in NorM-VC**
D36	D38	Cs^+/Rb^+-binding and perhaps structural maintenance
E255	E257	H^+/Na^+ binding and transport (empirical)
D371	D373	Rb^+-binding
N174	N176	Involved in Na^+-binding (empirical)
F259	F261	Contributes to Cs^+/Rb^+-binding site
Y367	F369	Contributes to Cs^+/Rb^+-binding site and perhaps the most important endogenous coordinating ligand for metal-ion binding
F429	L430	Contributes to Cs^+/Rb^+-binding site
S199	A201	Within H-bonding distance from D36

Interestingly, the pK_a of $D371^{NorM\text{-}VC}$ is predicted to be significantly affected by $Y367^{NorM\text{-}VC}$ (calculated using the online server H++). Furthermore, the oxygen atom of Y367 hydroxyl group is in close proximity to Rb^+/Cs^+, indicating its probable involvement in the metal-ion binding. Table 5.2 lists imporatnt residues that are predicted to contribute to the pK_a of $D371^{NorM\text{-}VC}$.

Table 5.2 Residues affecting the pK_a of D371

Residue in NorM-VC	**Contribution to the pka of D371**
Tyr144	0.19129
Glu255	0.783722
Tyr367	**1.64469**
Cys369	0.680222
Tyr398	0.917485

In addition to mutations in the C-lobe , the N174A$^{\text{NorM-VC}}$ mutation near D36 in the N-lobe is known to cause a drastic drop in the binding affinity for Na^+ [34]. This observation is supported by computational studies which predict the involvement of D36 in sodium movement through the protein [40]. Hence, it becomes important to also examine the differences in the D36-region between NorM-VC and NorM-PS. D36$^{\text{NorM-VC}}$ is surrounded by several polar amino acids (Figure 5.4).

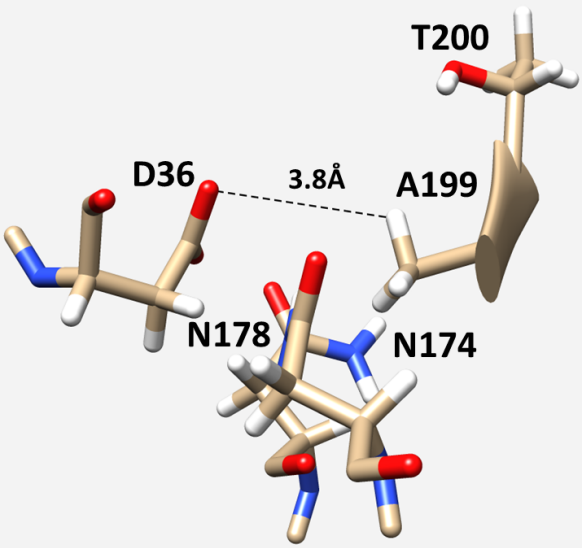

Fig. 5.4 Ala199$^{\text{NorM-VC}}$ closely approaches D36$^{\text{NorM-VC}}$, and is substituted by S201 in NorM-PS. It is likely that, by forming a H-bond, the serine residue raises the pk_a of the D38$^{\text{NorM-PS}}$ and causes the carboxylate to behave differently than its counterpart D36$^{\text{NorM-VC}}$.

All of the residues highlighted in Figure 5.4 are conserved in NorM-PS, with A199$^{\text{NorM-VC}}$ as the only exception that is substituted by S200$^{\text{NorM-PS}}$. The hydroxyl group of S200$^{\text{NorM-PS}}$ is very likely to be within hydrogen binding distance from D38$^{\text{NorM-PS}}$ and could be a factor in determining the ion-binding properties of NorM-PS. To test these hypotheses, a set of point mutants of NorM-VC and NorM-PS was prepared.

5.2 Restoration of the NorM-VC-like cation-binding site in NorM-PS does not alter the ion-coupling in NorM-PS

In order to investigate the amino acids in NorM-VC that contribute to its ion-binding properties, a range of rational ‘loss of function’ and ‘gain of function’ point mutations were introduced in NorM-VC and NorM-PS, respectively. Upon introduction of these

mutations, the mutant genes were subcloned and expressed in *L. lactis* cells. The ethidium transport assay was employed to test whether the mutants had an altered ability to interact with Na^+.

The introduction of F429L in the C-lobe of NorM-VC did not significantly affect the expression of the protein compared to the wild type protein (Figure 5.5).

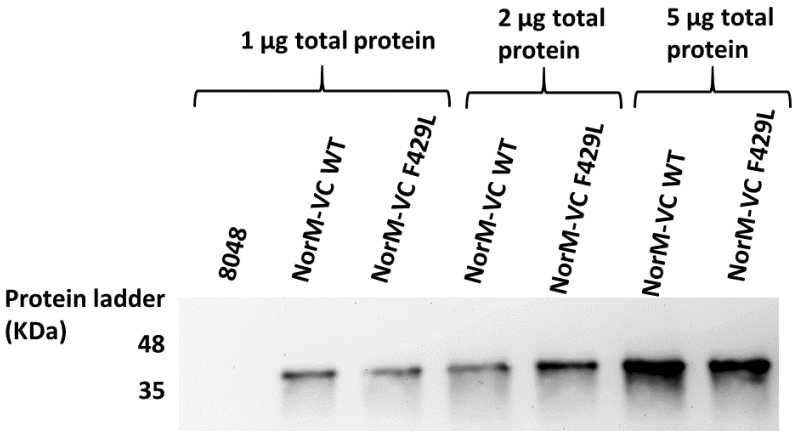

Fig. 5.5 The NorM-VC F429L mutant expresses to a level comparable with that of the wild type. 2 μg of total membrane protein was loaded onto each lane. The proteins were visualised using anti-His immunodetection.

In the ethidium transport assay (Figure 5.6), the F429L mutant was found to be transport-active. However, unlike wild type NorM-VC wild type, the ethidium efflux by the mutant was not stimulated by Na^+, indicating the loss of Na^+-binding in the mutant.

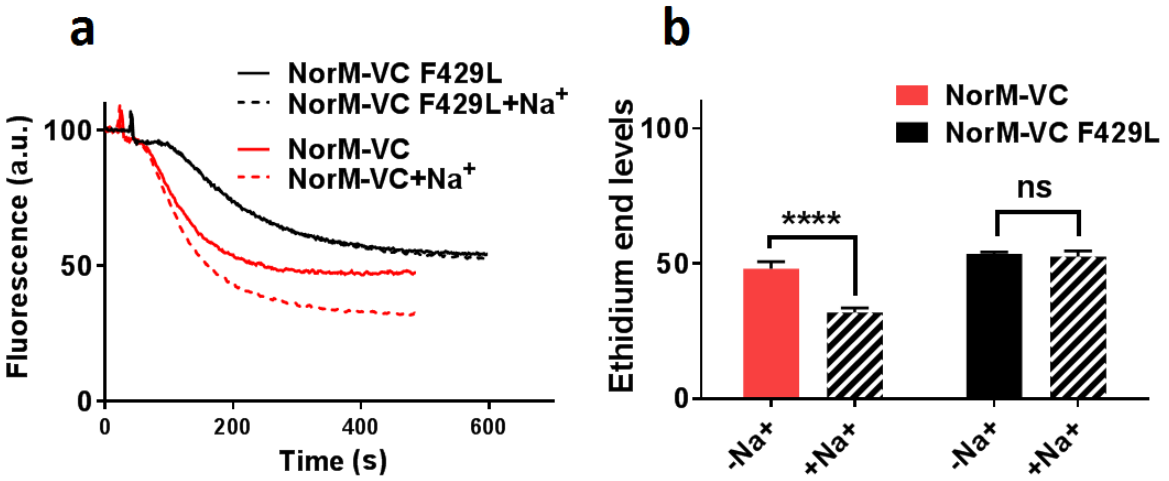

Fig. 5.6 F429 is a critical part of the Na^+-binding site in NorM-VC. Substitution of this aromatic residue by an aliphatic residue (leucine) causes loss of Na_+-dependent stimulation of ethidium export in whole cells. **a**, The traces shown are normalised for the initial fluorescence levels and are representative of the mean of the triplicates. **b**, The bars show end ($\pm$SD) ethidium fluorescence levels after extrusion without (no pattern) and with (ribbed) Na^+. N=3 (independent studies).

To confirm the involvement of F429$^{\text{NorM-VC}}$ in Na^+-binding, the NorM-VC F429L mutant protein was purified and the effect of Na^+ on the ethidium binding to the purified protein was tested in the fluorescence anisotropy assay.

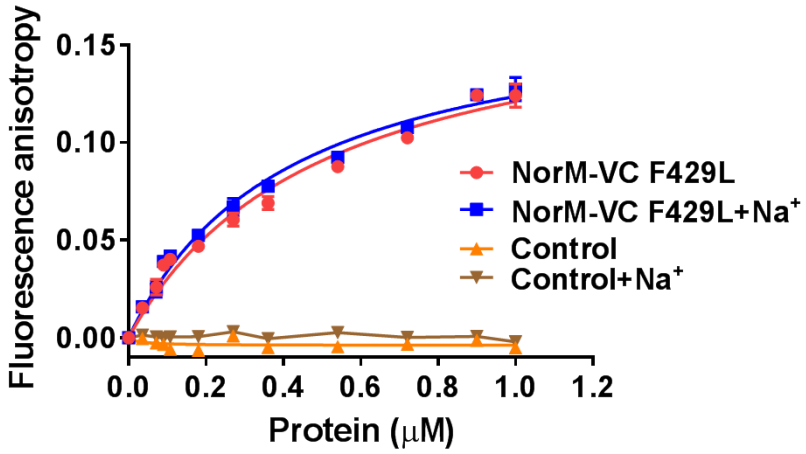

Fig. 5.7 The F429L mutation causes loss of Na^+-dependent stimulation of ethidium binding to NorM-VC. A fixed concentration of ethidium was titrated with increasing concentrations of purified NorM-VC. The fluorescence anisotropy was measured after each addition of protein. Equal amounts of elution buffer were added to generate the baseline (control). N=3 (independent studies).

In the anisotropy binding experiments, the affinity of ethidium for NorM-VC F429L with and without Na^+ was found to be statistically insignificant (k_d value=0.415 μM and 0.501 μM respectively). The loss of Na^+-stimulated transport in NorM-VC F429L shows that the Cs^+/Rb^+-binding site observed in the crystal structure [29], is physiologically relevant. These results emphasise the importance of the contribution of aromatic residues in metal-ion coordination, in addition to the commonly recognised charged- and polar-residues.

/sectionIntroduction of point mutations in NorM-PS

F429 was introduced at equivalent positions in NorM-PS (L426F$^{\text{NorM-PS}}$ and L430F $^{\text{NorM-PS}}$) to test whether the introduction of F429 in NorM-PS could make the transporter Na^+-responsive. Anti-His immunoblot showed that the mutants of NorM-PS used in this study expressed in *L. lactis* membrane to levels comparable with that of NorM-PS wildtype.

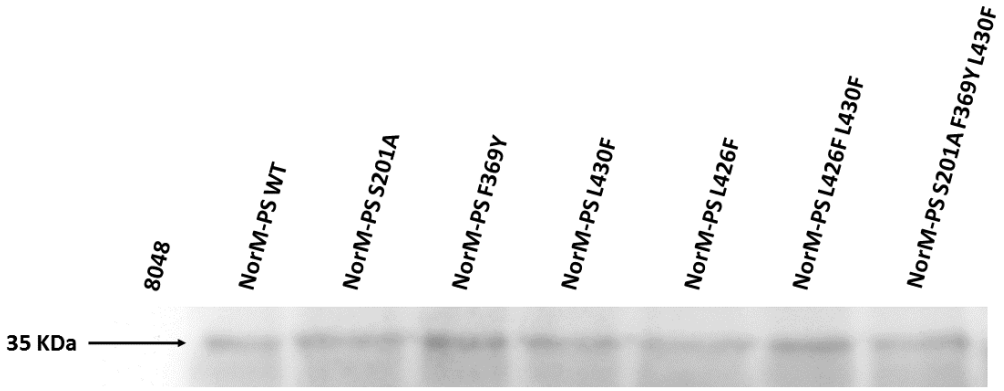

Fig. 5.8 Anti-His immunoblot showing the expression of NorM-PS mutants used in this study. 2 μg of total membrane protein was loaded onto each lane.

In ethidium efflux assay in whole cells, neither L430F nor L426F caused NorM-PS-mediated ethidium transport to be stimulated by Na^+.

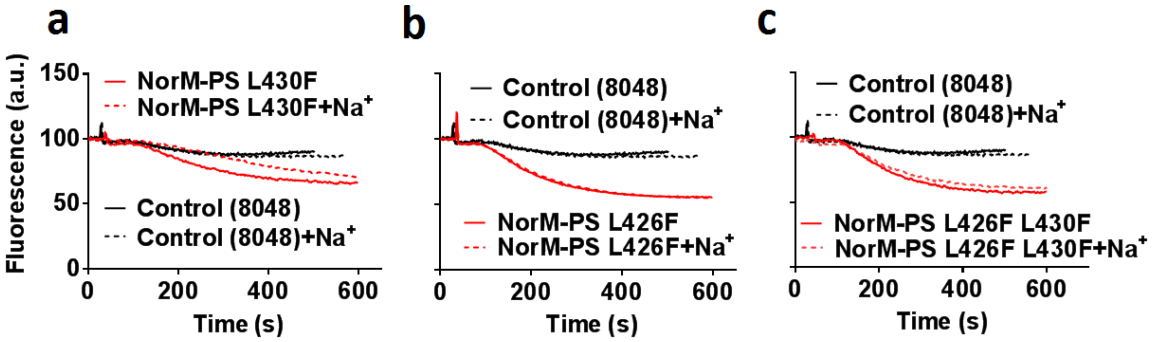

Fig. 5.9 **a** Insertion of F430, or **b**, F426 , or **c**, a combination of both does not confer Na^+-sensitivity to NorM-PS. The mutants were tested using ethidium export assay in *L. lactis* cells. The same control trace had been juxtaposed in all three graphs as all three results were part of the same study.

As previously mentioned, $Y367^{NorM\text{-}VC}$ interacts closely with the Cs^+ bound in the NorM-VC crystal structure, hence a F369Y mutation was introduced in NorM-PS and tested for its ability to facilitate Na^+-stimulated ethidium transport.

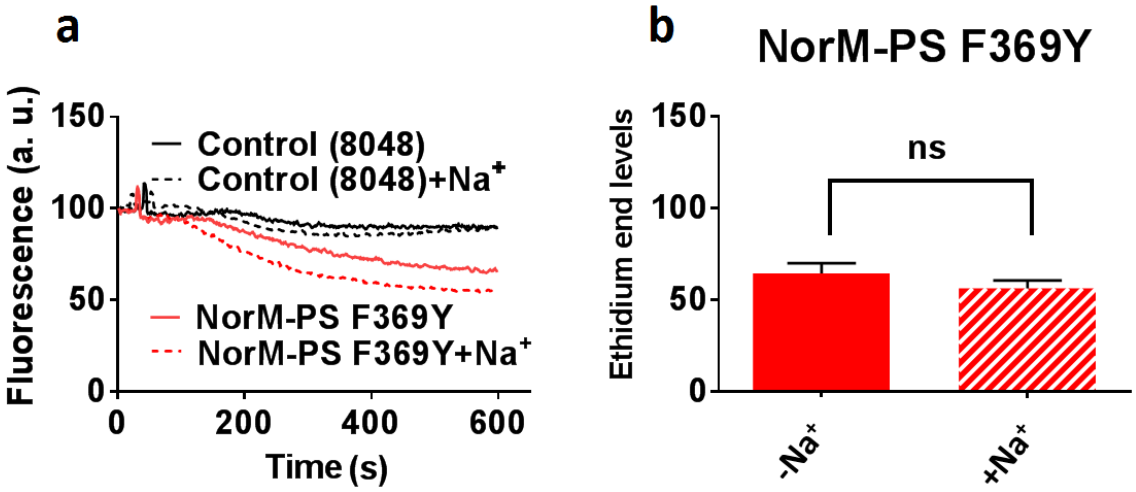

Fig. 5.10 **a**, The introduction of Y369 in NorM-PS does not confer any Na^+-dependence in ethidium export in whole cells. Notably, NorM-VC interacts with Cs^+/Rb^+ via the hydroxyl group of Y367 and in the crystal structures this side-chain appears to be most important endogenous ligand. **b**, No statistically significant enhancement of NorM-PS F369Y mediated ethidium transport was seen upon addition of Na^+. N=3 (independent studies).

As shown here, the F369Y mutation did not confer any significant Na^+ sensitivity to NorM-PS. This, combined with the information derived from L430F and L426F mutants, indicated that the differences between NorM-VC and NorM-PS in the C-lobe Cs^+/Rb^+-binding site alone are not responsible for the difference in the ion selectivity of these two transporters. Therefore, I investigated whether the $D36/N174^{NorM\text{-}VC}$ region in the N-lobe region could be could provide an explanation for the differences in Na^+-dependence of the two transporters. As mentioned earlier, $D36^{NorM\text{-}VC}$ ($D38^{NorM\text{-}PS}$) is in close vicinity to $A199^{NorM\text{-}VC}$($S201^{NorM\text{-}PS}$), but the $S200A^{NorM\text{-}PS}$ substitution did not impose any Na^+ dependence to NorM-PS-mediated transport.

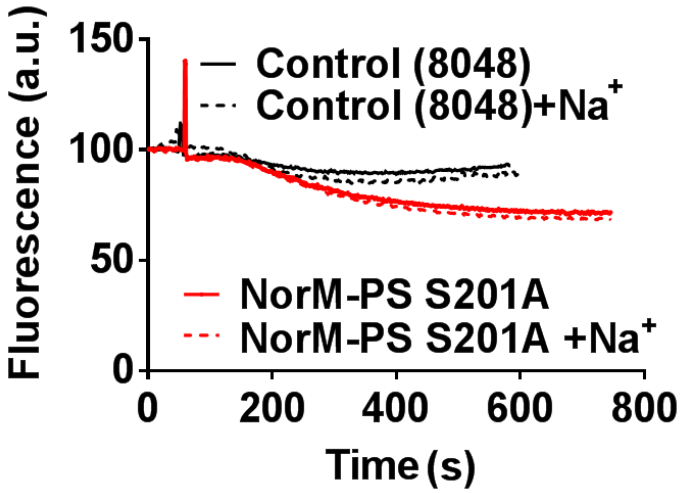

Fig. 5.11 The NorM-PS S201A mutant does not gain Na^+-dependency. In the X-ray structure of NorM-VC, A199 (counterpart of $S202^{NorM\text{-}PS}$) approaches D36 closely and it might be possible that in NorM-PS, S201 interacts with D38 too.

It can be speculated that if the Na^+-binding and transport events in NorM-VC require cooperation between the N- and C-lobe, then all of the above-mentioned mutations need to be introduced simultaneously in order to enable NorM-PS to bind and transport Na^+. To test the effect of the incorporation of these mutations in the N-lobe and C-lobe simultaneously, a triple point mutant was prepared and tested. As shown in Figure 11, a triple-mutant containing the mutations in the N-lobe (S201A) and C-lobe (F369Y, L430F) did not gain Na^+-dependence in the ethidium transport assay.

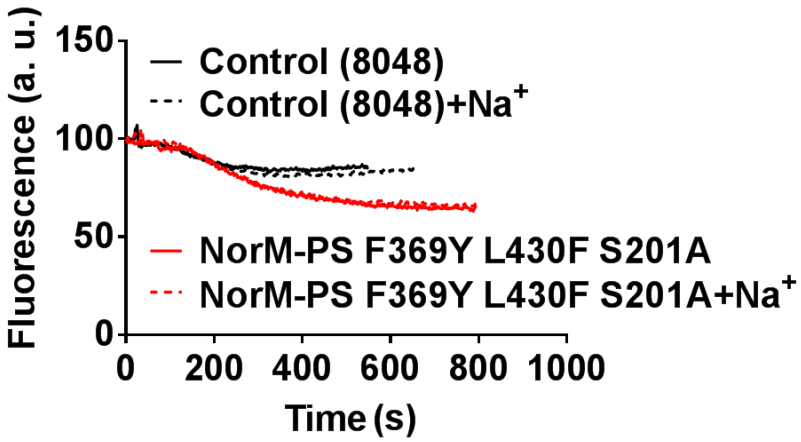

Fig. 5.12 Simultaneous mutations in the N- and C-lobe of NorM-PS do not result in Na^+-dependence of ethidium transport in *L. lactis* cells. The mutations were introduced with the objective of converting NorM-PS into a Na^+ dependent transorter.

The results shown here indicate that the Na^+-binding and transport in NorM-VC could not be transferred to NorM-PS through the introduction of a range of point mutations in the latter. Perhaps some of the main chain atoms in NorM-VC have interactions that are not feasible in NorM-PS due to differently oriented helices. With varying degrees of success, previous studies have attempted to alter the Na^+ versus H^+ selectivity of membrane proteins. A Na^+/K^+ pump from human blood cells that mediates Na^+/K^+ exchange by hydrolysing ATP was shown to mediate H^+/K^+ exchange reaction in absence of Na^+, and Na^+/H^+ exchange in the absence of K^+ [61]. The C-ring of the bacterial f_0/f_1-ATP synthases is notably well studied with regards to its promiscuity in H^+ and Na^+-coupling [62], and a range of hypotheses were suggested with regards to the question how the amino acid composition of the ion-binding site in the C-ring affects ion-selectivity. Furthermore, the flagellar motor system, BA-MotS, that can couple to both Na^+ and K^+, was shown to become strictly Na_+-coupled upon a single mutation [63]. Similarly, the flagellar stator MotB from alkaliphilic *Bacillus clausii*, which naturally has a promiscuous H^+ or Na^+-coupling behaviour, could be modified to couple to either H^+ or Na^+ exclusively by introducing two point mutations [59]. However, in the case of NorM-VC, the need for ion-coordination at the interface between two subunits and at different locations along the translocation pathway could make the situation more complex. It is not counter-intuitive that the number of mutations needed to alter the ion-specificity (or promiscuity) might be higher than in case of a system with a single ion-binding site. Furthermore, a more complex system is essentially more prone to disruption by mutations, and hence makes the identification of gain-of-function mutations more difficult. The loss of Na^+ depedendence in chimeric transporters shown in Chapter 3 indicates towards the same. Perhaps a high-throughput study would be more suitable to establish further structure-function correlations between NorM-VC and NorM-PS.

5.3 Δp or ΔpNa - which came first? An evolutionary conundrum

It is interesting to consider the evolution of the Na^+-dependent versus H^+-dependent transporters as it can provide insights into the question whether these two systems evolved independently or whether one is a downstream product of the other (a result of environmental demands). Also, another question is whether these systems are able to adopt each other's functionality. In other words, can a Na^+-dependent system always become a H^+-dependent system (and vice versa) by point mutation(s) or domain swapping?

From an evolutionary perspective, the primacy of one ion over the other has been a topic of debate. The proton motive force (Δp) appears to be the primary intermediate for energy conduction at present and is supported by the minimality of protonation as a chemical event. The minimality of protonation could have favoured the evolution of H^+-binding sites in proteins (and other macromolecules). However, the conductivity of biological membranes for H^+ is several orders of magnitude higher than for Na^+ [64]. This, combined with with the abundance of Na^+ in the prebiotic water (0.45 M NaCl), and the elevated temperature that make lipid bilayers too permeable for H^+, suggests that Na^+-gradient might have been more appropriate energy reservoir under these conditions.

Chapter 6

The pathway for Na^+ movement through NorM-VC

As described in Chapter 3, the Na^+-dependent stimulation of NorM-VC-mediated ethidium transport must involve both lobes of the transporter. Previously, molecular simulation and biochemical studies have shown that Na^+ binds in the D36 region and also near the E255/D371 dyad [40], [34]. A molecular simulation study predicted a physical cavity that acts as a pathway for Na^+-movement from the N-lobe to the C-lobe in NorM-VC in a parallel-lobed protein conformation that looks very different from the outward-open V-shaped crystal structure. To test that Na^+ does indeed first bind at $D36^{NorM\text{-}VC}$, ethidium export in NorM-VC D36N expressing cells was tested under different pH values in the absence or presence of ionophores and/or Na^+. The assay was done similarly as described in Chapter 4 for NorM-VC.

6.1 D36N mutation uncouples NorM-VC from Na^+-dependent ethidium transport

The ethidium export in NorM-VC D36N expressing cells (the immunoblot showing the expression of this mutant is present in Chapter 3, Figure 9) was tested at pH 6, 7, and 8 with or without 1 mM Na^+. To test the effect of different components of the Δp, the ionophores nigericin or valinomycin were added to provide cells with $\Delta\psi$ only or ΔpH only, or no Δp at all (control). In these experiments NorM-VC D36N exhibited significant ethidium export activity which was entirely dependent on the ΔpH. No activity was seen in presence of $\Delta\psi$. Also, the Δp-dependent activity was the same as the ΔpH-dependent activity. In essence, the electrogenic nature of the transport reaction was lost due to D36N mutation. Moreover, upon

addition of 1 mM Na^+, no enhancement of transport activity was seen. These results indicate that for NorM-VC to couple ethidium transport to Na^+, D36 is a critical residue.

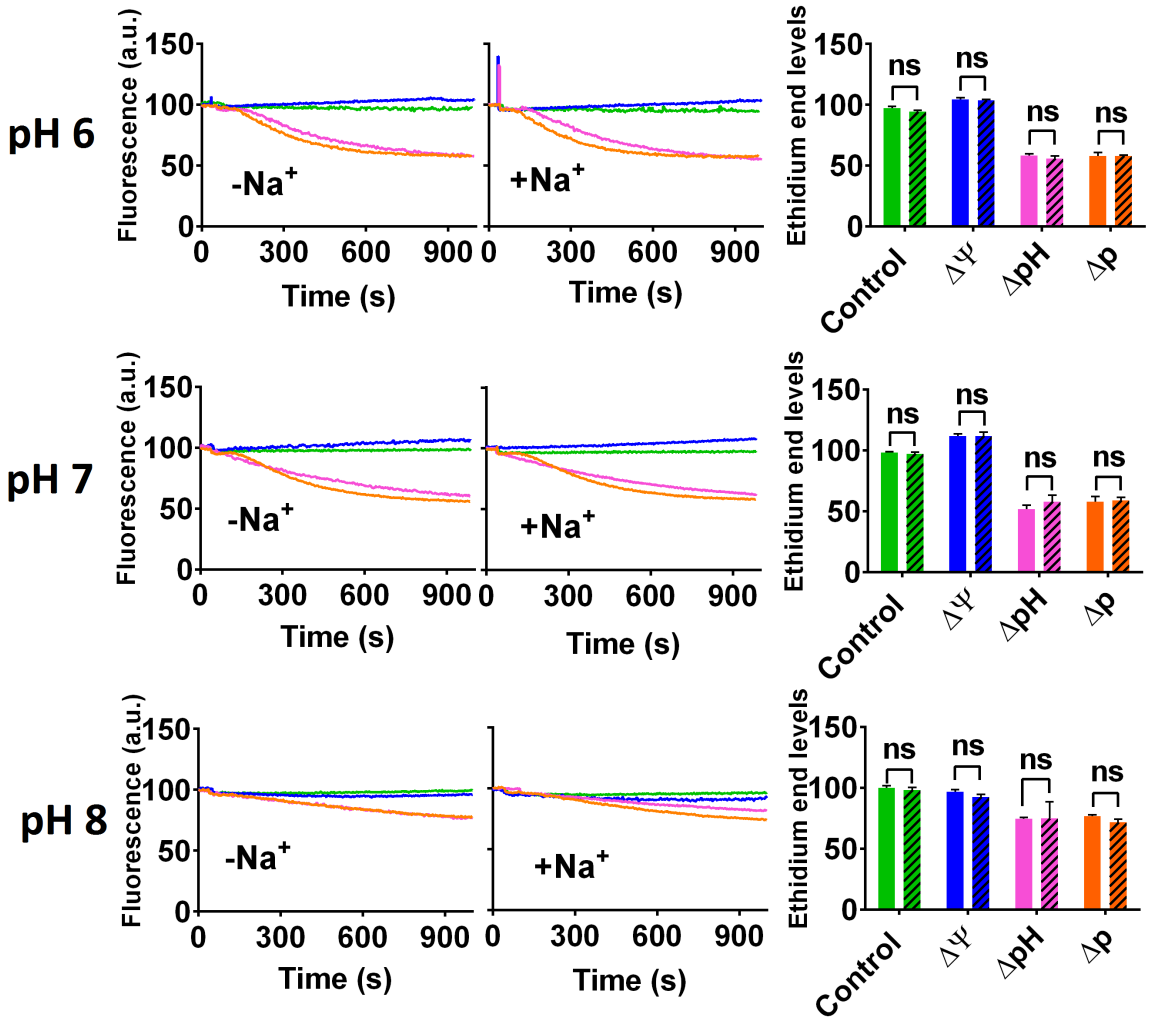

Fig. 6.1 NorM-VC D36N transports ethidium in an exclusively ΔpH dependent and electroneutral manner at pH 6, 7, and 8. At pH 8, unlike the wildtype, D36N mutant is not able to couple to ΔpNa in absence of the Δp. The traces shown here are closest to the mean value of triplicates. The bar charts on the right show mean (±SD) end ethidium fluorescence levels after extrusion. N=3 (independent studies).

To test the effect of the D36N mutation on ethidium-binding behaviour of NorM-VC, fluorescence anisotropy measurements with purified NorM-VC D36N protein were made. The effect of Na^+ was also tested by including 1 mM Na^+ in the buffer.

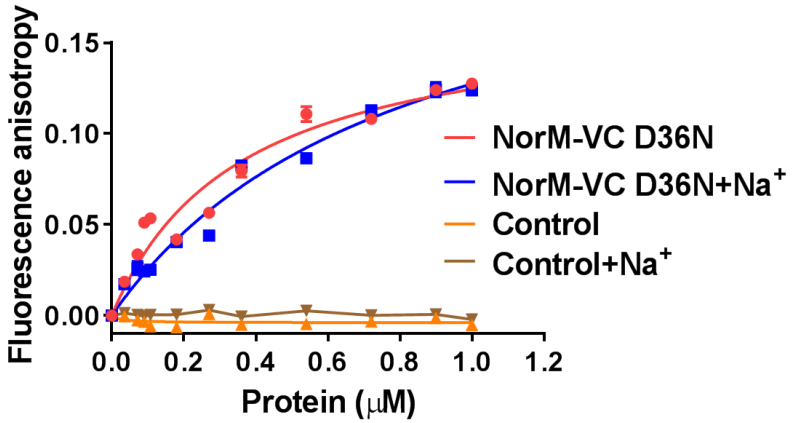

Fig. 6.2 The D36N mutation in NorM-VC causes disruption of Na^+-dependent stimulation of ethidium binding. As shown in Figure 3.7b, wildtype NorM-VC exhibits a significantly increased binding affinity for ethidium in the presence of Na^+. However, the D36N mutation leads to disruption of this stimulation in ethidium binding, indicating the importance of D36 in Na^+-binding to NorM-VC. N=3 (independent studies).

The ethidium binding results indicate that NorM-VC D36N binds ethidium with an affinity comparable to the wildtype without Na^+(K_d =0.357 ± 0.056^{D36N} mu*Mcomparedto*0.5620.037^{wildtype}$*mu*M No improvement in affinity for ethidium was seen in the presence of Na^+. On the contrary, there was an apparent drop in affinity under these conditions (K_d+Na^+= 0.811 ± 0.120 mu*M*).*Theseresultsindicatethatwhile*D36*maynotbeapartoftheethidium* − *bindingsiteinNorM* − *VC*, *itisapartofa*Na^+ − *bindingsite*.*Since*D36*isverycloseto theextracellularterminusofTMH*1, *itmightbeo*

6.2 A novel (putative) Na^+-binding site in NorM-VC

All structures of Na^+-coupled MATE transporters to date show the transporters in outward-open states, making it difficult to envisage how Na^+ moves from the N-lobe (D36 region) over to the C-lobe (E255/D371-dyad) in NorM-VC. In the outward-open crystal structure, the distance between D36 and D371 is about 25 Å, which is too large for any type of interactions to take place between the two residues. For the N-lobe to 'hand-over' the bound Na^+ to the C-lobe, the extracellular sides of the two lobes must come together - a configuration possible in the inward-open state. A possible solution to this problem is an alternative protein

conformation where the distance between the extracellular sides of the N- and C-lobes becomes shorter. To visualise such a conformation, a homology model of NorM-VC were prepared based on the MurJ crystal structure (described in Chapter 4). The MurJ-based homology model helps to visualise the inward-open state of NorM-VC. Interestingly, E255 which is sequestered in the outward-facing crystal structure (solvent accessible area = 35.5 $Å^2$) becomes relatively more solvent accessible in the MurJ based homology model (solvent accessible area = 79 $Å^2$). The exposure to the alkaline internal environment of the cell may allow E255 to become deprotonated, a very important event in the transport cycle. The solvent accessibility values were calculated using the online server Stride [65].

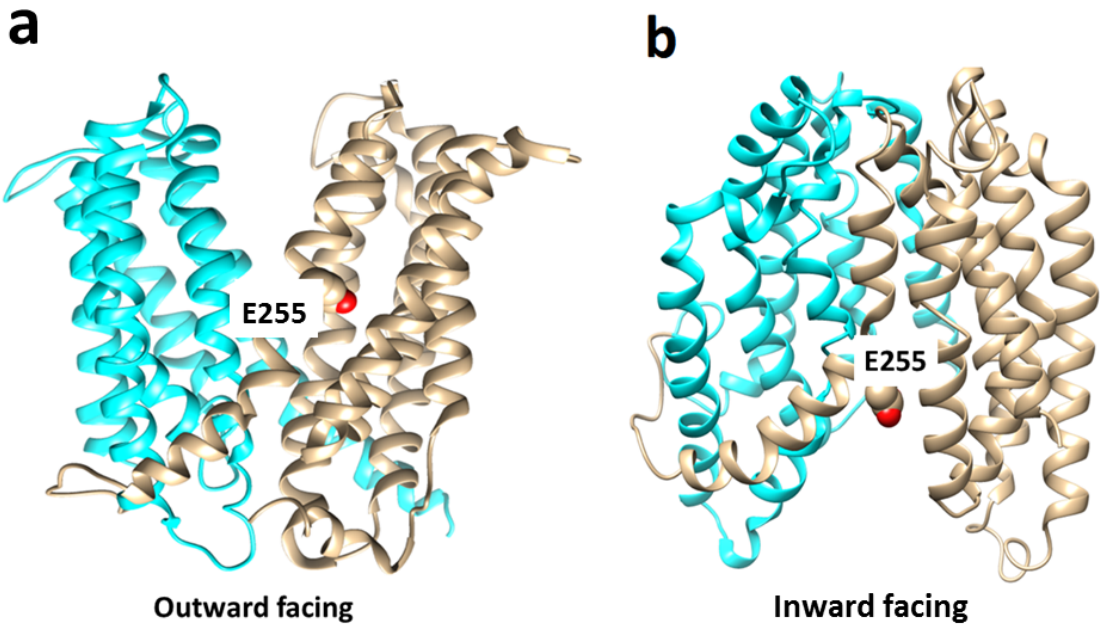

Fig. 6.3 $Glu255^{NorM\text{-}VC}$ is occluded in the outward-open state but becomes exposed to internal alkaline environment of the cell in the inward-open state. **a**, The X-ray crystal structure of NorM-VC (PDB ID: 3MKU). **b**, The MurJ-based homology model of NorM-VC. N-lobe shown in cyan ribbon and C-lobe shown in golden. E255 is shown as spheres.

In the NorM-VC crystal structure, D36 along with N174 and N178 might form a Na^+-binding site in the outward-open state. However, in the inward-open homology model, D36 (TMH1) and the two amides N174 and N178 (TMH5) move away from each other due to the movement of TMH1 towards TMH8 in the C-lobe (see cartoon below). The proximity of TMH1 and TMH8 is predicted to create a new Na^+-binding site that involves D36 and the Q278/N282-dyad at the extracellular side of the C-lobe. The distances between these two centres are short enough to allow them to coordinate the binding of Na^+.

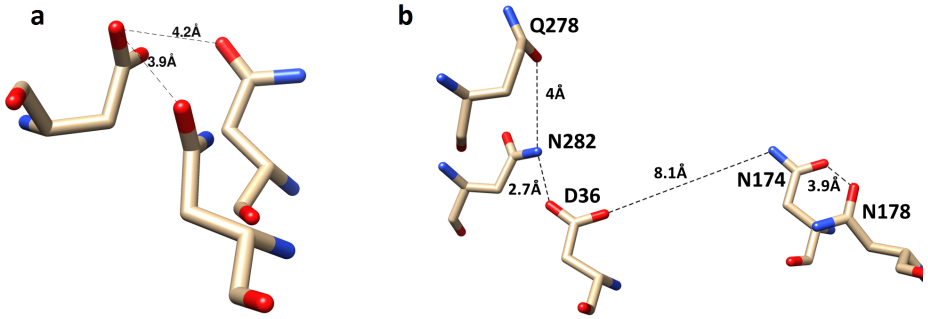

Fig. 6.4 Formation of a putative Na^+-binding site at the extracellular interface of N-lobe and C-lobe in the MurJ-based inward-open homology mode of NorM-VC. a, D36 closely interacts with N174 and N178 in the outward-open state. b, In the inward-open state, the D36 harbouring TMH1 rotates away from N174/N178 and approaches TMH8 which harbours two amides, Q278 and N282 positioned at an equivalent position as N174 and N178 in TMH5. This new arrangement of D36-Q278-N282 might allow the formation of a new Na^+-binding site at the interface between the N- and C-lobe in the inward-open conformation.

6.3 The amides Q278 and N282 are important for Na^+-coupling in NorM-VC

The possibility of a new Na^+-binding site in the inward-facing state provides scope for the Na^+ bound at the N-lobe helices to be transferred to C-lobe helices. To test this hypothesis, single point mutations were introduced to create NorM-VC Q278A and NorM-VC N282A. These two mutants were successfully expressed in the plasma membrane of *L. lactis* and the ethidium transport assay was used to test the effect of the mutations on the Na^+ sensitivity of NorM-VC.

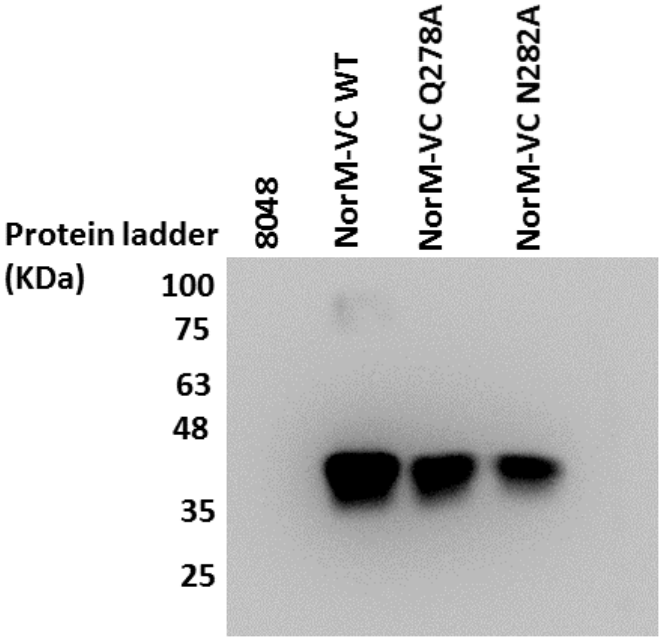

Fig. 6.5 Anti-His immunoblot showing the expression of NorM-VC WT, Q278A, and N282A in the plasma membrane of *L. lactis*. 2 μg of total membrane protein was loaded onto each lane. The non-expressing cells 8048 were used as negative control.

The activity of the amide (Q278 and N282) to alanine substitution mutants was tested in ethidium transport assays in intact cells. As shown in Figure 6.6, the NorM-VC Q278A mutant has similar activity as the wildtype, but the addition of 1 mM Na^+ does not cause stimulation of the ethidium export activity. The NorM-VC N282A mutant is less active than the wild type - which might be due to lower expression levels. However, similar to the Q278A mutant, the activity of N282A mutant is not stimulated by the addition of Na^+. Thus, both point mutations impair the stimulation of ethidium transport by Na^+.

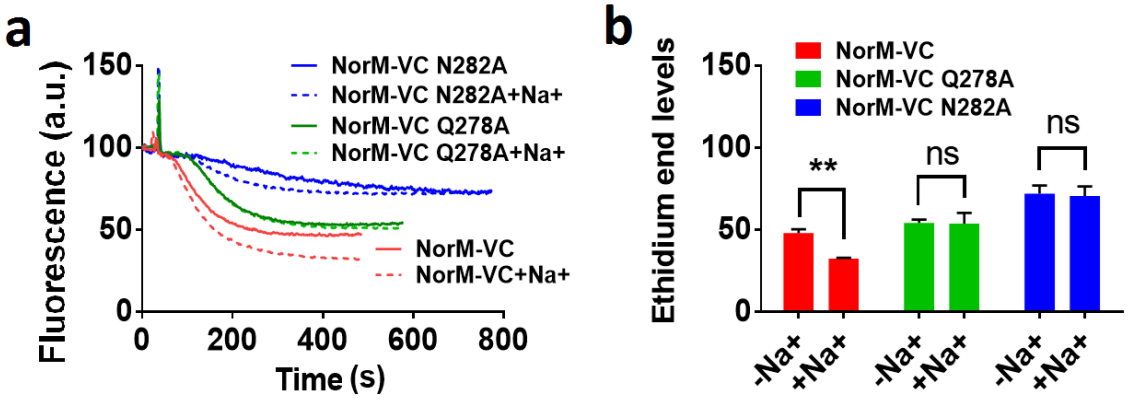

Fig. 6.6 The NorM-VC Q278A and N282A mutants lose Na^+-coupling, while still retaining either full (Q278A) or diminished (N282A) Δp-dependent ethidium export activity. NorM-VC WT was used as positive control. The fluorescence traces shown on the left are representative of 3 independent measurements, whereas the bar chart on the right shows mean values (± SD) of the fluorescence end levels.

To further confirm the loss of Na^+-binding to the NorM-VC Q278A and N282A mutants, the proteins were purified in DDM-containing buffer solution. Ethidium binding to purified mutant proteins was then measured in fluorescence anisotropy assays as described in the previous chapters. The addition of 1 mM Na^+ to the assay buffer did not cause any change in the ethidium binding behaviour of these mutants. For NorM-VC Q278A mutant, the apparent K_d values without and with Na^+ were 0.19 ± 0.05 μM and 0.32 ± 0.07 μM, respectively. For NorM-VC N282A mutant, the apparent K_d values without and with Na^+ were 0.13 ± 0.02 μM and 0.08 ± 0.02 μM, respectively. This is different from the wildtype where addition of Na^+ leads to a 10-fold increased affinity of NorM-VC for ethidium (see Chapter 3, Fig. 3.7).

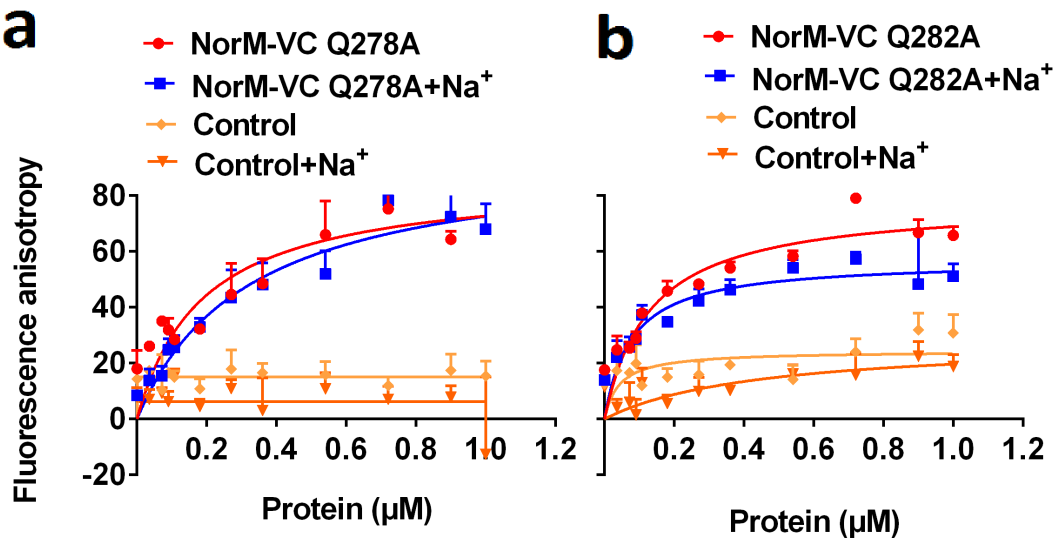

Fig. 6.7 Purified NorM-VC single point mutants Q278A **a**, and N282A **b**, lose Na^+-dependent stimulation of ethidium binding. Elution buffer was used as control to generate the baseline anisotropy. N=3 (independent studies).

The results shown above provide evidence for the involvement of residues Q278 and N282 in Na^+-binding and transport events in NorM-VC. Although, it is possible that the phenotypes observed here might be due to indirect effects of the mutations, I propose that these residues form a central Na^+-binding site in the translocation pathway for Na^+ that connects the otherwise distant Na^+-binding sites in the N- and C-lobes during the transition from the outward-open to the inward-open state. In the next chapter, all these observations are combined and a transport model, that explains the observations made on NorM-VC in this thesis, is discussed.

Chapter 7

Discussion and future directions

Membrane transporters in the MATE family have significant physiological and clinical relevance yet our current understanding of their structure-function relationship is very limited. It cannot be emphasised enough that the key to understanding these transport systems might be hidden between details and nuances. While it is very convenient to assume that two highly homologues proteins have very similar structures and similar functionality, my studies on NorM-VC and NorM-PS show that despite being very similar at the sequence level, these two systems show major differences in energy coupling. NorM-PS strictly depends on H^+ gradients and carries out a simpler H^+/ethidium antiport reaction with no net transloction of charge. In contrast, NorM-VC is more versatile in terms of its coupling-ion requirements and can utilise either Na^+ or H^+ gradient or both simultaneously. This versatility makes the dissection of the overall reaction more complex. Although the X-ray structure of NorM-VC provides a good starting point, the questions regarding the binding sites for the drugs, H^+, and Na^+ and their transport are essentially pertaining to dynamics in nature. For example, in the crystal structure, the cation-binding site was seen in the C-lobe of NorM-VC but the chimeric proteins characterised in this thesis indicate that the transport must involve a pathway composed of a sequence of sites in both the N-lobe and C-lobe. Also, it is very important to understand how these binding events affect each other and in what order they take place.

7.1 A novel transport model for NorM-VC

Based on the observations made in this thesis, a transport model is presented here. This model incorporates H^+, Na^+, and substrate binding and dissociation in the transport cycle. The following steps describe the events as they might take place per transport cycle:

Step 1 Binding of a proton and switch to the inward-open conformation: The Na^+ binds at the D36 region, coordinated by D36, N174, and N178 (perhaps also by T200 [66]). The binding of a H^+ at the $E255^{TMH7}$/$D371^{TMH10}$-dyad makes the carboxylate groups of these two residues come closer and form a H-bond, which leads to introduction of a kink at G245 (GFP motif in TMH7). This event is similar to the TMH7 bending in plant MATE AtDTX14, and is also analogous with the helix-bending event in pfMATE [36] where P26 and G30 in TMH1 form a flexible switch that can introduce a helix kink at acidic pH. The bending of TMH7 in NorM-VC causes a dramatic conformational switch to the inward-open state. Based on the currently available data, it is difficult to say whether the binding of the two coupling-ions (Na^+ and H^+) is ordered, and if so, which ion will bind first. If the crystal structure of outward-facing NorM-VC is taken as the initial conformation in the transport cycle, then a simple cavity analysis can provide a clue which of the two ions has easier accessibility to its binding site. To look for cavities in NorM-VC structure, the online server CastP 3.0 [67] was used. A probe of radius 1.4 Å (radius of the water molecule) was used to search for cavities. The results provided by CastP 3.0 include the cavity volume, area, number of openings and the exposed residues. NorM-VC appears to have numerous cavities of which only two are near D36 and N174 (the first binding site for Na^+ from the extracellular side). Both cavities, occluded by surrounding helices, lack openings and are inaccessible to Na^+.

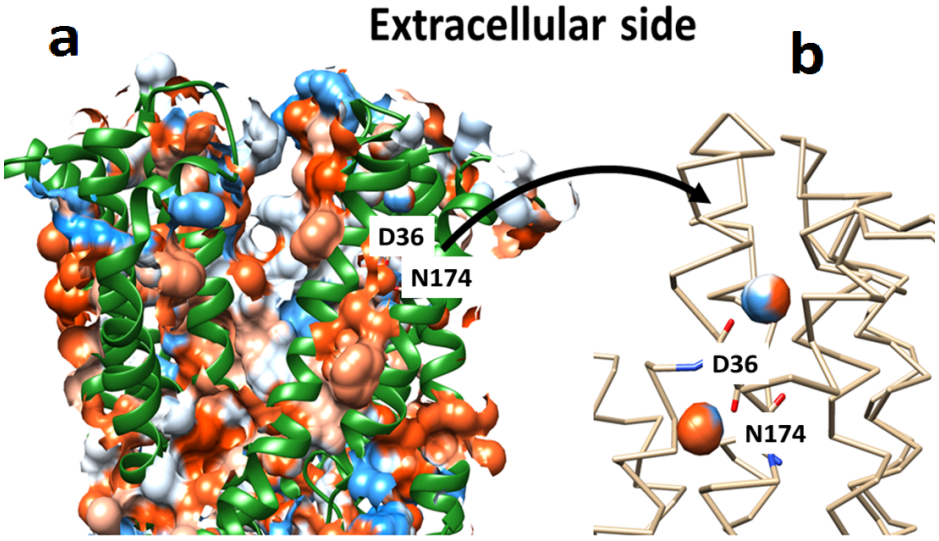

Fig. 7.1 Cavity surface of NorM-VC crystal structure (PDB ID: 3MKU). **a**, Of all the cavities formed in NorM-VC, only two occluded cavities are formed near D36 and N174. **b**, the cavities close to D36 and N174 are small in volume (15^3 Å, each) and have no openings.

On the other hand, the H^+-binding site formed by E255/D371 is accessible via the biggest cavity in the outward-open conformation. This cavity is open to the extracellular environment and hence a proton ($H3O^+$) could directly approach the E255/D371-dyad from the outside. It is therefore possible that the binding of H^+ is the precondition for Na^+-binding to NorM-VC.

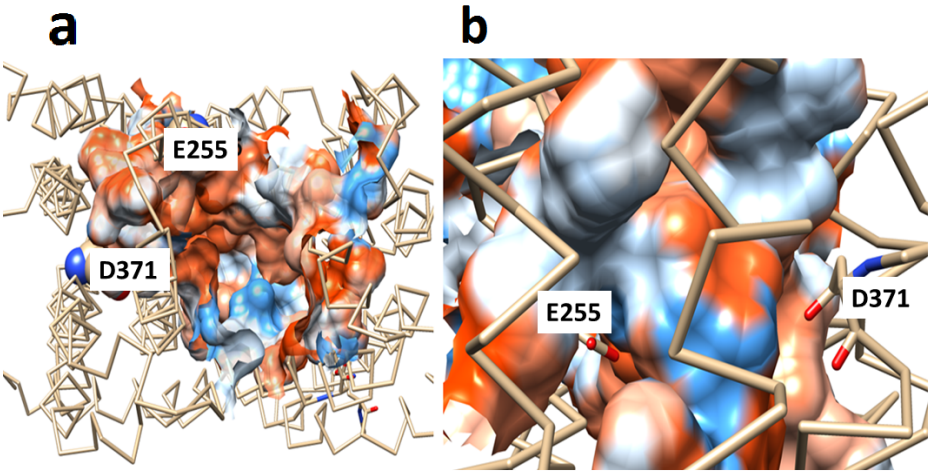

Fig. 7.2 **a**, in NorM-VC (PDB ID: 3MKU),a large cavity with four openings exposes E255 and D371 to the external aqueous environment.**a**, the cavity as seen from the top. **b**, Close-up view showing these two residues exposed to the cavity.

Step 2 The intermediate/transition state with Na^+-binding at the extracellular interface: The inward-open state brings the extracellular sides of the N-lobe and C-lobe together. A novel higher affinity Na^+-binding site is formed involving TMH1 (D36) and TMH8 (Q278 and N282). The semi-parallel structure of DinF-BH (PDB ID: 4LZ6) shows similarly proximally spaced extracellular sides of TMH1 and TMH8 too. Na^+ binds at this newly formed binding-site on its way from the D36 centre in the N-lobe to the final binding-site at the E255-D371 centre in the C-lobe.

Step 3 Release of H^+ and substrate binding: The switch from the outward-open state to the inward-open state exposes E255 to the alkaline interior. The H^+ that was shared by E255 and E371 dissociates and is replaced by the incoming Na^+ from the D36-Q278-N282 site. H^+-release and Na^+-binding create a high-affinity binding site for the drug molecule (ethidium). Previously, molecular dynamics simulations suggested that in order for Na^+ to bind, D371 should be protonated and E255 should be deprotonated [39]. Yet, experimentally it has been shown that deprotonation at D371 leads to ethidium binding. Na^+- and ethidium-binding events must overlap temporally for Na^+ to promote ethidium-binding to NorM-VC. Hence it can be deduced that H^+-release coincides with Na^+ and ethidium-binding as observed in biochemical experiments [34].

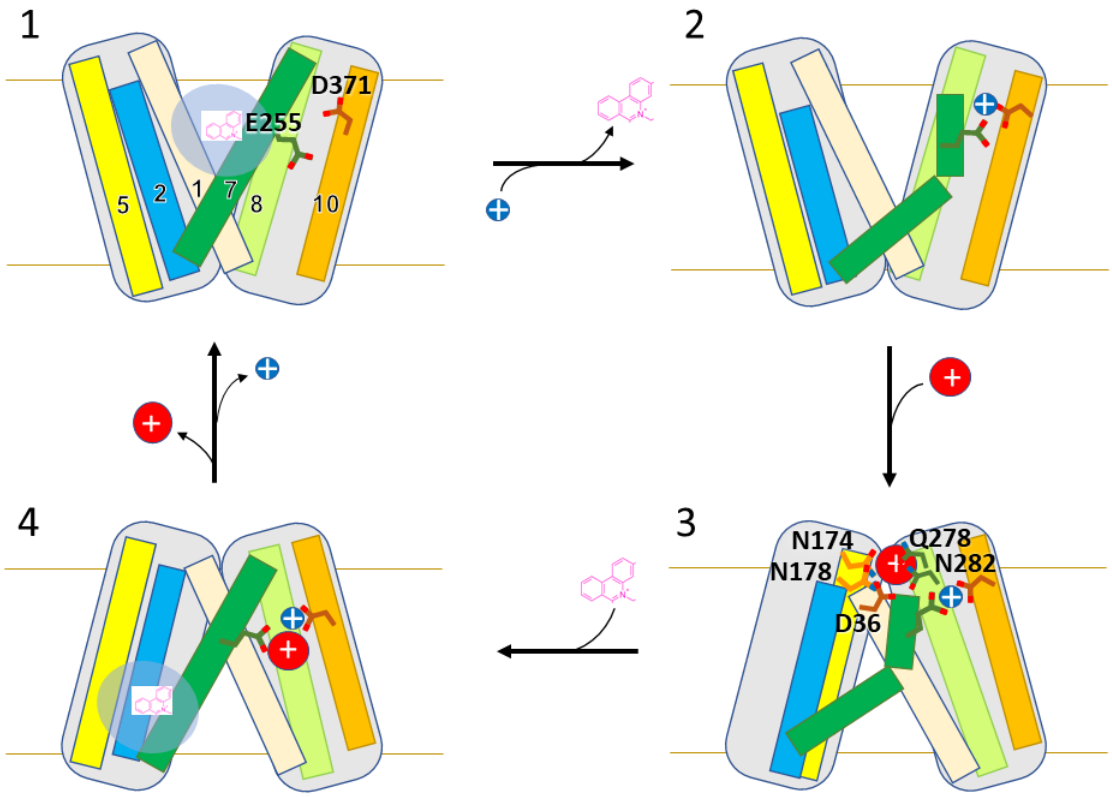

Fig. 7.3 A cartoon representation of the proposed NorM-VC transport model. Red ball=sodium ion, blue ball=proton, numbered cylinders represent transmembrane helices and the amino acid residues taking part in transport cycle are numbered.

Step 4 The substrate and Na^+ are released and the initial conformation is restored: H^+-release causes the transporter to switch back to the outward-open state which has lower affinity for the bound substrate and Na^+. The substrate is released into the exterior whereas Na^+ is released into the cellular interior, and the transporter assumes the original conformation – ready to undergo another transport cycle.

This model explains most of the empirical observation for NorM-VC and places all the players (H^+, Na^+ and drug molecule) together from a functional perspective. Based on this model, the positive cooperation between Na^+ and ethidium binding and the competition between H^+ and ethidium binding can be explained. The cooperativity between the N- and C-lobes for Na^+-binding explains why the NorM-VC and NorM-PS chimeras (discussed in Chapter 3) do not show Na^+-dependent stimulation of the ethidium transport activity.

The stoichiometry of 1 Na^+-1 H^+-/ethidium$^+$- antiport in the model suggests the existence of three driving forces for ethidium transport by NorM-VC from cells: (i) ΔpH (interior alkaline), (ii) $\Delta\psi$ (interior negative), and (iii) the chemical concentration gradient of ethidium

(ΔpEthidium, interior high). Under physiological conditions during normal drug efflux with low interior ethidium concentration, the ΔpEthidium will actually be inhibitory for drug efflux. With an established apparent K^d for Na^+ of 4.7±0.6 μM [34] , the affinity of NorM-VC for Na^+ is so high that the contamination of Na^+ in cell suspensions will be sufficient to support transport even when the ion is not added to my biochemical buffers. In my experiments in Chapters 3 and 4, the ethidium efflux reaction in cells was found to be dependent on the ΔpH plus $\Delta\psi$ at pH 7 and 8. Addition of Na^+ to the buffer, thus creating a ΔpNa (interior low), further stimulated ethidium efflux. Under conditions where the ΔpH prevails in cells (pH 6), the efflux reaction showed a bias towards the ΔpH. The lack of coupling to the $\Delta\psi$ in the presence of the ionophore nigericin at pH 6.0 might be a consequence of the very low internal pH (pH^{in} = pH^{out} under these conditions, which is inhibitory for NorM-VC and other membrane transporters. Following the initial and ground-breaking studies on the lactose-proton symporter LacY [68], it is generally assumed that secondary-active membrane transporters are molecular machines that operate with a fixed ion coupling stoichiometry under all environmental conditions. It is the differences in the availability of driving forces under the various experimental conditions that creates an experimental bias towards one driving force over another. Most of my data can be explained if the stoichiometry of NorM-VC is fixed at 1 Na^+-1 H^+/ethidium$^+$ antiport. However, the possibility still exists that NorM-VC contains promiscuous ion binding sites that can interact with Na^+ and/or H^+ in a fashion that depends on their availability. The existence of promiscuous Na^+/H^+ binding sites has been studied in other membrane proteins before [62]. In this scenario, it is conceivable that at higher pH values the ratio of Na^+ over H^+ changes and more Na^+ is transported than H^+. In other words, the H^+ binding sites in NorM-VC would act as Na^+ binding sites at basic pH.

Although all the key residues relevant for this model are conserved in NorM-PS, it can be reasoned that there are additional structural features, such as helical rotations or main-chain interactions that allow NorM-VC to transport Na^+ and are not available in NorM-PS.

In support of this model, molecular dynamics simulations have suggested that Na^+-binding in NorM-NG involves D41 ($D36^{NorM\text{-}VC}$), D52, D355, and D356, before Na^+ finally moves to the cation-binding site at E261 ($E255^{NorM\text{-}VC}$) [69]. Also, the same study reported that a D41A mutation completely abolishes the binding of the Na^+ - a finding consistent with the experimental data on NorM-VC D36N in this thesis. During the final stages of the research presented here, a new EPR spectroscopy study provided information on the conformational changes occurring in NorM-VC upon binding of H^+ and Na^+ [66]. The distance measurements show that Na^+-binding and substrate-binding stabilise two mutually exclusive states (outward-open and inward-open, respectively). But the results with ethidium

anisotropy results in Chapter 4, along with the ethidium-monoazide binding studies [34] and the EPR studies on Ruboxyl binding to NorM-VC [43], clearly show that Na^+ and substrate binding to NorM-VC are not mutually exclusive, in fact, the presence of Na^+ promotes the binding of ethidium to NorM-VC. This observation is also consistent with the non-overlapping binding-sites for Cs^+ and TPP in NorM-NG.

The H^+- and Na^+-coupled drug transport model presented here has the potential to be applicable to other MATE transporters. As discussed in Chapter 1, MATE transporters have a conserved sequence motifs (the GXP motif in TMH-7) and carboxyl residues. The model allocates functional relevance to these structural features. For example, the human MATE transporter, hMATE1 might function by the same carboxylate-dyad protonation and TMH7-bending mechanism. It is possible that in absence of a $D36^{NorM\text{-}VC}$ equivalent carboxylate, hMATE1 functions as a H^+/$drug^+$ antiporter. This antiport reaction might be analogues to the electroneutral antiport carried out by the NorM-VC D36N mutant.

The DinF-family MATE transporters achieve a similar mechanism by forming a carboxylate dyad in the N-lobe and the 'structural spur' comes from the bending of TMH1, a feature that accentuates the existence of two-fold structural and functional symmetry in MATE transporters. The transport-active chimeric MATE proteins discussed in Chapter 3 also point towards a functional symmetry between the N- and C-lobes in MATE transporters.

The results presented in this thesis also provide insights into the ecological relevance of the ion-coupling versatility exhibited by NorM-VC. As discussed in Chapter 4, under alkaline conditions, the Δp-independent, Na^+-coupled ethidium transport by NorM-VC indicates toward an adaptive feature in NorM-VC that might enable *Vibrio cholera* to thrive in constantly fluctuating pH and saline conditions in the estuaries where this bacterium resides.

7.2 Future research directions

The following section contain a brief account of the potential studies that can be carried out to better probe the transport cycle and overall structural dynamics in NorM-VC and NorM-PS.

1. To determine of the protonation states of the catalytic carboxylates in NorM proteins: The protonation of carboxylate residues in membrane proteins has been studied before and one of the successful approaches is the dicyclohexylcarbodiimide (DCCD) labelling of the proteins [70]. DCCD reacts with protonated (especially membrane-buried) carboxylates and the label can be detected by means of mass-spectrometric techniques. DCCD treatment was shown to inhibit the facilitated influx of ethidium by NorM-VC (reverse transport) in deenergised *L. lactis* cells (Figure 7.4). However, due to incomplete digestion of the purified DCCD-labelled protein, the mass spectrometric coverage was poor and identification of the labelled carboxylate(s) was inconclusive. Cyanogen bromide (CNBr) has been found to be more effective at cleavage of membrane proteins and hence the experiments can be repeated with CNBr cleavage of DCCD labelled NorM-VC (or NorM-PS). Since NorM-PS has the same catalytic carboxylates as NorM-VC but only antiports one H^+ per cycle, it will be interesting to know which of the three carboxylates (D38, E257, and D373) has catalytic importance in proton coupling. DCCD labelling could be used for this purpose. The effect of single, double, and triple carboxylate substitutions (NorM-PS D38N, E257N and D373N) on ethidium transport activity of NorM-PS expressing *L. lactis* cells was tested by me; the preliminary results require further repeats. In a previous study, substitution of any of these three carboxylates by amides led to disruption of the DAPI/H^+ antiport activity by mutant proteins [42]. In the same study E257 and D373 were found to be important for substrate binding and D38 was stated to be involved in H^+-coupling, which is not analogous with their counterpart residues in NorM-VC.

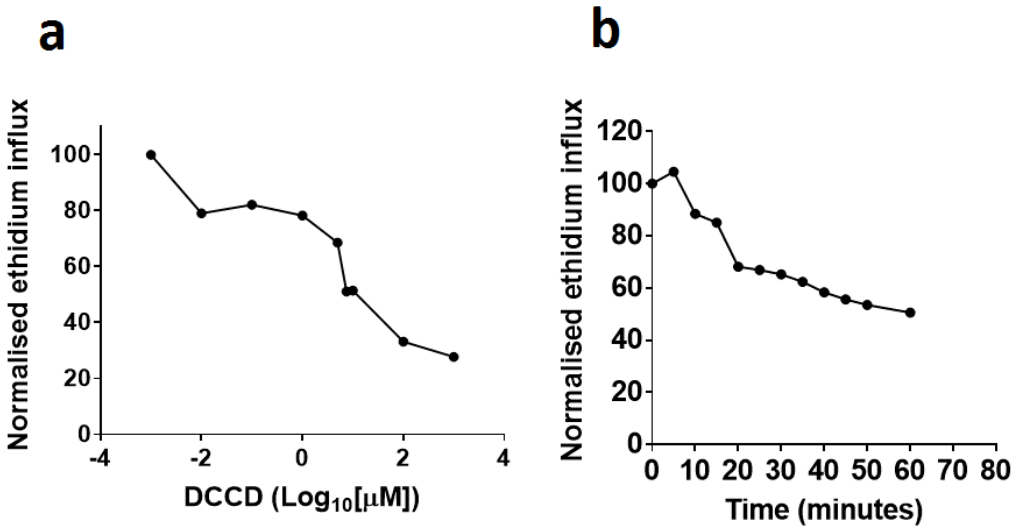

Fig. 7.4 DCCD reacts with NorM-VC and inhibits proton-coupled NorM-VC mediated influx of ethidium in deenergized cells in a dose-dependent **a**, and time dependent **b**, manner. NorM-VC expressing *L. lactis* cells were incubated with varying concentrations of DCCD, after which 2 μM ethidium bromide was added to the buffer. The ethidium accumulation rate in the linear phase was then determined and normalised against the rate of influx in the no-DCCD control.

2. To probe the structural switch in NorM transporters: Different opinions exist in the published literature on whether all MATE transporters function by the same conformational switch as that of pfMATE (protonation-driven helix bending) or not. MATE transporters appear to conserve a $G(X)_nP$ motif in helices that harbour catalytic carboxylates. Interestingly, upon comparing the crystal structure of outward-facing NorM-VC with our MurJ-based homology model of the inward-open state, a significant torsional difference is seen at the Gly245 (part of the GXP motif in NorM-VC) site of the TMH7 (phi value changes by 78 degrees). In order to assess the importance of this GXP motif in NorM transporters, the effect of bulkier amino acid substitutions in this motif can be tested in drug transport and binding assays. If it is indeed the bending of the TMH7 that exposes the drug binding site in the transporter, rendering the helix inflexible (by introducing bulkier side-groups) should cause disruption of drug binding and transport. Also, the disruption of the conformational switch can be tested by distance measurements between amino acid positions using EPR techniques.

3. To explore the (pseudo) two-fold symmetry in NorM proteins: As discussed in Chapter 1, MATE transporters are suspected to function by an alternative two-state mechanism that relies on the symmetry between the two lobes. As was shown in Chapter 3, chimeras generated by swapping the N- and C-lobes of NorM-VC and NorM-PS were

found to be transport-active proteins. This further strengthens the notion of a two-fold symmetry-based mode of operation in MATE transporters. One way to test this hypothesis could be to examine whether a protein composed of two N-lobes or two C-lobes is transport active. Also, such proteins can be used to study whether or not the binding-sites for substrates and ions fully reside in one of the two domains or whether they utilise both domains in a sequential fashion and/or bind at the interface between the domains.

4. To study the pH-dependence of Na^+-mediated stimulation of ethidium transport activity of NorM-VC: The studies of the effects of the proton availability on the ion-coupling in NorM-VC, as described in Chapter 4, could potentially be extended to NorM-VC incorporated in proteoliposomes . The effect of H^+ availability on the Na^+-dependent stimulation of ethidium efflux to NorM-VC can be studied to explore the relationship between H^+ versus Na^+ availability and transport. Previously, NorM-VC reconstituted in liposomes was shown to couple ethidium transport to ΔpNa under mildly acidic conditions (internal buffer pH= 6.8) [34]. In these experiements, NorM-VC was reconstituted in inside-out orientation and the extracellular side of the protein, which contains D36, faced acidic buffer. To further corroborate the findings in this thesis, NorM-VC can be reconstituted in liposomes prepared with internal buffer containing a fixed concentration of Na^+. If Na^+-dependent stimulation of ethidium transport is truly pH-dependent then more ethidium should be transported in liposomes with alkaline internal buffer than in liposomes with acidic internal buffer.

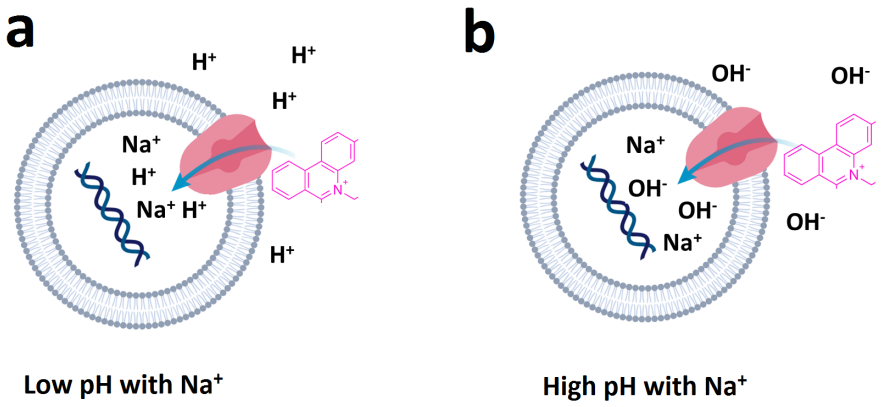

Fig. 7.5 Ethidium transport by NorM-VC reconstituted in liposomes loaded with DNA. In these experiments, the external buffer can be changed to test the effect of various factors on transport. Previously, reconstituted NorM-VC was shown to utilise Na^+ to transport ethidium while the extracellular side of the protein faced low pH buffer, a condition similar to **a**. In order to test the stimulation of Na^+-driven ethidium transport by NorM-VC, the same experiment can be done at alkaline pHs, a condition similar to **b**.

The relationship between H^+ and Na^+ binding to NorM-VC can also be studied using ethidium binding as a reporter in fluorescence anisotropy experiments. The measurements presented in this thesis show that the addition of Na^+ leads to enhanced binding of ethidium to purified NorM-VC. However, it is not yet known how this phenomenon is affected by pH. In experiments, the binding of ethidium to NorM-VC could be measured at a fixed Na^+ concentration and a range of pH values. These and other studies would increase our understanding of how H^+ and Na^+ interact with NorM-VC.

References

[1] WHO, "Antimicrobial resistance: global report on surveillance 2014," 2014.

[2] B. Wilkinson, K. Dorian, and L. Sabath, "Cell wall composition and associated properties of methicillin-resistant Staphylococcus aureus strains," *Journal of Bacteriology*, vol. 136, no. 3, 1978.

[3] G. D. Wright, "Bacterial resistance to antibiotics: Enzymatic degradation and modification," *Advanced Drug Delivery Reviews*, vol. 57, no. 10, pp. 1451–1470, 2005.

[4] N. Woodford and M. J. Ellington, "The emergence of antibiotic resistance by mutation," *Clinical Microbiology and Infection*, vol. 13, no. 1, pp. 5–18, 2007.

[5] A. Donhofer, S. Franckenberg, S. Wickles, O. Berninghausen, R. Beckmann, and D. N. Wilson, "Structural basis for TetM-mediated tetracycline resistance," *Proceedings of the National Academy of Sciences*, vol. 109, no. 42, pp. 16900–16905, 2012.

[6] L. J. V. Piddock, "Clinically relevant chromosomally encoded multidrug resistance efflux pumps in bacteria," *Clinical Microbiology Reviews*, vol. 19, no. 2, pp. 382–402, 2006.

[7] M. H. Saier, V. S. Reddy, B. V. Tsu, M. S. Ahmed, C. Li, and G. Moreno-Hagelsieb, "The Transporter Classification Database (TCDB): Recent advances," *Nucleic Acids Research*, vol. 44, no. D1, pp. D372–D379, 2016.

[8] ECDC, *The bacterial challenge : time to react*, vol. 6 July 201. 2009.

[9] L. J. Goldstein, H. Galski, A. Fojo, M. Willingham, S. L. Lai, A. Gazdar, R. Pirker, A. Green, W. Crist, G. M. Brodeur, M. Lieber, J. Cossman, M. M. Gottesman, and I. Pastan, "Expression of a multidrug resistance gene in human cancers.," *Journal of the National Cancer Institute*, vol. 81, no. 2, pp. 116–124, 1989.

[10] L. A. Doyle, W. Yang, L. V. Abruzzo, T. Krogmann, Y. Gao, A. K. Rishi, and D. D. Ross, "A multidrug resistance transporter from human MCF-7 breast cancer cells.," *Proceedings of the National Academy of Sciences of the United States of America*, vol. 95, no. 26, pp. 15665–15670, 1998.

[11] M. J. Zamek-Gliszczynski, K. A. Hoffmaster, D. J. Tweedie, K. M. Giacomini, and K. M. Hillgren, "Highlights from the international transporter consortium second workshop," in *Clinical Pharmacology and Therapeutics*, vol. 92, pp. 553–556, 2012.

[12] A. Yonezawa and K.-i. Inui, "Importance of the multidrug and toxin extrusion mate/slc47a family to pharmacokinetics, pharmacodynamics/toxicodynamics and pharmacogenomics," *British Journal of Pharmacology*, vol. 164, no. 7, pp. 1817–1825.

[13] S. Matsushima, K. Maeda, K. Inoue, K. Y. Ohta, H. Yuasa, T. Kondo, H. Nakayama, S. Horita, H. Kusuhara, and Y. Sugiyama, "The inhibition of human multidrug and toxin extrusion 1 is involved in the drug-drug interaction caused by cimetidine," *Drug Metabolism and Disposition*, vol. 37, no. 3, pp. 555–559, 2009.

[14] M. H. Saier and I. T. Paulsen, "Phylogeny of multidrug transporters," *Seminars in Cell and Developmental Biology*, vol. 12, no. 3, pp. 205–213, 2001.

[15] K. A. Hassan, L. D. Elbourne, L. Li, H. K. Gamage, Q. Liu, S. M. Jackson, D. Sharples, A. B. Kolstø, P. J. Henderson, and I. T. Paulsen, "An ace up their sleeve: A transcriptomic approach exposes the AceI efflux protein of Acinetobacter baumannii and reveals the drug efflux potential hidden in many microbial pathogens," *Frontiers in Microbiology*, vol. 6, 2015.

[16] K. G. Chen and B. I. Sikic, "Molecular pathways: regulation and therapeutic implications of multidrug resistance.," *Clinical cancer research : an official journal of the American Association for Cancer Research*, vol. 18, no. 7, pp. 1863–1869, 2012.

[17] J. Xu, H. Peng, and J. T. Zhang, "Human multidrug transporter ABCG2, a target for sensitizing drug resistance in cancer chemotherapy," *Current Medicinal Chemistry*, vol. 14, no. 6, pp. 689–701, 2007.

[18] N. Cant, N. Pollock, and R. C. Ford, "CFTR structure and cystic fibrosis," *International Journal of Biochemistry and Cell Biology*, vol. 52, pp. 15–25, 2014.

[19] R. Zhao and I. D. Goldman, "Folate and thiamine transporters mediated by facilitative carriers (SLC19A1-3 and SLC46A1) and folate receptors," *Molecular Aspects of Medicine*, vol. 34, no. 2-3, pp. 373–385, 2013.

[20] R. Augustin, "The protein family of glucose transport facilitators: It's not only about glucose after all," *IUBMB Life*, vol. 62, no. 5, pp. 315–333, 2010.

[21] E. M. Quistgaard, C. Löw, F. Guettou, and P. Nordlund, "Understanding transport by the major facilitator superfamily (MFS): structures pave the way," *Nature Publishing Group*, vol. 17, no. 2, pp. 1–10, 2016.

[22] D. M. Posadas, F. A. Martín, J. V. Sabio Y Garcïa, J. M. Spera, M. V. Delpino, P. Baldi, E. Campos, S. L. Cravero, and A. Zorreguieta, "The TolC homologue of Brucella suis is involved in resistance to antimicrobial compounds and virulence," *Infection and Immunity*, vol. 75, no. 1, pp. 379–389, 2007.

[23] I. Nasie, S. Steiner-Mordoch, and S. Schuldiner, "New substrates on the block: Clinically relevant resistances for EmrE and homologues," *Journal of Bacteriology*, vol. 194, no. 24, pp. 6766–6770, 2012.

[24] T. Kuroda and T. Tsuchiya, "Multidrug efflux transporters in the MATE family," *Biochimica et Biophysica Acta - Proteins and Proteomics*, vol. 1794, no. 5, pp. 763–768, 2009.

[25] S. Eskandari, "Remarkable commonalities of electrogenic and electroneutral Na+-phosphate cotransporters," *Journal of Physiology*, vol. 587, no. 17, pp. 4131–4132, 2009.

[26] E. Ficici, W. Zhou, S. Castellano, and J. D. Faraldo-Gómez, "Broadly conserved na+-binding site in the n-lobe of prokaryotic multidrug mate transporters," *Proceedings of the National Academy of Sciences*, vol. 115, no. 27, pp. E6172–E6181, 2018.

[27] Y. Morita, A. Kataoka, S. Shiota, T. Mizushima, and T. Tsuchiya, "NorM of Vibrio parahaemolyticus is an Na+-driven multidrug efflux pump," *Journal of Bacteriology*, vol. 182, no. 23, pp. 6694–6697, 2000.

[28] F. Long, C. Rouquette-Loughlin, W. M. Shafer, and E. W. Yu, "Functional cloning and characterization of the multidrug efflux pumps NorM from Neisseria gonorrhoeae and YdhE from Escherichia coli," *Antimicrobial Agents and Chemotherapy*, vol. 52, no. 9, pp. 3052–3060, 2008.

[29] X. He, P. Szewczyk, A. Karyakin, M. Evin, W. X. Hong, Q. Zhang, and G. Chang, "Structure of a cation-bound multidrug and toxic compound extrusion transporter," *Nature*, vol. 467, no. 7318, pp. 991–994, 2010.

[30] M. Otsuka, T. Matsumoto, R. Morimoto, S. Arioka, H. Omote, and Y. Moriyama, "A human transporter protein that mediates the final excretion step for toxic organic cations," *Proceedings of the National Academy of Sciences*, vol. 102, no. 50, pp. 17923–17928, 2005.

[31] K. Toyama, A. Yonezawa, S. Masuda, R. Osawa, M. Hosokawa, S. Fujimoto, N. Inagaki, K. Inui, and T. Katsura, "Loss of multidrug and toxin extrusion 1 (MATE1) is associated with metformin-induced lactic acidosis," *British Journal of Pharmacology*, vol. 166, no. 3, pp. 1183–1191, 2012.

[32] J. J. Mousa, Y. Yang, S. Tomkovich, A. Shima, R. C. Newsome, P. Tripathi, E. Oswald, S. D. Bruner, and C. Jobin, "MATE transport of the *E. Coli*-derived genotoxin colibactin," *Nature Microbiology*, vol. 1, no. 1, 2016.

[33] M. Radchenko, R. Nie, and M. Lu, "Disulfide cross-linking of a Multidrug and toxic compound extrusion transporter impacts Multidrug efflux," *Journal of Biological Chemistry*, vol. 291, no. 18, pp. 9818–9826, 2016.

[34] Y. Jin, A. Nair, and H. W. van Veen, "Multidrug transport protein norM from vibrio cholerae simultaneously couples to sodium- and proton-motive force.," *The Journal of biological chemistry*, vol. 289, no. 21, pp. 14624–14632, 2014.

[35] M. Lu, J. Symersky, M. Radchenko, A. Koide, Y. Guo, R. Nie, and S. Koide, "Structures of a Na+-coupled, substrate-bound MATE multidrug transporter," *Proceedings of the National Academy of Sciences*, vol. 110, no. 6, pp. 2099–2104, 2013.

[36] Y. Tanaka, C. J. Hipolito, A. D. Maturana, K. Ito, T. Kuroda, T. Higuchi, T. Katoh, H. E. Kato, M. Hattori, K. Kumazaki, T. Tsukazaki, R. Ishitani, H. Suga, and O. Nureki, "Structural basis for the drug extrusion mechanism by a MATE multidrug transporter," *Nature*, vol. 496, no. 7444, pp. 247–251, 2013.

[37] M. Radchenko, J. Symersky, R. Nie, and M. Lu, "Structural basis for the blockade of MATE multidrug efflux pumps," *Nature Communications*, vol. 6, 2015.

[38] H. Miyauchi, S. Moriyama, T. Kusakizako, K. Kumazaki, T. Nakane, K. Yamashita, K. Hirata, N. Dohmae, T. Nishizawa, K. Ito, T. Miyaji, Y. Moriyama, R. Ishitani, and O. Nureki, "Structural basis for xenobiotic extrusion by eukaryotic MATE transporter," *Nature Communications*, vol. 8, no. 1, 2017.

[39] A. Krah and U. Zachariae, "Insights into the ion-coupling mechanism in the MATE transporter NorM-VC," *Physical Biology*, vol. 14, no. 4, 2017.

[40] S. Vanni, P. Campomanes, M. Marcia, and U. Rothlisberger, "Ion binding and internal hydration in the multidrug resistance secondary active transporter NorM investigated by molecular dynamics simulations," *Biochemistry*, vol. 51, no. 6, pp. 1281–1287, 2012.

[41] J. Song, C. Ji, and J. Z. H. Zhang, "Insights on Na+ binding and conformational dynamics in multidrug and toxic compound extrusion transporter NorM," *Proteins: Structure, Function and Bioinformatics*, vol. 82, no. 2, pp. 240–249, 2014.

[42] L. Nie, E. Grell, V. N. Malviya, H. Xie, J. Wang, and H. Michel, "Identification of the high-affinity substrate-binding site of the multidrug and toxic compound extrusion (MATE) family transporter from Pseudomonas stutzeri," *Journal of Biological Chemistry*, vol. 291, no. 30, pp. 15503–15514, 2016.

[43] P. R. Steed, R. A. Stein, S. Mishra, M. C. Goodman, and H. S. McHaourab, "Na+-substrate coupling in the multidrug antiporter NorM probed with a spin-labeled substrate," *Biochemistry*, vol. 52, no. 34, pp. 5790–5799, 2013.

[44] O. P. Kuipers, P. G. G. A. De Ruyter, M. Kleerebezem, and W. M. De Vos, "Quorum sensing-controlled gene expression in lactic acid bacteria," *Journal of Biotechnology*, vol. 64, no. 1, pp. 15–21, 1998.

[45] I. Mierau and M. Kleerebezem, "10 Years of the nisin-controlled gene expression system (NICE) in Lactococcus lactis," 2005.

[46] H. Holo and I. F. Nes, "High-frequency transformation, by electroporation, of Lactococcus lactis subsp. cremoris grown with glycine in osmotically stabilized media," *Applied and Environmental Microbiology*, vol. 55, no. 12, pp. 3119–3123, 1989.

[47] A. Hemsley, N. Arnheim, M. D. Toney, G. Cortopassi, D. J. Galas, and L. Angeles, "A simple method for site-directed mutagenesis using the polymerase chain reaction," *Nucleic Acids Research*, vol. 17, no. 16, pp. 6545–6551, 1989.

[48] C. Li, A. Wen, B. Shen, J. Lu, Y. Huang, and Y. Chang, "FastCloning: A highly simplified, purification-free, sequence- and ligation-independent PCR cloning method," *BMC Biotechnology*, vol. 11, 2011.

[49] O. P. Kuipers, M. M. Beerthuyzen, P. G. G. A. De Ruyter, E. J. Luesink, and W. M. De Vos, "Autoregulation of nisin biosynthesis in Lactococcus lactis by signal transduction," *Journal of Biological Chemistry*, vol. 270, no. 45, pp. 27299–27304, 1995.

[50] L. Balakrishnan, H. Venter, R. A. Shilling, and H. W. van Veen, "Reversible transport by the ATP-binding cassette multidrug export pump LmrA: ATP synthesis at the expense of downhill ethidium uptake," *Journal of Biological Chemistry*, vol. 279, no. 12, pp. 11273–11280, 2004.

[51] T. Abee, K. J. Hellingwerf, and W. N. Konings, "Effects of potassium ions on proton motive force in rhodobacter sphaeroides," *Journal of Bacteriology*, vol. 170, no. 12, pp. 5647–5653, 1988.

[52] Y. Zhang and J. Skolnick, "TM-align: A protein structure alignment algorithm based on the TM-score," *Nucleic Acids Research*, vol. 33, no. 7, pp. 2302–2309, 2005.

[53] A. Vergara-Jaque, C. Fenollar-Ferrer, D. Kaufmann, and L. R. Forrest, "Repeat-swap homology modeling of secondary active transporters: Updated protocol and prediction of elevator-type mechanisms," *Frontiers in Pharmacology*, vol. 6, 2015.

[54] L. R. Forrest, "Structural Symmetry in Membrane Proteins," *Annual Review of Biophysics*, vol. 44, no. 1, pp. 311–337, 2015.

[55] A. V. Nair, H. Singh, S. Raturi, A. Neuberger, Z. Tong, N. Ding, K. Agboh, and H. W. Van Veen, "Relocation of active site carboxylates in major facilitator superfamily multidrug transporter LmrP reveals plasticity in proton interactions," *Scientific Reports*, vol. 6, no. August, pp. 1–12, 2016.

[56] C. Von Ballmoos and P. Dimroth, "Two distinct proton binding sites in the ATP synthase family," *Biochemistry*, vol. 46, no. 42, pp. 11800–11809, 2007.

[57] N. W. Luedtke, Q. Liu, and Y. Tor, "On the electronic structure of ethidium," *Chemistry - A European Journal*, vol. 11, no. 2, pp. 495–508, 2005.

[58] M. L. Eisinger, L. Nie, A. R. Dörrbaum, J. D. Langer, and H. Michel, "The Xenobiotic Extrusion Mechanism of the MATE Transporter NorM_PS from Pseudomonas stutzeri," *Journal of Molecular Biology*, vol. 430, no. 9, pp. 1311–1323, 2018.

[59] N. Terahara, T. A. Krulwich, and M. Ito, "Mutations alter the sodium versus proton use of a Bacillus clausii flagellar motor and confer dual ion use on Bacillus subtilis motors," *Proceedings of the National Academy of Sciences*, vol. 105, no. 38, pp. 14359–14364, 2008.

[60] J. C. Gordon, J. B. Myers, T. Folta, V. Shoja, L. S. Heath, and A. Onufriev, "H++: A server for estimating pKas and adding missing hydrogens to macromolecules," *Nucleic Acids Research*, vol. 33, no. Suppl. 2, 2005.

[61] C. Polvani and R. Blostein, "Protons as substitutes for sodium and potassium in the sodium pump reaction," *Journal of Biological Chemistry*, vol. 263, no. 32, pp. 16757–16763, 1988.

[62] K. Schlegel, V. Leone, J. D. Faraldo-Gomez, and V. Muller, "Promiscuous archaeal ATP synthase concurrently coupled to Na+ and H+ translocation," *Proceedings of the National Academy of Sciences*, vol. 109, no. 3, pp. 947–952, 2012.

[63] N. Terahara, M. Sano, and M. Ito, "A Bacillus Flagellar Motor That Can Use Both Na+ and K+ as a Coupling Ion Is Converted by a Single Mutation to Use Only Na+," *PLoS ONE*, vol. 7, no. 9, 2012.

[64] H. L. Tepper and G. A. Voth, "Mechanisms of passive ion permeation through lipid bilayers: Insights from simulations," *Journal of Physical Chemistry B*, vol. 110, no. 42, pp. 21327–21337, 2006.

[65] M. Heinig and D. Frishman, "STRIDE: A web server for secondary structure assignment from known atomic coordinates of proteins," *Nucleic Acids Research*, vol. 32, no. WEB SERVER ISS., 2004.

[66] D. P. Claxton, K. L. Jagessar, P. R. Steed, R. A. Stein, and H. S. Mchaourab, "Sodium and proton coupling in the conformational cycle of a mate antiporter from vibrio cholerae," *Proceedings of the National Academy of Sciences*, vol. 115, no. 27, pp. E6182–E6190, 2018.

[67] T. A. Binkowski, S. Naghibzadeh, and J. Liang, "CASTp: Computed Atlas of Surface Topography of proteins," *Nucleic Acids Research*, vol. 31, no. 13, pp. 3352–3355, 2003.

[68] P. Viitanen, M. L. Garcia, and H. R. Kaback, "Purified reconstituted lac carrier protein from escherichia coli is fully functional," *Proceedings of the National Academy of Sciences*, vol. 81, no. 6, pp. 1629–1633, 1984.

[69] Y. M. Leung, D. A. Holdbrook, T. J. Piggot, and S. Khalid, "The NorM MATE transporter from N. gonorrhoeae: Insights into drug and ion binding from atomistic molecular dynamics simulations," *Biophysical Journal*, vol. 107, no. 2, pp. 460–468, 2014.

[70] M. A. Seeger and H. W. van Veen, "Molecular basis of multidrug transport by ABC transporters.," *Biochimica et biophysica acta*, vol. 1794, no. 5, pp. 725–37, 2009.

Appendix A

Online resources

1. PrabiClustalW: https://npsa-prabi.ibcp.fr/cgi-bin/npsa_automat.pl?page=/NPSA/npsa_clustalw.html
2. CASTp: http://sts.bioe.uic.edu/castp/index.html?1ycs
3. ESPript3.0: http://espript.ibcp.fr/
4. GraphPad Prism: https://www.graphpad.com/
5. H++: http://biophysics.cs.vt.edu/
6. IDT codon optimisation tool: http://www.idtdna.com/codonopt
7. SWISS-MODEL: https://swissmodel.expasy.org/
8. Stride: http://webclu.bio.wzw.tum.de/cgi-bin/stride/stridecgi.py
9. Thermo Scientific: https://www.thermofisher.com/uk/en/home.html
10. TM-align: https://zhanglab.ccmb.med.umich.edu/TM-align/
11. UCSF Chimera: https://www.cgl.ucsf.edu/chimera/

Appendix B

Abbreviations and symbols

1. ABC: ATP binding cassette
2. ADP: Adenosine diphosphate
3. ANOVA: Analysis of variation
4. ATP: Adenosine triphosphate
5. BSA: Bovine serum albumin
6. CNBr: Cyanogen bromide
7. DAPI: 4,6-diamidino-2-phenylindole
8. DCCD: N,N'-Dicyclohexylcarbodiimide
9. DDM: n-dodecyl--D-maltoside
10. $DiOC_2(3)$: 3,3'-Diethyloxacarbocyanine Iodide
11. DNP: 2,4-dinitrophenol
12. DNA: Deoxyribonucleic acid
13. DTT: Dithiothreitol
14. EPR: Electron paramagnetic resonance
15. HRP: Horse radish peroxidase
16. IgG: Immunoglobulin G

17. ISOV: Inside-out vesicles:
18. K-EDTA: Potassium-Ethylene diamine tetraacetate
19. LB: Lysogeny broth
20. MATE: Multidrug and toxic compound extrusion
21. MDT: Multidrug transporters
22. MOP: Multidrug/oligosaccharidyl-lipid/polysaccharide
23. OD_x: optical density at wavelength x nm
24. P_i: Phosphate group
25. PMF: Proton motive force
26. Kp_i: Potassium phosphate group
27. *norM-PS*: NorM gene from *Pseudomonas stutzeri*
28. *norM-VC*: NorM gene from *Vibrio Cholerae*
29. NorM-PS: NorM protein from *Pseudomonas stutzeri*
30. NorM-VC: NorM protein from *Vibrio Cholerae*
31. SCOP: Strcutural classification of proteins
32. SD: Standard deviation
33. SDS-PAGE: Sodium dodecyl sulphate-polyacrylamide gel electrophoresis
34. PCR: Polymerase chain reaction
35. PDB: Protein data bank
36. PNK: Polynucleotide kinase
37. RPM: Rotations per minute
38. RTH: Round-the-horn
39. TBST: Tris buffered saline-Tween 20
40. TMH: Transmembrane helix

41. UV: Ultraviolet
42. Δp: Proton motive force
43. ΔpH: pH gradient across membrane
44. ΔpNa: Na^+ gradient across membrane
45. $\Delta\psi$: Transmembrane potential